

**PREPARATION, CHARACTERIZATION AND  
FLUORESCENCE QUENCHING OF WATER-SOLUBLE  
LIGHT-EMITTING NANOPARTICLES BASED ON  
CONJUGATED POLYMERS AND OLIGOMERS**

**LU XIAOMEI**

*(B.Sc., Fudan Univ.)*

**A THESIS SUBMITTED  
FOR THE DEGREE OF MASTER OF SCIENCE  
DEPARTMENT OF CHEMISTRY  
NATIONAL UNIVERSITY OF SINGAPORE**

**2007**

## ACKNOWLEDGEMENTS

It is a great pleasure to thank my supervisors, Prof. CHAN Sze On Hardy, for his invaluable guidance and advice throughout these years of my work. He has greatly devoted his valuable time to help me in this project and thesis, not only for sharing his knowledge but also encouragement and constant concern.

Special thanks to Prof. Huang Wei at Fudan University as well as all the staffs and students there. I have learnt so much from them that simple words cannot express my indebtedness to them.

I would like to express my sincere gratitude to all research staffs and postgraduate students in my group, especially to Dr. Cheng Daming, Dr. Xia Haibin, Dr. Tang Jiecong, Zhang Sheng, Che Huijuan, Xu Changhua and Fan Dongmei for their kind help, collaboration and friendship.

I would also like to express my gratitude to the National University of Singapore for the award of the research scholarship and Department of Chemistry for using the facilities to carry out my research.

Last but not least, I am very thankful to my family especially my parents and husband for their warmest patience, encouragement and great helps. Special mention must be made of my daughter, who is so sweet and her coming brightens up my life.

Thank you.

# TABLE OF CONTENTS

ACKNOWLEDGEMENTS.....	I
TABLE OF CONTENTS .....	II
SUMMARY.....	VII
NOMENCLATURE .....	IX
LIST OF TABLES .....	I
LIST OF SCHEMES.....	II
LIST OF FIGURES .....	III
<b>CHAPTER ONE INTRODUCTION.....</b>	<b>1</b>
1.1 CONJUGATED POLYMERS .....	1
1.1.1 Structures of Conjugated Polymers .....	1
1.1.2 Applications of Conjugated Polymers .....	4
1.2 CONJUGATED POLYMERS APPLIED AS CHEMOSENSORS OR BIOSENSORS.....	6
1.3 WATER-SOLUBLE CONJUGATED POLYMERS .....	10
1.4 NONCOVALENTLY CONNECTED MICELLES (NCCM).....	16
1.5 PROJECT OBJECTIVES .....	20
REFERENCES .....	21
<b>CHAPTER TWO WATER-SOLUBLE LIGHT-EMITTING NANOPARTICLES PREPARED</b>	
<b>    BY NON-COVALENT BOND SELF-ASSEMBLY OF FUNCTIONALIZED</b>	
<b>    POLY(P-PHENYLENEETHYNYLENE)S AND POLY(ACRYLIC ACID).....</b>	<b>30</b>

2.1	INTRODUCTION .....	30
2.2	MOLECULAR DESIGN .....	32
2.3	EXPERIMENTAL .....	33
2.3.1	<i>Materials</i> .....	33
2.3.2	<i>Characterization Methods</i> .....	33
2.3.3	<i>Synthesis</i> .....	34
	1,4-Diiodo-2,5-dimethoxybenzene (1) .....	34
	1,4-Diiodo-2,5-hydroquinone (2) .....	35
	1,4-Diiodo-2,5-bis(hexyloxy)benzene (3) .....	35
	1,4-Bis(ethynyl)-2,5-bis(hexyloxy)benzene (Monomer 1) .....	36
	2,5-Bis((3-propanol)oxy)-1,4-diiodobenzene (Monomer 2) .....	37
	2,5-Bis[3-( <i>N,N</i> -diethylamino)-1-oxapropyl]-1,4-diiodobenzene (Monomer 3) .....	38
	OHPPE .....	39
	NEt <sub>2</sub> PPE .....	40
2.4	RESULTS AND DISCUSSION .....	41
2.4.1	<i>Synthesis of Monomers and Polymers</i> .....	41
2.4.2	<i>Solubility and Color Study</i> .....	42
2.4.3	<i>NMR Spectroscopy</i> .....	42
2.4.4	<i>FT-IR Spectroscopy</i> .....	45
2.4.5	<i>Thermal Stability</i> .....	46
2.4.6	<i>Optical Properties</i> .....	47
2.4.7	<i>Water-Soluble Light-Emitting Nanoparticles</i> .....	48

2.5 CONCLUSION .....	55
REFERENCES .....	56

### CHAPTER THREE WATER-SOLUBLE LIGHT-EMITTING NANOPARTICLES

#### PREPARED BY NON-COVALENT BOND SELF-ASSEMBLY OF HYDROXYL

#### GROUP FUNCTIONALIZED OLIGO(P-PHENYLENEETHYNYLENE)S WITH

#### DIFFERENT MOLECULAR ARCHITECTURES AND WATER-SOLUBLE

#### POLYMERS CONTAINING DIFFERENT ACTIVE HYDROGEN ATOMS..... 59

3.1 INTRODUCTION .....	59
3.2 MOLECULAR DESIGN .....	61
3.3 EXPERIMENTAL .....	62
3.3.1 <i>Materials</i> .....	62
3.3.2 <i>Characterization Methods</i> .....	62
3.3.3 <i>Synthesis</i> .....	63
2,5-Diiodo-1,4-dimethoxybenzene (1) .....	63
1,4-Diiodo-2,5-hydroquinone (2) .....	64
1,4-Diiodo-2,5-bis(hexyloxy)benzene (3) .....	65
2,5-Bis(hexyloxy)-4-[(trimethylsilyl)ethynyl]iodobenzene (4) .....	65
2-(4-Iodophenoxy)-tetrahydro-2H-pyran (5) .....	66
2-(4-Ethynylphenoxy)-tetrahydro-2H-pyran (6) .....	66
2-(4-(2-(4-Ethynyl-2,5-bis(hexyloxy)phenyl)ethynyl)phenoxy)-tetrahydro-2H-pyran (7) .....	67
1-Ethynyl-2,5-bis(hexyloxy)-4-(2-phenylethynyl)benzene (8) .....	69
4-(Hexyloxy)-2,5-diiodophenol (9) .....	70

6-(4-(Hexyloxy)-2,5-diiodophenoxy)hexanol (10).....	71
1,4-Bis((6-hexanol)oxy)-2,5-diiodobenzene (11).....	72
Oligo(2,5-dihexyloxy-1,4-phenyleneethynylene (MOPE).....	73
Linear-shaped OH-functionalized OPE (OHOPE <sub>L</sub> ).....	74
T-shaped OH-functionalized OPE (OHOPE <sub>T</sub> ).....	75
Cross-shaped OH-functionalized OPE (OHOPE <sub>C</sub> ).....	77
3.4 RESULTS AND DISCUSSION.....	78
3.4.1 <i>Synthesis of Oligomers</i> .....	78
3.4.2 <i>NMR Spectroscopy</i> .....	79
3.4.3 <i>Water-Soluble Light-Emitting Nanoparticles</i> .....	81
3.4.4 <i>Optical Properties</i> .....	84
3.4.4.1 Solution-state Photophysics.....	84
3.4.4.2 Solid-state Photophysics.....	86
3.4.4.3 Optical Properties of Nanoparticles.....	88
3.5 CONCLUSION.....	91
REFERENCES.....	92

## CHAPTER FOUR STUDY ON OPTICAL PROPERTIES AND FLUORESCENCE

### QUENCHING OF WATER-SOLUBLE LIGHT-EMITTING NANOPARTICLES .96

4.1 INTRODUCTION.....	96
4.2 MOLECULAR DESIGN.....	97
4.3 EXPERIMENTAL.....	98
4.3.1 <i>Materials</i> .....	98

4.3.2	<i>Characterization Methods</i> .....	99
4.3.3	<i>Preparation of anionic nanoparticles</i> .....	99
4.4	RESULTS AND DISCUSSION .....	100
4.4.1	<i>General properties of OHOPE<sub>1</sub>/PAA<sup>-</sup> nanoparticles</i> .....	100
4.4.2	<i>Fluorescence quenching of nanoparticles by MV<sup>2+</sup></i> .....	101
4.4.3	<i>The influence of electrostatic interaction on fluorescence quenching</i> .....	105
4.4.4	<i>The influence of the nanoparticles concentration on fluorescence quenching</i> .....	106
4.4.5	<i>The influence of pH on fluorescence quenching</i> .....	108
4.4.6	<i>The influence of ionic strength on fluorescence quenching</i> .....	111
4.5	CONCLUSION .....	112
	REFERENCES .....	113
	<b>CHAPTER FIVE CONCLUSION REMARKS</b> .....	<b>116</b>

## SUMMARY

Water-soluble conjugated polymers (WSCPs) have shown great potential for use as fluorescent chemo- or biosensors due to their special solubility and optoelectronic properties. However, the general synthetic method to realize their water-solubility is complex. We have developed an alternative approach involving the convenient preparation of water-soluble light-emitting nanoparticles by combining light-emitting conjugated polymers/oligomers and water-soluble polymers via hydrogen bonds.

To be more specific, a series of conjugated polymer/oligomer based water-soluble light-emitting nanoparticles, made by non-covalent bond self-assembly with poly- or oligo(*p*-phenyleneethynylene) (PPE or OPE) and water-soluble polymers (PAA, PEG, PG), have been prepared and characterized.

The OPE-based nanoparticles exhibit a good water-solubility and a low degree of size dispersity, which are highly desired for applications in chemo- and bio-sensors. Furthermore, the results show a strong correlation between strength of hydrogen bonds between the water soluble polymer and the conjugated oligomer, size and degree of dispersity of the nanoparticles. Surprisingly, the formation of the nanoparticles are little influenced by the molecular architecture of conjugated molecules.



The optical properties and fluorescence quenching of the nanoparticles are systematically investigated. The optical properties of these nanoparticles are similar to those found in PPE or OPE films.

The effect of nanoparticle concentration, pH and ionic strength on the fluorescent quenching process will be discussed.

## Nomenclature

ATRP	Atom transfer radical polymerization
CNC	Charge neutral complex
CP	Conjugated polymer
CPB	Carboxyl-ended polybutadiene
CPS	Carboxyl-end polystyrene
DNT	2,4-dinitrotoluene
DSC	Differential scanning calorimetry
FWSCPs	Fluorescent water-soluble conjugated polymers
GPC	Gel permeation chromatography
HIJP	Hybrid ink-jet printing
LED	Light-emitting diodes
MOPE	Oligo(2,5-dihexyloxy-1,4-phenyleneethynylene)
MV <sup>2+</sup>	Methyl viologen
NCCM	Noncovalently connected micelles
NE <sub>t</sub> <sub>2</sub> PPE	Amino-functionalized PPE
OPE	Oligo(p-phenyleneethynylene)
OHOPE <sub>C</sub>	Cross-shaped OH-functionalized OPE
OHOPE <sub>L</sub>	Linear-shaped OH-functionalized OPE
OHOPE <sub>T</sub>	T-shaped OH-functionalized OPE
OHPPE	Hydroxyl-functionalized PPE

P2VP	Poly(2-vinyl pyridine)
P4VP	Poly(4-vinyl pyridine)
PA	Polyacetylene
PAA	Poly(acrylic acid)
PCL	Poly( $\epsilon$ -caprolactone)
PEG	Poly(ethylene glycol)
PF	Polyfluorene
PG	Poly(galactose)
PI	Polyimide
PL	Photoluminescence
PNA	Peptide nucleic acid
PPE	Poly(p-phenyleneethynylene)
PPV	Poly(phenylenevinylene)
PPV-SO <sub>3</sub> <sup>2-</sup>	Anionic sulfonated PPV
PSOH	Hydroxyl-containing polystyrene
PVPy	Poly(4-vinylpyridine)
TGA	Thermogravimetric analysis
THF	Tetrahydrofuran
TNT	2,4,6-trinitrotoluene
UV-vis	Ultraviolet-visible
WSCP	Water-soluble conjugated polymer

## LIST OF TABLES

TABLE 1.1 THE STRUCTURES OF SOME COMMON CONJUGATED POLYMERS5 .....	3
TABLE 2.1 GPC AND SPECTROSCOPIC DATA FOR PPES .....	42
TABLE 2.2 DLS CHARACTERIZATION DATA OF THE NANOPARTICLES AND THE PREPARING PROPORTION OF PPE AND PAA .....	48
TABLE 2.3 PHOTOPHYSICAL PROPERTIES OF FUNCTIONALIZED PPES IN THF AND THEIR NANOPARTICLES IN AQUEOUS SOLUTION.....	55
TABLE 3.1 DLS CHARACTERIZATION DATA OF THE NANOPARTICLES AND THE PREPARING PROPORTION OF OPES AND PAA .....	81
TABLE 3.2 DLS DATA OF THE NANOPARTICLES AND THE PREPARED BY OHOPEL AND WATER-SOLUBLE POLYMERS (PEG, PG OR PAA) .....	82
TABLE 3.3 PHOTOPHYSICAL PROPERTIES OF FUNCTIONALIZED OPES IN THF, OPES AS FILMS AND OPE/PAA NANOPARTICLES IN AQUEOUS SOLUTION.....	90
TABLE 4.1 PHOTOPHYSICAL PROPERTIES OF THE NEUTRAL OHOPEL/PAA AND ANIONIC OHOPEL/PAA- NANOPARTICLES IN AQUEOUS SOLUTION .....	101

## LIST OF SCHEMES

SCHEME 2.1 FUNCTIONALIZED PPES AND THE WATER-SOLUBLE POLYMER FOR PREPARING WATER-SOLUBLE NANOPARTICLES .....	32
SCHEME 2.2 SYNTHETIC ROUTES FOR FUNCTIONALIZED MONOMERS .....	36
SCHEME 2.3 SYNTHETIC ROUTES FOR FUNCTIONALIZED PPES .....	39
SCHEME 3.1 FUNCTIONALIZED OPES AND WATER-SOLUBLE POLYMERS FOR THE PREPARATION OF WATER-SOLUBLE NANOPARTICLES .....	61
SCHEME 3.2.1 SYNTHETIC ROUTES FOR COMPOUND 1-4 .....	64
SCHEME 3.2.2 SYNTHETIC ROUTES FOR COMPOUND 5-7 .....	67
SCHEME 3.2.3 SYNTHETIC ROUTES FOR COMPOUND 8-11.....	70
SCHEME 3.2.4 SYNTHETIC ROUTES FOR MOPE .....	73
SCHEME 3.2.5 SYNTHETIC ROUTES FOR OHOPE <sub>L</sub> AND OHOPE <sub>T</sub> .....	76
SCHEME 3.2.6 SYNTHETIC ROUTE FOR OHOPE <sub>C</sub> .....	77
SCHEME 4.1 NEUTRAL/ANIONIC WATER-SOLUBLE NANOPARTICLES AND QUENCHERS	98
SCHEME 4.2 PREPARATION OF ANIONIC WATER-SOLUBLE NANOPARTICLES .....	100

# LIST OF FIGURES

FIGURE 1.1 SOME TYPICAL CPS FOR DETECTING ALKALI OR ALKALINE-EARTH METAL IONS .....	7
FIGURE 1.2 PYRIDYL-BASED CONJUGATED POLYMERS AS CHEMOSENSORS .....	8
FIGURE 1.3 BAND DIAGRAM ILLUSTRATING THE MECHANISM OF QUENCHING BEHAVIOR FOR CONJUGATED POLYMERS.....	9
FIGURE 1.4 A: THE FIRST REPORTED CONJUGATED POLYMER AS FLUORESCENCE CHEMOSENSOR. B: THE PPE DERIVATIVES UTILIZED FOR DETECTING TNT .....	10
FIGURE 1.5 DIAGRAM ILLUSTRATING THE DETECTION MECHANISM OF CONJUGATED POLYELECTROLYTE FOR BIOMOLECULES .....	12
FIGURE 1.6 DIAGRAMMATIC REPRESENTATION FOR THE USE OF A WATER-SOLUBLE CP WITH A SPECIFIC PNA-C* OPTICAL REPORTER PROBE TO DETECT A COMPLEMENTARY SSDNA SEQUENCE.95 .....	13
FIGURE 1.7 MOLECULAR STRUCTURE OF WSCPS USED AS CHEMO OR BIOSENSORS ..	14
FIGURE 1.8 MOLECULAR STRUCTURE OF WATER-SOLUBLE CONJUGATED-IONIC AND CONJUGATED-ACIDIC BLOCK COPOLYMERS .....	16
FIGURE 2.1 <sup>1</sup> H NMR SPECTRA OF THE FUNCTIONALIZED PPES .....	43
FIGURE 2.2 <sup>13</sup> C NMR SPECTRA OF THE FUNCTIONALIZED PPES .....	44
FIGURE 2.3 FT-IR SPECTRA OF THE FUNCTIONALIZED PPES.....	45
FIGURE 2.4 THERMOGRAVIMETRIC ANALYSIS OF THE FUNCTIONALIZED PPES .....	46
FIGURE 2.5 UV-VIS AND PL SPECTRA OF THE FUNCTIONALIZED POLYMERS IN THF ....	47
FIGURE 2.6 REPRESENTATIVE FLUORESCENCE MICROGRAPH OF THE OHPPE/PAA (1:25) NANOPARTICLES. THE SAMPLE WAS OBSERVED IN WATER. THE PICTURE WAS RECORDED WITH 500 TIMES ZOOM. ....	50
FIGURE 2.7 REPRESENTATIVE TEM MICROGRAPHS OF THE NANOPARTICLES OBTAINED BY FREEZE DRYING. THE PICTURE WAS RECORDED WITH 50,000 TIMES ZOOM. ....	50

FIGURE 2.8	UV-VIS AND PL SPECTRA OF THE OHPPE/PAA AND NET2PPE/PAA NANOPARTICLES IN AQUEOUS SOLUTION .....	52
FIGURE 2.9	UV-VIS AND PL SPECTRA OF THE OHPPE AND NET2PPE AS FILMS.....	53
FIGURE 3.1	<sup>1</sup> H NMR SPECTRA OF THE FUNCTIONALIZED OPES.....	79
FIGURE 3.2	<sup>13</sup> C NMR SPECTRA OF THE FUNCTIONALIZED OPES.....	80
FIGURE 3.3	REPRESENTATIVE FLUORESCENCE MICROGRAPH OF THE OHOPEL/PAA (1:50) NANOPARTICLES. THE SAMPLE WAS OBSERVED IN WATER.....	84
FIGURE 3.4	REPRESENTATIVE TEM MICROGRAPHS OF THE OHOPEL/PAA NANOPARTICLES OBTAINED BY FREEZE DRYING. ....	84
FIGURE 3.5	UV-VIS AND PL SPECTRA OF THOSE OPES IN THF (10 <sup>-6</sup> MG/ML).....	85
FIGURE 3.6	NORMALIZED PL EMISSION SPECTRA OF OHOPEL IN THE DILUTE AND CONCENTRATED SOLUTIONS .....	86
FIGURE 3.7	NORMALIZED UV AND PL SPECTRA OF OHOPEL IN THE SOLID STATE.....	87
FIGURE 3.8	UV-VIS AND PL SPECTRA OF THE FUNCTIONALIZED OPE/PAA NANOPARTICLES IN AQUEOUS SOLUTION .....	89
FIGURE 4.1	UV-VIS AND PL SPECTRA OF THE NEUTRAL OHOPEL/PAA AND ANIONIC OHOPEL/PAA- NANOPARTICLES IN AQUEOUS SOLUTION .....	100
FIGURE 4.2	UV-VIS ABSORBANCE AND PL EMISSION SPECTRA OF NANOPARTICLES IN AQUEOUS SOLUTION QUENCHED BY MV <sup>2+</sup> IN DIFFERENT CONCENTRATIONS .....	103
FIGURE 4.3	UNMODIFIED STERN-VOLMER PLOT OF ANIONIC OHOPEL/PAA- NANOPARTICLES QUENCHED BY MV <sup>2+</sup> .....	104
FIGURE 4.4	MODIFIED STERN-VOLMER PLOT FOR ANIONIC OHOPEL/PAA- NANOPARTICLES IN FIGURE 4.3 .....	105
FIGURE 4.5	A: UNMODIFIED AND B: MODIFIED STERN-VOLMER PLOTS OF OHOPEL/PAA- NANOPARTICLES QUENCHED BY FE(CN) <sub>6</sub> <sup>4-</sup> AND OHOPEL/PAA NANOPARTICLES QUENCHED BY FE(CN) <sub>6</sub> <sup>4-</sup> AND MV <sup>2+</sup> .....	106
FIGURE 4.6	UV-VIS ABSORPTION AND EMISSION SPECTRA OF OHOPEL/PAA- NANOPARTICLES IN DIFFERENT CONCENTRATIONS (C = 1, 10 AND 50 μM)	

.....	107
FIGURE 4.7 KSV VERSUS THE CONCENTRATION OF OHOPEL/PAA- NANOPARTICLES RANGING FROM 1 TO 50 $\mu$ M IN THE PRESENCE OF MV <sup>2+</sup> .....	108
FIGURE 4.8 UV-VIS ABSORBANCE AND PL EMISSION SPECTRA OF OHOPEL/PAA- NANOPARTICLES IN AQUEOUS SOLUTION OF DIFFERENT PHS .....	109
FIGURE 4.9 KSV VALUES OF OHOPEL/PAA- VERSUS PHS .....	110
FIGURE 4.10 KSV VALUES OF OHOPEL/PAA- NANOPARTICLES VERSUS PHS IN DIFFERENT NANOPARTICLE CONCENTRATIONS .....	111
FIGURE 4.11 (A) PH-DEPENDENCE OF UV-VIS ABSORPTION MAXIMA; (B) PH-DEPENDENCE OF EMISSION MAXIMA; (C) FLUORESCENCE QUENCHING BY MV <sup>2+</sup> OF OHOPEL/PAA-NA <sup>+</sup> NANOPARTICLES IN AQUEOUS SOLUTION WITH AND WITHOUT NA <sub>2</sub> CO <sub>3</sub> .....	112



# CHAPTER ONE

## Introduction

### 1.1 Conjugated Polymers

Since the high conductivity of doped polyacetylene (PA) was discovered in 1977, the investigation of conjugated organic polymers has been carried out by research groups all around the world.<sup>1</sup> Conjugated polymers (CPs) with good electric properties are excellent alternatives to those widely used silicone based materials in electronic devices. In addition, these polymers have good stability, low density, flexibility in design, and they are easy to prepare. Their electronic properties can be well controlled by doping and by modification of the backbone chemical structures. During the past two decades, because of their theoretically interesting properties and their technologically promising future, conjugated polymers have become a focus of materials research.

#### 1.1.1 Structures of Conjugated Polymers

The term conjugated polymers refers to organic macromolecules represented by alternating double and single bonds or alternating triple and single bonds, and is indicative of an  $\sigma$ -bonded C-C backbone with  $\pi$ -electron delocalization.<sup>2</sup> The conjugation length is defined as the extent over which the  $\pi$ -electrons are delocalized. Conjugated polymers are organic semiconductors which combine the desirable processing characteristics of polymer systems with the electrical and optical

properties of semiconductors.<sup>3,4</sup>

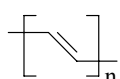
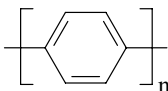
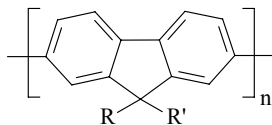
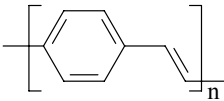
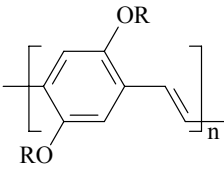
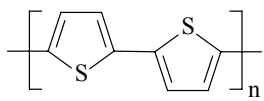
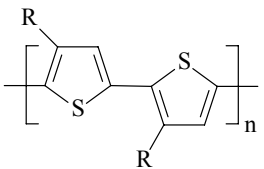
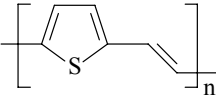
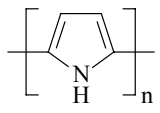
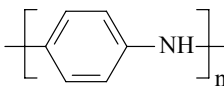
The semiconducting behaviour of conjugated polymers can be easily understood from the types of bonding operating along the main chain. The double or triple bonds between carbon atoms in the polymer main chain each have an electron excess to that normally required for just  $\sigma$ -bonds.<sup>5</sup> These extra electrons are in the  $p_z$  orbitals which are mainly perpendicular to the bonding orbitals between adjacent carbon atoms. These electrons overlap with adjacent  $p_z$  orbitals to form a delocalized  $\pi$ -electron cloud that spreads over several units along the polymer backbone. When this happens, delocalised  $\pi$  valence (bonding) and  $\pi^*$  conduction (anti-bonding) bands with defined bandgap are formed—which meets the requirements for semiconducting behaviour. Normally the electrons reside in the lower energy valence band but, if given sufficient energy, they can be excited into the normally empty upper conduction band, giving rise to a  $\pi$ - $\pi^*$  transition. Intermediate states are forbidden by quantum mechanics. The delocalized  $\pi$ -electron system confers the semiconducting properties on the polymer and gives it the ability to support positive and negative charge carriers with relatively high mobilities along the chain.<sup>6</sup>

As a semiconductor, a conjugated polymer must also satisfy two other conditions.<sup>7</sup>

One is that the  $\sigma$  bonds should be much stronger than the  $\pi$  bonds so that they can hold the molecule intact even when there are excited states – such as electrons and holes—in the  $\pi$  bonds. Without the linkage of the  $\sigma$  bonds, the molecule would split apart because these semiconductor excitations weaken the  $\pi$  bonds. The other requirement is that  $\pi$ -orbitals on neighbouring polymer molecules should overlap with

each other so that electrons and holes can move in three dimensions between molecules. Fortunately many conjugated polymers satisfy these three requirements. The semiconductor band gaps of most conjugated polymers are ranged from 1.5 to 3 eV, indicating that they are good candidates as optoelectronic devices.

**Table 1.1 The structures of some common conjugated polymers<sup>5</sup>**

Polymer	Chemical Name	Formula	Bandgap (eV)
PA	trans-polyacetylene		1.5
PPP	poly( <i>p</i> -phenylene)		3.0
PF	polyfluorene		3.2
PPV	poly( <i>p</i> -phenylene vinylene)		2.5
RO-PPV	poly(2,5-dialkoxy- <i>p</i> -phenylene vinylene)		2.2
PT	polythiophene		2.0
P3AT	poly(3-alkylthiophene)		2.0
PTV	poly(2,5-thiophenylene vinylene)		1.8
PPy	polypyrrole		3.1
PANi	polyaniline		3.2

Up to now, many conjugated polymers (structure are showed in Table 1.1) such as polyacetylene (PA), polyaniline (PAni), polypyrrole (PPy), polythiophene (PT), poly(*p*-phenylenevinylene) (PPV), poly(*p*-phenylene) (PPP), and polyfluorene (PF) have been thoroughly investigated.

PPP and its derivatives are interesting materials because they act as an excellent organic conductor upon doping. Another major interest of PPP is that it can be used as the active component in blue light-emitting diodes (LEDs).<sup>8,9</sup> Oligo(*p*-phenylene)s are generally utilized as model compounds for studying the electrical mechanisms of PPPs which are related to intra- and inter-chain charge transport or distribution and stabilization of charges and spins on  $\pi$ -conjugated chains. These mechanisms are important to the potential application of PPPs in rechargeable batteries.<sup>10,11</sup> PPV and its derivatives are one of the most extensively studied systems since the first ever reported light-emitting devices (LEDs) utilized PPV as the emission layer.<sup>12</sup> This has stimulated further interest in related types of structures such as poly(*p*-phenyleneethynylene) (PPE), which exhibit large photoluminescence efficiencies both in solution and in the solid state because of their high degree of chain rigidity.<sup>13</sup>

### **1.1.2 Applications of Conjugated Polymers**

Conjugated polymers display unusual electronic properties such as low ionization potential and high electron affinity, and the ability to be oxidized or reduced more reversibly than conventional polymers due to their unique molecular structures. These

polymers combine the processing advantages of the traditional polymers with the electrical and optical properties of metals, and the mechanical properties of the plastics.

There are two interesting properties of conjugated polymers used as conducting polymers that attracted much attention. The first is their reversible redox properties (i.e. electroactivity) and the second is their electrically conductive properties (i.e. conductivity).

The exploitation of the two properties have enabled the polymers to used as electronic devices,<sup>14</sup> rechargeable batteries,<sup>15</sup> and controlled drug release systems.<sup>16</sup> The combination of electroactivity and a good stability in aqueous solutions makes feasible the use of selected conjugated polymers in areas of bioscience.<sup>17</sup> PPy has been exploited as an electroactive film for the timed release of chemicals.<sup>18</sup>

In the area of sensors, considerable attention has also been directed towards the use of conducting polymers in amperometric sensors, primarily for the monitoring of glucose.<sup>19-21</sup> Conducting polymers have also been used in potentiometric sensors, conductometric sensors,<sup>22</sup> colorimetric sensors,<sup>23</sup> fluorescent sensors,<sup>24</sup> chemosensors,<sup>25</sup> and biosensors.<sup>26</sup> Conducting polymers are also used in the manufacturing of electrically conducting textiles<sup>27</sup> and production of artificial muscles.<sup>28</sup>

In addition, it has been reported that PA,<sup>29</sup> PANi,<sup>30</sup> PPy<sup>31</sup> can be used as conducting resists in lithographic applications. PANi is used as shielding material for electromagnetic radiation and to reduce electromagnetic interference.<sup>32-34</sup>

One of the most important applications of conjugated polymers is their role as active materials in optoelectronic devices such as light-emitting diodes,<sup>35</sup> photodiodes,<sup>36-38</sup> laser diodes,<sup>39</sup> light-emitting electrochemical cells,<sup>40,41</sup> photodetectors,<sup>42</sup> polymer rigid triodes,<sup>43</sup> optocouplers,<sup>44</sup> electrostatic shielding, non-linear optics,<sup>45,46</sup> electrochromic windows,<sup>47</sup> and field effect transistors.<sup>48-54</sup> Some of these polymer-based devices have reached performance levels comparable to or even better than those of their inorganic counterparts. In particular, polymer light emitting diodes have spurred special interest in recent years.

## **1.2 Conjugated Polymers Applied as Chemosensors or Biosensors**

Conjugated polymers are widely used as sensors. CP-based sensors can be made very sensitive to trace analytes.<sup>26</sup> CP-based sensors can be divided into four types, which are conductometric, potentiometric, colorimetric and fluorescence sensors. Conductometric sensors show dramatic changes of their electrical conductivity after perturbation by an analyte. Potentiometric sensors exhibit the changes of chemical potential. Colorimetric sensors are the sensors which display changes of UV-vis absorption properties. Fluorescence sensors are also widely used in chemical sensing which is based on the changes of their fluorescence intensity, energy transfer, wavelength, and lifetime and the efficient signal amplification. Much effort in the area of CP-based sensors has been directed to the enhancement of sensitivity of the devices.<sup>55,56</sup>

The selectivity of CP-based sensors can be realized through introducing special

receptors into the molecular structure. The polyalkyl ether chain-, crown ether-, aza crown ether-functionalized CPs are the most widely investigated.<sup>57</sup> Poly[3-(3,6-dioxahexyl)thiophene], the first conjugated polymer used for ion detection, was reported to exhibit high sensitivity to  $\text{Bu}_4\text{N}^+$  and  $\text{Li}^+$  ions through investigation of the changes of its voltammetric properties after complexation with these ions.<sup>58,59</sup> A series of polythiophene and polypyrrole-based CPs have been developed to detect alkali or alkaline-earth metal ions.<sup>60-71</sup> (Figure 1.1)

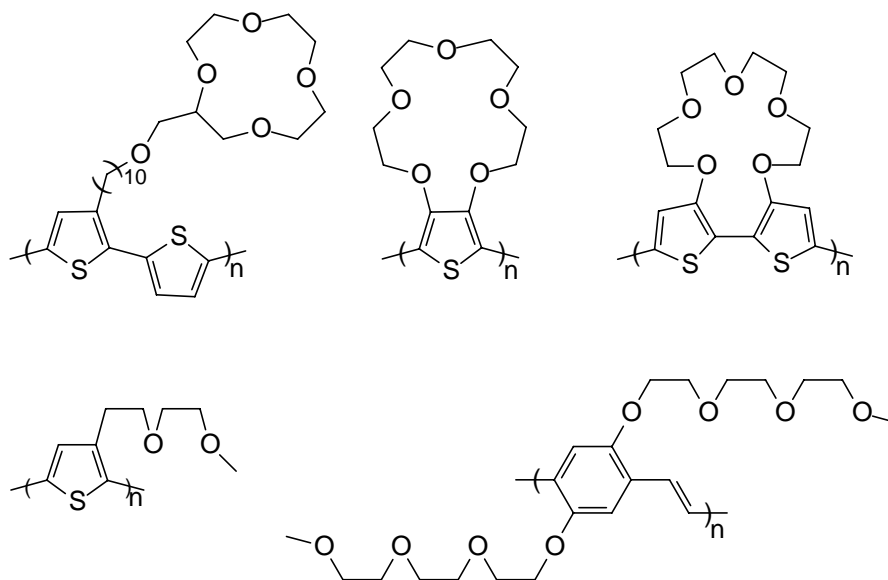


**Figure 1.1** Some typical CPs for detecting alkali or alkaline-earth metal ions

Beside crown ether-functionalized CP sensors, CPs containing pyridyl-based ligands which coordinate with a variety of transition metal ions were also studied. Generally, the pyridyl-based ligands were introduced into the conjugated backbone or tethered on the conjugated backbone to form the  $\pi$ - $\pi$  conjugation (Figure 1.2). After chelating with the transition metal ions, the ligands will become more planar and thus increase the  $\pi$ - $\pi$  conjugation along the polymer chains. Concomitantly, the optoelectronic

properties of the CPs will change significantly and can be used to detect transition metal ions. Thus, many bipyridine-based conjugated polymers were synthesized to detect transition metal ion.<sup>72-76</sup>

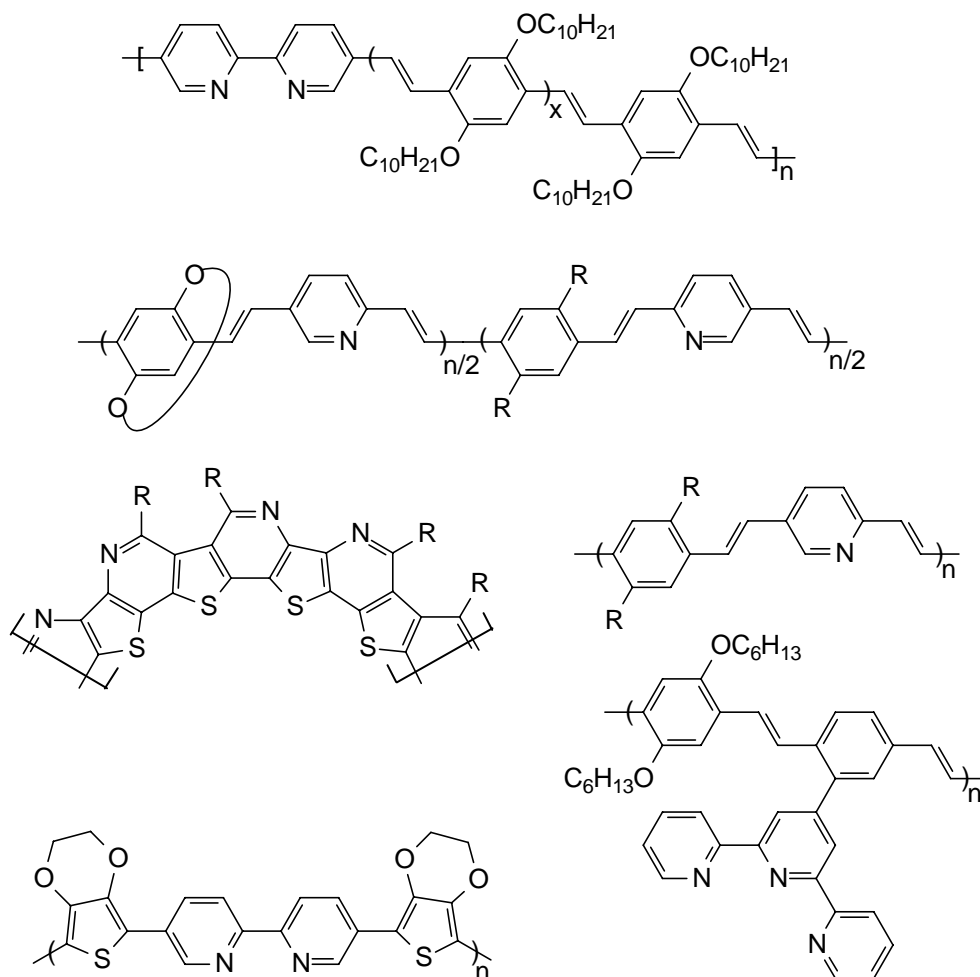


**Figure 1.2** Pyridyl-based conjugated polymers as chemosensors

Such crown ether or pyridyl group-containing CPs have been widely investigated to detect metal ions as conductometric, potentiometric and colorimetric sensors. Recently, fluorescence sensors which detect analytes through the fluorescence quenching and recovering have received much attention because of their real-time and amplified responses. The utility of CPs as fluorescence sensors was first reported by Swager's group.<sup>77,78</sup> It was found that these fluorescent conjugated polymers display



very high sensitivity to trace amounts of analytes. The observed superior sensitivity is anticipated to result from the CP's delocalized conjugated molecular structure which can facilitate efficient electron and energy migration along the whole conjugated backbone (Figure 1.3).

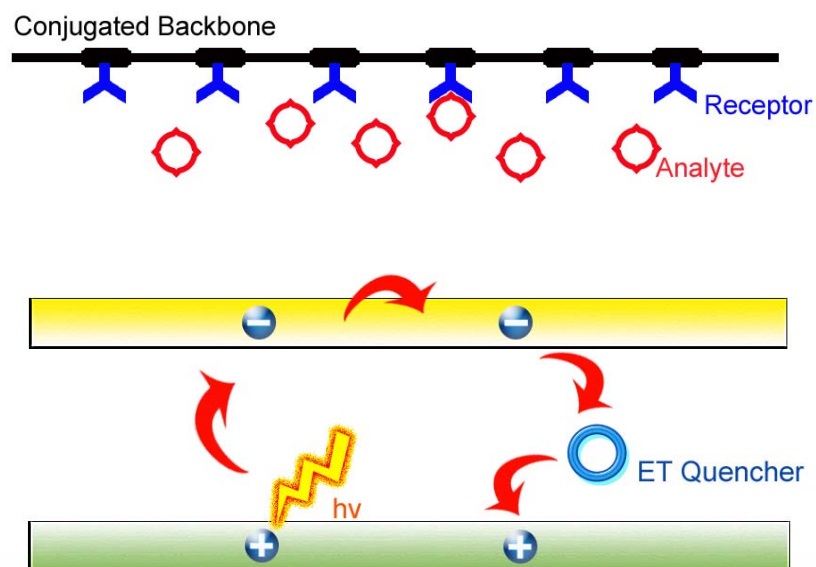


**Figure 1.3 Band diagram illustrating the mechanism of quenching behavior for conjugated polymers**

In Swager's work, the fluorescent conjugated polymers with a cyclophane receptor at every repeat unit and their monomeric counterpart compound, a small molecule containing a cyclophane receptor, were compared to demonstrate this principle. The cyclophane receptors were afforded to bind paraquat and its derivatives which are electron-transfer molecules for fluorescence quenching (Figure 1.4 A). It was shown that the fluorescence of both the monomer and polymer can be quenched after the binding of the paraquat by the cyclophane to form a rotaxane complex. However, the polymer showed a 3 orders of increase in quenching efficiency when compared to the

monomeric compound. The efficient quenching resulted from the facile electron and energy migration from the binding receptor sites to the whole polymer backbone (Figure 1.3). This approach was also used by Swager's group to detect explosives, such as 2,4,6-trinitrotoluene (TNT) and 2,4-dinitrotoluene (DNT)<sup>55,56</sup> (Figure 1.4 B).

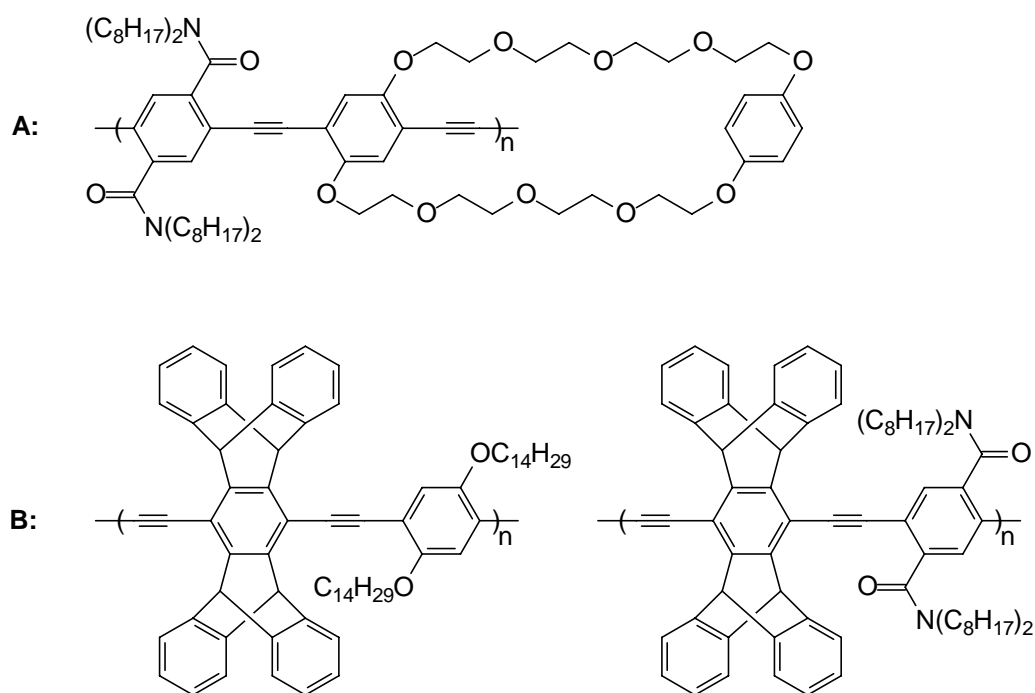


**Figure 1.4 A: The first reported conjugated polymer as fluorescence chemosensor. B: the PPE derivatives utilized for detecting TNT**

### 1.3 Water-Soluble Conjugated Polymers

Currently, water-soluble conjugated polymers (WSCPs) have displayed great potential in optoelectronic<sup>79-81</sup> and biological fields<sup>82</sup> due to their water solubility and optoelectronic properties. The most common way to prepare conjugated polymers with good water solubility is to introduce hydrophilic groups such as quaternized ammonium, carboxylate or sulfonate into the polymer chains to form conjugated polyelectrolytes. The optoelectronic properties of WSCPs can be conveniently

adjusted by changing the molecular structure of the conjugated backbone. Also, the ionic group on the conjugated polymer can be further used to afford electrostatic attraction force to construct supramolecular structures.<sup>83-86</sup>

Previously WSCPs were applied to fabricate optoelectronic devices through the layer-by-layer self-assembly,<sup>87</sup> ink-jet printing<sup>88</sup> or screen printing techniques.<sup>89</sup> The above novel developed film deposition techniques showed great potential to fabricate films with large area multilayers by a relative cheap method. Yang's group first reported fabrication of the blue and orange-red dual-color polymeric light-emitting pixels via hybrid ink-jet printing method (HIJP).<sup>90</sup> Rubner's group later reported the multilayer LEDs through layer-by-layer self-assembly using cationic and anionic blue-light emitting conjugated polymers.<sup>90</sup> Furthermore, the same layer-by-layer self-assembly method was applied to study the Förster energy transfer between conjugated polymers with different band-gaps.<sup>91</sup> Most importantly, the water-based techniques have been paid more attention because they can be used to prevent the unfavorable inter-surface diffusion or erosion between the neighboring layers which is inevitable in the organic solvent-based fabrication processes.<sup>92</sup>

Although previous research has demonstrated that conjugated polymers exhibit amplified sensitivity to detect small amounts of analytes, these conjugated polymer-based sensors are limited in practical application because these polymers can only dissolve in organic solvents while most of sensing applications are conducted in an aqueous environment. Water-soluble conjugated polymers therefore show great potential as a new class of chemo- and bio-sensors with high sensitivity and

selectivity.<sup>93</sup> WSCPs with ionic groups could attach oppositely charged quenchers more closely through electrostatic attraction and lead to amplified fluorescence quenching by those trace quenchers via energy transfer or electron transfer. Cheng first reported the amplified fluorescence quenching of anionic sulfonated PPV (PPV-SO<sub>3</sub><sup>2-</sup>) to cationic methyl viologen (MV<sup>2+</sup>).<sup>93</sup>

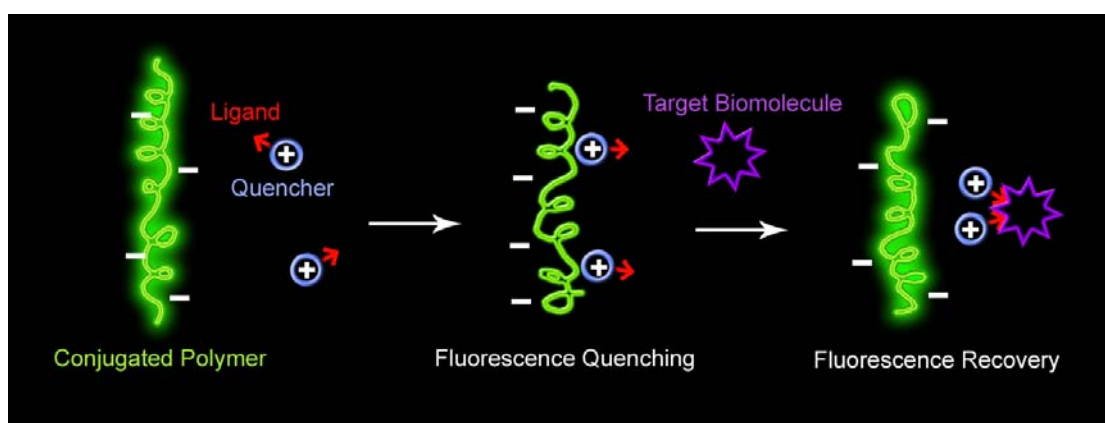


**Figure 1.5 Diagram illustrating the detection mechanism of conjugated polyelectrolyte for biomolecules**

This method can also be applied to detect biomolecules by coupling the quencher with a biological ligand. In aqueous solution, when the quencher–ligand conjugates is attached to the conjugated polyelectrolytes through electrostatic interactions, the fluorescence of conjugated polyelectrolytes will be quenched. When biospecific receptors are added, the quencher–ligand conjugates will combine with the biological receptor and detach from the conjugated polyelectrolytes, and thus the fluorescence will be recovered (Figure 1.5).<sup>93</sup> In 2002, Wang et al modified this method. They first fabricated a charge neutral complex (CNC) in aqueous solution by combining PPV-SO<sub>3</sub><sup>-</sup> and a saturated cationic polyelectrolyte at a 1:1 ratio (per repeat unit) and

then successfully used them to detect the anti-DNP IgG.<sup>94</sup> The advantage of this modified method is that it can significantly decrease the nonspecific interactions between conjugated polyelectrolytes and biomolecules.

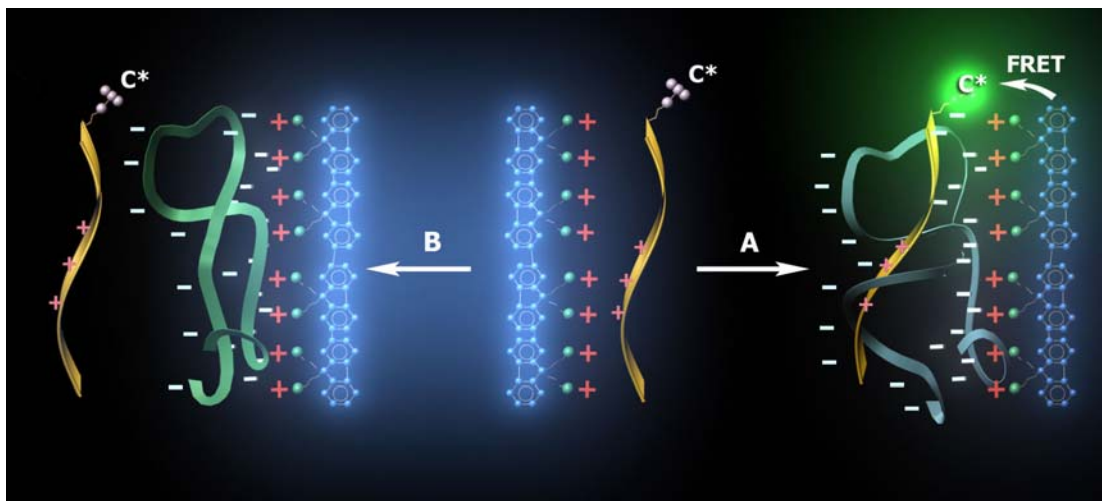


**Figure 1.6** Diagrammatic representation for the use of a water-soluble CP with a specific PNA-C\* optical reporter probe to detect a complementary ssDNA sequence.<sup>95</sup>

Recently, the cationic blue-light emitting conjugated polymers, PFs, are successfully developed by G. C. Bazan et al to detect DNA and RNA through sensitizing the fluorescence of a dye on a specific peptide nucleic acid (PNA) sequence.<sup>95</sup> The mechanism of this method is illustrated in Figure 1.6. The cationic PF and PNA with dye were dissolved in the same aqueous solution and DNA was then added. The anionic DNA swiftly combined with cationic PF through electrostatic attraction. If the PNA with dye is the specific PNA for the DNA, the PNA will be attached close to the DNA-PF complex and produce the energy transfer from PF to the dye on PNA. Finally the blue-light emitting of PF in the aqueous solution will turn into green light-emitting of the dye. On the contrary, if the PNA with dye is not the specific PNA

for the DNA, the PNA will not be absorbed by the DNA-PF complex and the aqueous solution will still retain blue-light emitting.

Most recently, Swager's group has used a carbohydrate-functionalized fluorescent polymer, which contains many carbohydrate ligands on a single polymer chain, to allow for multivalent detection of pathogens. The multivalent interactions between the mannose-functionalized polymer and mannose receptors located on the bacterial pili can cause aggregation of the polymer and form brightly fluorescent clusters.<sup>96</sup>

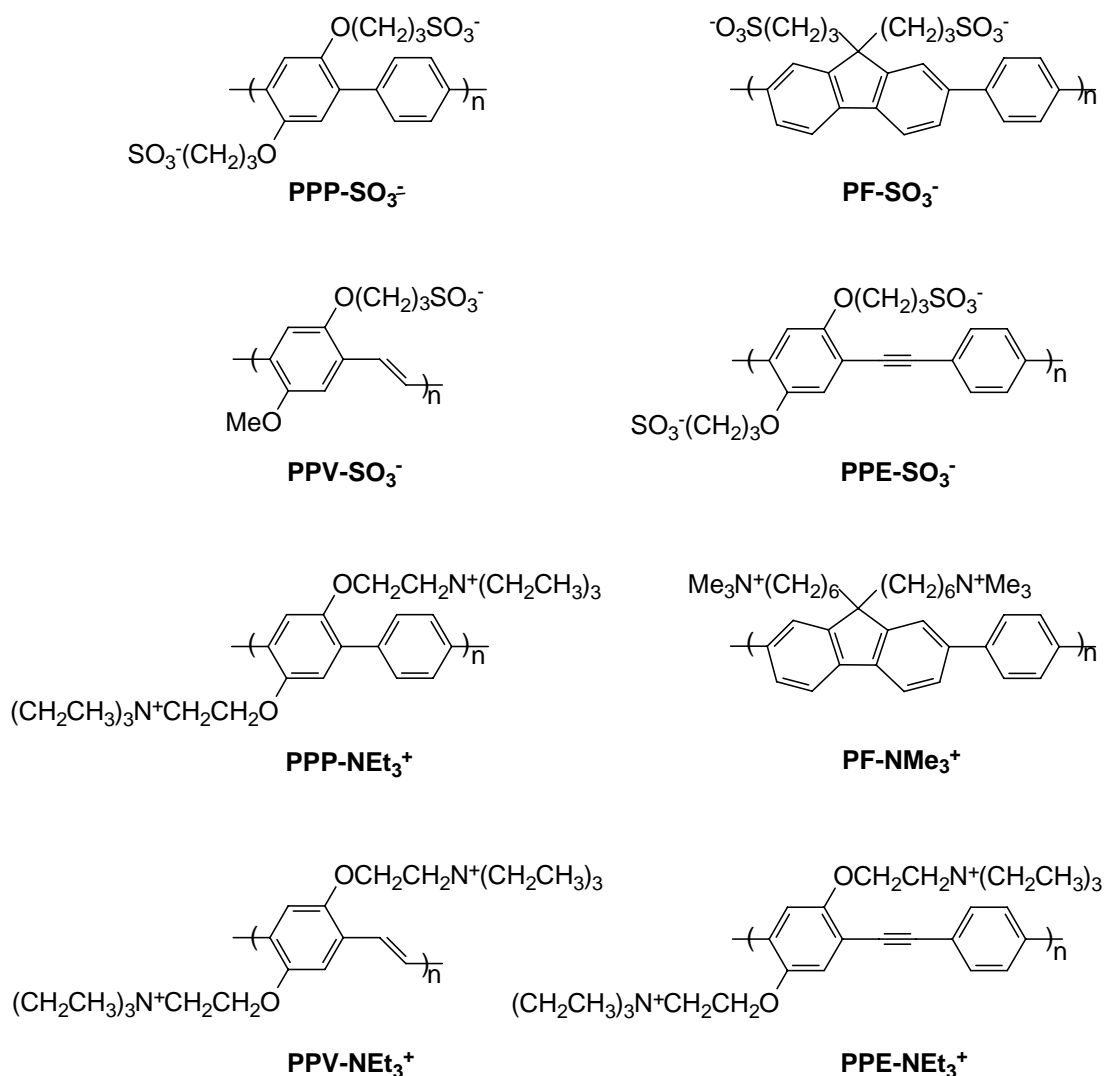


**Figure 1.7** Molecular structure of WSCPs used as chemo or biosensors

Because of the potential application of WSCPs as biosensors, the influence on the fluorescence quenching of WSCPs have been significantly investigated. Recent research shows that the quenching ability of WSCPs is influenced by the structures of conjugated polymers themselves and the local environments, such as conjugated length,<sup>97</sup> charge of quenching,<sup>98</sup> ionic strength,<sup>99</sup> substrate,<sup>100</sup> complex of WSCPs with oppositely charged surfactant<sup>101,102</sup> or polyelectrolytes<sup>100,103</sup> and aggregation states.<sup>104</sup> It was found that the more fluorescent quenching will be obtained if the longer conjugated length of WSCPs and the more opposite charge on the quencher exist.<sup>97,98</sup> The increased ionic strength of the local environment is likely to screen the electrostatic attraction between conjugated polymer and quencher, and finally leads to a decrease in the quenching ability.<sup>99</sup>

Further study showed that if the fluorescent WSCPs are absorbed onto the oppositely charged surfaces, their quenching ability may be significantly changed. For example, when PPV-SO<sub>3</sub><sup>-</sup> chains were absorbed on the surface of polystyrene microsphere, these anionic conjugated polymers can only be used to detect analytes with the same anionic charges instead of that with opposite cationic charge.<sup>100</sup> Similarly, after anionic PPV-SO<sub>3</sub><sup>-</sup> chains were combined with cationic surfactant, these conjugated polymers exhibit higher sensitivity on those neutral quenchers (for example, trinitrotoluene) but a lower sensitivity to oppositely charged quenchers.<sup>101</sup>

The first reported water-soluble conjugated polymer was polythiophene.<sup>105</sup> Other fluorescent water-soluble conjugated polymers (Figure 1.7) soon followed, which included poly(phenylene ethylene),<sup>106</sup> poly(phenylene vinylene)<sup>107</sup> and

polyfluorene.<sup>108</sup> Generally, their water-solubility was realized through chemically attach ionic or neutral water-soluble groups to the polymer chains.

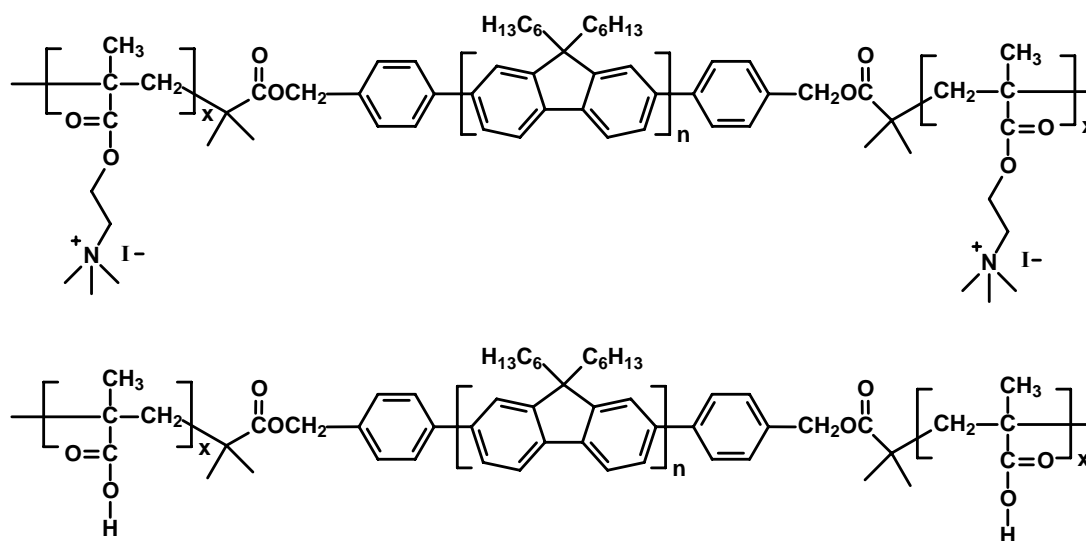


**Figure 1.8 Molecular structure of water-soluble conjugated-ionic and conjugated-acidic block copolymers**

Recently, a novel method to achieve water-solubility was reported. This involves the self-assembly of block copolymer in aqueous solution, by combining the neutral conjugated polymer segments with the water-soluble polymer soft segments. Lu et al.<sup>109,110</sup> synthesized the water-soluble conjugated-acidic and conjugated-ionic block copolymers via atom transfer radical polymerization (ATRP) with the polyfluorene-based macroinitiator and reported their good water-solubility through their self-assembly in aqueous solution (Figure 1.8).

#### 1.4 Noncovalently Connected Micelles (NCCM)

Recently, hydrogen bonding and ion-ion interaction has been used as the main driving forces to self-assemble one-, two- or three-dimensional structures.<sup>111,112</sup> It is



well-known that introducing the specific interactions into multicomponent polymers is an efficient method to enhance the miscibility and finally form interpolymer complexes.<sup>113</sup> However, most polymers contain flexible and long-chain properties, resulting in the uncontrollable interactions between complementary polymers and therefore the formation of irregular structures.<sup>113</sup> Thus, efficient control of specific interactions between polymeric blocks to realize regular supramolecular structures is highly desirable. Generally, such assemblies are realized through the micellization of block copolymers in one selected solvent, the driving force of which is from the extremely different solubility of the polymer blocks in such a solvent.<sup>114-116</sup>

Most recently, polymeric micelles and hollow spheres are developed from the self-assemblies of two different types of polymers with intermolecular-specific interactions (hydrogen bonding). This novel method to prepare polymeric self-assembly is called “block copolymer-free strategies”.

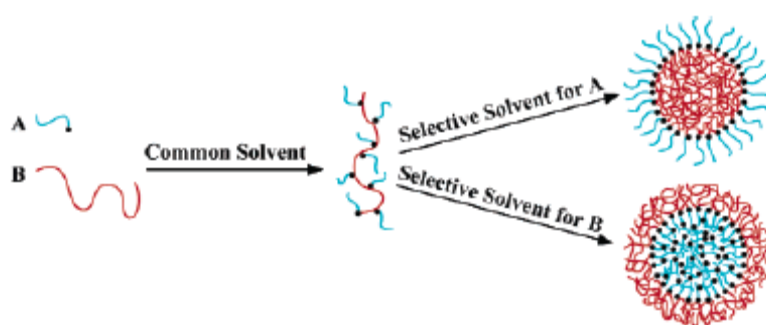


**Figure 1.9 Schematic representation of the formation of hydrogen bonding grafting polymers and their assembly in selective solvents.**

To realize this strategy, an oligomer (A) equipped with a single interaction site at one end of the short chain and a polymer (B) pending with many interacting sites which could interact with A must be chosen.<sup>117-119</sup> Under the interaction between B and the

end of A, a graft-like soluble complex with B and A is first formed in the same solvent. After adding another solvent in which only A or B has good solubility, the complex can assemble into a core-shell structure (Figure 1.9). This strategy was first reported by Jiang's group. They successfully prepared the polymeric micells using poly(4-vinyl pyridine) (P4VP) as a proton-accepting polymer and a low-molecular-weight carboxyl-end polystyrene (CPS) as a proton-donating polymer.<sup>118</sup> CPS and P4VP were first mixed in chloroform to form the soluble complex and then after adding toluene (which could only dissolve CPS) the complex self-assembled into stable micelles.<sup>118,119</sup> Because the CPS shell and the P4VP core are connected with each other by hydrogen bonding which are different with covalent bonding in the micelles of blockpolymers, they were called "noncovalently connected micelles" (NCCM). The above strategy was further applied to prepare other NCCMs composed of carboxyl-ended polybutadiene (CPB) and P4VP<sup>120</sup>, and poly(2-vinyl pyridine) (P2VP) and polyisoprene with a sulfonic acid end (suPI)<sup>121</sup>.

In the above strategy, restricting one kind of interaction sites to the end of polymer chain is necessary. Recently, a new strategy named "Assembly of Polymer Pairs in Solvent/Precipitant" which does not need the above restriction and which is applicable to those polymers with one or more interacting sites was developed as follows.<sup>122</sup> All of those polymers which have one or more interacting sites can be used in this new strategy. Firstly, polymers A and B were dissolved in different solvents and the solvent for B must be a precipitant for A. When solution with A was added into solution with B, the chains of A would aggregate into nano- or submicrometer

size particles and quickly embedded with the chains of B through the formation of hydrogen bonding between A and B, and therefore the micelle-like particles were formed and the precipitation A would be prevented. Based on this new strategy, several NCCMs were prepared using slightly sulfonated polystyrene/P4VP,<sup>123,124</sup> poly(styrene-co-methacrylic acid)/poly(vinyl pyrrolidone),<sup>125</sup> hydroxyl-containing polystyrene (PSOH)/P4VP,<sup>126</sup> CPB/poly(vinyl alcohol),<sup>127</sup> and poly( $\epsilon$ -caprolactone) (PCL)/poly(acrylic acid).<sup>128</sup> For example, chloroform is a good solvent for both PSOH and P4VP, while nitromethane is a good solvent for P4VP but a poor solvent for PSOH. When PSOH in  $\text{CHCl}_3$  was added into nitromethane with P4VP, the NCCMs was formed because of the hydrogen bonding between the pyridine ring in P4VP and hydroxyl in PSOH. As shown in Figure 1.10, it was found that the mutual interaction between P4VP and PSOH could be adjusted by changing the hydroxyl density in PSOH and resulted in different morphologies of the NCCMs.

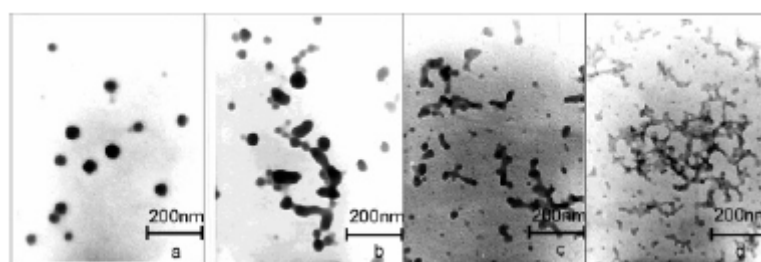


**Figure 1.10** TEM micrographs of NCCM of (PSOH-x)-P4VP (x, the molar content of hydroxyl-containing units in PSOH) showing morphological change with hydrogen-bonding density, (a) PSOH-2/P4VP, (b) PSOH-20/P4VP, (c) PSOH-27/P4VP, and (d) PSOH-42/P4VP.<sup>147</sup>

All the above research showed that as long as the proper special interaction are utilised, most polymers, such as functionalized oligomers, ionomers, homopolymers, random copolymers, and graft copolymers, can be assembled into supermolecular

structures. These new strategies for self-assembly are characterized by simplicity of the preparing process and broadness of the available materials. These opens up further intriguing prospects for obtaining water-soluble conjugated polymer-based light-emitting materials (nanoparticles).

### **1.5 Project Objectives**

It has been shown in the previous paragraphs that the noncovalent self-assembly via hydrogen bonds is a powerful way to prepare water-soluble materials directly from non-water-soluble polymers in conjunction with water-soluble polymers. Thus this method is anticipated to be suitable for the preparation of water-soluble conjugated polymer-based fluorescent nanomaterials.

The aim of our project is to produce water-soluble conjugated polymers or oligomers through the noncovalent self-assembly method described above. In our work, conjugated polymers PPEs and oligomers OPEs with functional groups capable of forming hydrogen bonds with water-soluble polymers will be characterized as light-emitting materials. The optoelectronic properties and fluorescence quenching of the light-emitting nanoparticles prepared will be evaluated for potential application as sensors. The influence of non-covalent self-assembly system with different types of hydrogens on the conformational change and the related optical behavior of conjugated polymers in aqueous environments will also be discussed.

## References

1. Chiang, C. K.; Fincher, C. R.; Park, Y. W.; Heeger, A. J.; Shirakawa, H.; Louis, E. J.; Gau, S. C.; MacDiarmid, A. G. *Phys. Rev. Lett.*, **1977**, *39*, 1098.
2. Brown, A. R. *Electroluminescence in Poly(p-phenylenevinylene) and Derivatives*, Ph. D. dissertation, University of Cambridge, **1992**.
3. Bradley, D. D. C. *Chem. Br.*, **1991**, *21*, 719.
4. Bradley, D. D. C.; Brown, A. R.; Burn, P. L.; Burroughes, J. H.; Friend, R. H.; Greenham, N. C.; Gymer, R. W.; Holmes, A. B.; Kraft, A. M.; Marks, R. N. "Conjugated Polymer Electro-optic Devices" in *Photochemistry and Polymeric Systems*, Royal Society of Chemistry, **1993**, 120.
5. Friend, R. H.; Greenham, N. C. "Conjugated Polymer Electroluminescence" in *Physical Properties of Polymers Handbook*, AIP Press, **1996**, *35*, 479.
6. May, P. *Physics World*, **1995**, 52.
7. Friend, R. H.; Burroughes, J. H.; Shimoda, T. *Physics World*, **1999**, 35.
8. Kraft, A.; Grimsdale, A. C.; Holmes, A. B. *Angew. Chem.*, **1998**, *110*, 416.
9. Kraft, A.; Grimsdale, A. C.; Holmes, A. B. *Angew. Chem. Int. Ed.*, **1998**, *37*, 403.
10. Novák, P.; Müllen, K.; Santhanam, K. S. V.; Hass, O. *Chem. Rev.*, **1997**, *97*, 207.
11. Bohnen, A.; Heitz, W.; Müllen, K.; Räder, H. J.; Schenk, R. *Makromol. Chem.*, **1991**, *192*, 1679.
12. Burroughes, J. H.; Bradley, D. D. C.; Brown, A. R.; Marks, R. N.; Mackay, K.; Friend, R. H.; Burn, P. L.; Holmes, A. B. *Nature*, **1990**, *347*, 539.
13. Chen, W. *Design, Synthesis, Characterization and Study of Novel Conjugated*

- Polymers*, Ph. D dissertation, Iowa State University, **1997**.
14. Potember, R. S.; Hoffmann, R. C.; Hu, H. S.; Cocchiaro, J. E.; Viands, C. V.; Murphy, R. A.; Poehler, T. O. *Polymer*, **1987**, *28*, 574.
  15. Bond, S. F.; Howie, A.; Friend, R. H. *Sur. Sci.*, **1995**, *333*, 196.
  16. Blankespoor, R. L.; Miller, L. L. *J. Chem. Soc., Chem. Commun.*, **1985**, 90.
  17. Couves, L. D.; Porter, S. J. *Synth. Met.*, **1989**, *28*, C761.
  18. Zinger, B.; Miller, L. L. *J. Am. Chem. Soc.*, **1984**, *106*, 6861.
  19. Umana, M.; Weller, J. *Anal. Chem.*, **1986**, *58*, 2979.
  20. Barlett, P. N.; Whitaker, R. G. *J. Electroanal. Chem.*, **1987**, *37*, 224.
  21. Caglar, P.; Wnek, G. E. *J. Macromol. Sci. Pure. Appl. Chem.*, **1995**, *A32*, 349.
  22. Paul, E. W.; Ricco, A. J.; Wrighton, M. S. *J. Phys. Chem.*, **1985**, *89*, 1441.
  23. McQuade, D. T.; Pullen, A. E.; Swager, T. M. *Chem. Rev.*, **2000**, *100*, 2537.
  24. Thomas, K. G.; Thomas, K. J.; Das, S.; George, M. V. *Chem. Commun.*, **1997**, 597.
  25. Jung, S. K.; Wilson, G. S. *Anal. Chem.*, **1996**, *68*, 591.
  26. Swager, T. M. *Acc. Chem. Res.*, **1998**, *31*, 201.
  27. Okoniewski, M. *Modifizierung der Synthesefasern zur Erzielung von leitfähigen, Ferromagnetischen, Anderen Eigenschaften, Melliand textilber*, **1990**, *71*, 94.
  28. Kuhn, W.; Hargitay, B.; Katchalsky, A.; Eisenberg, H. *Nature*, **1950**, *165*, 514.
  29. Clarke, T. C.; Krounbi, M. T.; Lee, V. Y.; Street, G. B. *J. Chem. Soc., Chem. Commun.*, **1981**, *8*, 384.
  30. Angelopoulos, M.; Shaw, J. M.; Kaplan, R. D.; Perreault, S. *J. Vac. Sci. Technol. B*,

- 1989**, 7, 1519.
31. Pitchumani, S.; Willig, F. *J. Chem. Soc., Chem. Commun.*, **1983**, 13, 809.
  32. Joo, J.; Epstein, A. *J. Appl. Phys. Lett.*, **1994**, 65, 2278.
  33. Colaneri, N. F.; Shacklette, L. W. *IEEE Trans. Instrum. Meas.*, **1992**, IM-41, 291.
  34. Taka, T. *Synth. Met.*, **1991**, 41, 1777.
  35. Gustafsson, G.; Cao, Y.; Treacy, G. M.; Klavetter, F.; Colaneri, N.; Heeger, A. J. *Nature*, **1992**, 357, 1789.
  36. Yu, G.; Heeger, A. J. *J. Appl. Phys.*, **1995**, 78, 4510.
  37. Hals, J. J. M.; Walsh, C. A.; Marseglia, E. A.; Friend, R. H.; Moratti, S. C.; Holmes, A. B. *Nature*, **1995**, 396, 498.
  38. Yu, G.; Cao, Y.; Hummelen, J. C.; Wudl, F.; Heeger, A. J. *Science*, **1995**, 270, 1789.
  39. Hide, F.; Diaz-Garcia, M. A.; Schwartz, B. J.; Heeger, A. J. *Acc. Chem. Res.*, **1997**, 30, 430.
  40. Pei, Q.; Yu, G.; Zhang, C.; Yang, Y.; Heeger, A. J. *Science*, **1995**, 269, 1086.
  41. Pei, Q.; Yang, Y.; Yu, G.; Zhang, C.; Heeger, A. J. *J. Am. Chem. Soc.*, **1996**, 118, 3922.
  42. Yu, G.; Wang, J.; McElvain, J.; Heeger, A. J. *Adv. Mater.*, **1998**, 10, 1431.
  43. Yang, Y.; Heeger, A. J. *Nature*, **1994**, 372, 344.
  44. Yu, G.; Pakbaz, K.; Heeger, A. J. *J. Electron. Mater.*, **1994**, 23, 925.
  45. Halvorson, C.; Hays, A.; Kraabel, B.; Wu, R.; Wudl, F.; Heeger, A. J. *Science*, **1992**, 265, 1215.

46. Halger, T. W.; Heeger, A. J. *Phys. Rev. B*, **1994**, *49*, 7313.
47. Reynolds, J. R.; Kumar, A.; Reddinger, J. L.; Sankaran, B.; Sapp, S. A.; Sotzing, G. A. *Synth. Met.*, **1997**, *85*, 1295.
48. Burroghes, J. H.; Jones, C. A.; Friend, R. H. *Nature*, **1998**, *335*, 137.
49. Garnier, F.; Hajlaoui, R.; Yasser, A.; Srivastava, P. *Science*, **1994**, *265*, 1684.
50. Brown, A. R.; Pomp, A.; Hart, C. M.; de Leeuw, D. M. *Science*, **1995**, *270*, 972.
51. Torsi, L.; Dodabalapur, A.; Rothberg, L. J.; Fung, A. W. P.; Katz, H. E. *Science*, **1996**, *272*, 1462.
52. Sirringhaus, H.; Tessler, N.; Friend, R. H. *Science*, **1998**, *280*, 1741.
53. Horowitz, G. *Adv. Mater.*, **1998**, *10*, 365.
54. Drury, C. J.; Mutsaers, C. M. J.; Hart, C. M.; Matters, M.; de Leeuw, D. M. *Appl. Phys. Lett.*, **1998**, *73*, 108.
55. Yang, J.-S.; Swager, T. M. *J. Am. Chem. Soc.* **1998**, *120*, 5321.
56. Yang, J.-S.; Swager, T. M. *J. Am. Chem. Soc.* **1998**, *120*, 11864.
57. Moutet, J.-C.; Saint-Aman, E.; Tran-Van, F.; Angibeaud, P.; Uthle, J.-P. *Adv. Mater.* **1992**, *4*, 511.
58. Roncali, J.; Garreau, R.; Delabouglise, D.; Garnier, F.; Lemaire, M. *J. Chem. Soc., Chem. Commun.* **1989**, 679.
59. Shi, L. H.; Garnier, F.; Roncali, J. *Synth. Met.* **1991**, *41-43*, 547.
60. Bartlett, P. N.; Benniston, A. C.; Chung, L.-Y.; Dawson, D. H.; Moore, P. *Electrochim. Acta* **1991**, *36*, 1377.
61. Yousoufi, H. K.; Hmyene, M.; Garnier, F.; Delabouglise, D. *J. Chem. Soc., Chem.*



- Commun.* **1993**, 1550.
62. Garnier, F.; Korri, H.; Hmyene, M.; Yassar, A. *Polym. Prepr.* **1994**, 35 (1), 205.
  63. Youssoufi, H. K.; Yassar, A.; Baý'teche, S.; Hmyene, M.; Garnier, F. *Synth. Met.* **1994**, 67, 251.
  64. Marsella, M. J.; Swager, T. M. *J. Am. Chem. Soc.* **1993**, 115, 12214.
  65. Swager, T. M.; Marsella, M. J. *Adv. Mater.* **1994**, 6, 595.
  66. Swager, T. M.; Marsella, M. J.; Bicknell, L. K.; Zhou, Q. *Polym. Prepr.* **1994**, 35 (1), 206.
  67. Marsella, M. J.; Swager, T. M. *Polym. Prepr.* **1994**, 35 (1), 271.
  68. Marsella, M. J.; Newland, R. J.; Swager, T. M. *Polym. Prepr.* **1995**, 36 (1), 594.
  69. Bäuerle, P.; Scheib, S. *Acta Polym.* **1995**, 46, 124.
  70. Scheib, S.; Bäuerle, P. *J. Mater. Chem.* **1999**, 9, 2139.
  71. Inoue, M.; Sotelo, M.; Machi, L.; Inoue, M. B.; Nebesny, K. W.; Fernando, Q. *Synth. Met.* **1989**, 32, 91.
  72. Wang, B.; Wasielewski, M. R. *J. Am. Chem. Soc.* **1997**, 119, 12.
  73. Zhang, Q. T.; Tour, J. M. *J. Am. Chem. Soc.* **1997**, 119, 9624.
  74. Fu, D.-K.; Xu, B.; Swager, T. M. *Tetrahedron* **1997**, 53, 15487.
  75. Kimura, M.; Horai, T.; Hanabusa, K.; Shirai, H. *Adv. Mater.* **1998**, 10, 459-.
  76. Zotti, G.; Zecchin, S.; Schiavon, G.; Berlin, A.; Penso, M. *Chem. Mater.* **1999**, 11, 3342.
  77. Zhou, Q.; Swager, T. M. *J. Am. Chem. Soc.* **1995**, 117, 7017.
  78. Zhou, Q.; Swager, T. M. *J. Am. Chem. Soc.* **1995**, 117, 12593.

79. Cimrova, V.; Schmidt, W.; Rulkens, R.; Schulze, M.; Meyer, W.; Neher, D. *Adv. Mater.* **1996**, *8*, 585.
80. Baur, J. W.; Kim, S.; Balanda, P. B.; Reynolds, J. R.; Rubner, M. F. *Adv. Mater.* **1998**, *10*, 1452.
81. Ho, P. K. H.; Granstrom, M.; Friend, R. H.; Greenham, N. C. *Adv. Mater.* **1998**, *10*, 769.
82. McQuade, D. T.; Pullen, A. E.; Swager, T. M. *Chem. Rev.* **2000**, *100*, 2537.
83. Chen, L.; Yu, S.; Kagami, Y.; Gong, J.; Osada, Y. *Macromolecules* **1998**, *31*, 787.
84. Decher, G. *Science* **1997**, *277*, 1232.
85. McCullough, R. D.; Ewbank, P. C.; Loewe, R. S. *J. Am. Chem. Soc.* **1997**, *119*, 633.
86. (a) Thünemann, A. F. *Adv. Mater.* **1999**, *11*, 127. (b) Thünemann, A. F.; Ruppelt, D. *Langmuir* **2001**, *17*, 5098.
87. (a) Ferreira, M.; Rubner, M. F. *Macromolecules* **1995**, *28*, 7107. (b) Fou, A. C.; Rubner, M. F. *Macromolecules* **1995**, *28*, 7115. (c) Fou, A. C.; Onitsuka, O.; Ferreira, M.; Rubner, M. F. *J. Appl. Phys.* **1996**, *79*, 7501.
88. Bharathan, J.; Yang, Y. *Appl. Phys. Lett.* **1998**, *72*, 2660.
89. Bao, Z.; Feng, Y.; Dodabalapur, A.; Raju, V. R.; Lovinger, A. J. *Chem. Mater.* **1997**, *9*, 1299.
90. Chang, S. C.; Bharathan, J.; Yang, Y. *Appl. Phys. Lett.* **1998**, *73*, 2561.
91. Baur, J. W.; Rubner, M. F.; Reynolds, J. R.; Kim, S. *Langmuir* **1999**, *15*, 6460.
92. Landfester, K.; Montenegro, R.; Scherf, U.; Güntner, R.; Asawapirom, U.; Patil, S.;

- Neher, D.; Kietzke, T. *Adv. Mater.* **2002**, *14*, 651.
93. Chen, L.; McBranch, D. W.; Wang, H.-L.; Helgeson, R.; Wudl, F.; Whitten, D. G. *Proc. Natl. Acad. Sci. U. S. A.* **1999**, *96*, 12287.
94. Wang, D.; Gong, X.; Heeger, P. S.; Rininsland, F.; Bazan, G. C.; Heeger, A. J. *Proc. Natl. Acad. Sci. U. S. A.* **2002**, *99*, 49.
95. Gaylord, B. S.; Heeger, A. J.; Bazan, G. C. *Proc. Natl. Acad. Sci. U. S. A.* **2002**, *99*, 10954. b) Liu, B.; Bazan, G. C. *Chem. Mater.* **2004** *16*, 4467. c) Liu, B.; Gaylord, B. S.; Wang, S.; Bazan, G. C. *J. Am. Chem. Soc.* **2003**, *125*, 6705. d) Wang, S.; Liu, B.; Gaylord, B. S.; Bazan, G. C. *Adv. Funct. Mater.* **2003**, *13*, 463. e) Liu, B.; Bazan, G. C. *J. Am. Chem. Soc.* **2004**, *126*, 1942. f) Gaylord, B. S.; Heeger A. J.; Bazan G. C. *J. Am. Chem. Soc.* **2003**, *125*, 896. g) Wang, S.; Gaylord, B. S.; Bazan, G. C. *J. Am. Chem. Soc.* **2004**, *126*, 5446. h) Liu, B.; Baudrey, S.; Jaeger, L.; Bazan, G. C. *J. Am. Chem. Soc.* **2004**, *126*, 4076.
96. Disney, M. D.; Zheng, J.; Swager, T. M.; Seeberger, P. H. *J. Am. Chem. Soc.* **2004**, *126*, 13343.
97. Gaylord, B. S.; Wang, S.; Heeger, A. J.; Bazan, G. C. *J. Am. Chem. Soc.* **2001**, *123*, 6417.
98. Wang, D. L.; Wang, J.; Moses, D.; Bazan; G. C.; Heeger, A. J. *Langmuir* **2001**, *17*, 1262.
99. Wang, J.; Wang, D. L.; Miller, E. K.; Moses, D.; Bazan; G. C.; Heeger, A. J. *Macromolecules* **2000**, *33*, 5153.
100. Jones, R. M.; Bergstedt, T. S.; McBranch, D. W.; Whitten, D. G. *J. Am. Chem. Soc.*

- 2001**, 123, 6726.
101. Chen, L.; McBranch, D.; Wang, R.; Whitten, D. G. *Chem. Phys. Lett.* **2000**, 330, 27.
102. Chen, L.; Xu, S.; McBranch, D.; Whitten, D. G. *J. Am. Chem. Soc.* **2000**, 122, 9302.
103. Stork, M.; Gaylord, B. S.; Heeger, A. J.; Bazan, G. C. *Adv. Mater.* **2002**, 14, 361.
104. Tan, C.; Mauricio, R. P.; Schanze, K. S. *Chem. Commun.* **2002**, 446.
105. Patil, S.; Ikenoue, Y.; Wudl, F.; Heeger, A. J. *J. Am. Chem. Soc.* **1987**, 109, 1858.
106. Kuroda, K.; Swager, T. M. *Chem. Commun.* **2003**, 26.
107. (a) Shi, S.; Wudl, F. *Macromolecules* **1990**, 23, 2119. b) Fan, Q. L.; Lu, S.; Lai, Y. H.; Hou, X. Y.; Huang, W. *Macromolecules* **2003**, 36, 6976.
108. (a) Liu, B.; Yu, W. L.; Lai, Y. H.; Huang, W. *Chem. Commun.* **2000**, 551. b) Huang, F.; Wu, H. B.; Wang, D.; Yang, W.; Cao, Y. *Chem. Mater.* **2004**, 16, 708.
109. Lu, S.; Fan, Q. L.; Liu, S. Y.; Chua, S. J.; Huang, W. *Macromolecules* **2002**, 35, 98751.
110. Lu, S.; Fan, Q. L.; Chua, S. J.; Huang, W. *Macromolecules* **2003**, 36, 304.
111. Fyfe, M. C.; Stoddart, J. F. *Acc. Chem. Res.* **1997**, 30, 393.
112. Ciferri, A. *Macromol. Rapid Commun.* **2002**, 23, 511.
113. Jiang, M.; Li, M.; Xiang, M. L.; Zhou, H. *Adv. Polym. Sci.* **1999**, 146, 121.
114. Soo, P. L.; Eisenberg, A. *J. Polym. Sci., Part B: Polym. Phys.* **2004**, 42, 923.
115. Jain, S.; Bates, F. S. *Science* **2003**, 300, 460.
116. Jenekhe, S. A.; Chen, X. L. *Science* **1998**, 279, 1903.

117. Liu, S. Y.; Zhang, G. Z.; Jiang, M. *Polymer* **1999**, *40*, 5449.
118. Liu, S. Y.; Pan, Q. M.; Xie, J. W.; Jiang, M. *Polymer* **2000**, *41*, 6919.
119. Liu, S. Y.; Jiang, M.; Liang, H. J.; Wu, C. *Polymer* **2000**, *41*, 8697.
120. Wang, M.; Zhang, G. Z.; Chen, D. Y.; Jiang, M.; Liu, S. Y. *Macromolecules* **2001**, *34*, 7172.
121. Orfanou, K.; Topouza, D.; Sakellariou, G.; Pispas, S. *J. Polym. Sci., Part A: Polym. Chem.* **2003**, *41*, 2454.
122. Jiang, M.; Duan, H. W.; Chen, D. Y. *Macromol. Symp.* **2003**, *195*, 165.
123. Zhao, H. Y.; Gong, J.; Jiang, M.; An, Y. L. *Polymer* **1999**, *40*, 4521.
124. Yuan, X. F.; Zhao, H. Y.; Jiang, M.; An, Y. L. *Acta Chim. Sin.* **2000**, *58*, 118.
125. Yuan, X. F.; Jiang, M.; Zhao, H. Y.; Wang, M.; Zhao, Y.; Wu, C. *Langmuir* **2001**, *17*, 6122.
126. Wang, M.; Jiang, M.; Ning, F. L.; Chen, D. Y.; Liu, S. Y.; Duan, H. W. *Macromolecules* **2002**, *35*, 5980.
127. Zhang, Y. W.; Jiang, M.; Zhao, J. X.; Zhou, J.; Chen, D. Y. *Macromolecules* **2004**, *37*, 1537.
128. Zhang, Y. W.; Jiang, M.; Zhao, J. X.; Wang, Z. X.; Dou, H. J.; Chen, D. Y. *Langmuir* **2004**, *21*, 1531.

## CHAPTER TWO

### **Water-Soluble Light-Emitting Nanoparticles Prepared by Non-Covalent Bond Self-Assembly of Functionalized Poly(p-phenyleneethynylene)s and Poly(acrylic acid)**

#### **2.1 Introduction**

In recent years intense efforts have been devoted to the study of conjugated polymers for applications as fluorescent chemo- or biosensors.<sup>1</sup> Water-soluble conjugated polymers have particularly attracted increasing attention as sensory materials to detect chemical or bioactive species, such as protein, DNA and RNA.<sup>2</sup>

To be a good candidate for use as biosensors, water-solubility is important since most of the biomolecules are water-soluble. The first water-soluble conjugated polymer reported was 3-substituted polythiophene<sup>3</sup> and subsequently a series of conjugated polyelectrolytes were developed, such as poly(phenyleneethylene) (PPE),<sup>4</sup> poly(phenylenevinylene) (PPV)<sup>5</sup> and polyfluorene (PF).<sup>6</sup> Their water-solubility was mostly obtained through introducing ionic functions to their side chains. Another way to achieve water-solubility is through the use of block copolymer, e.g. combining neutral conjugated polymer segment with the water-soluble polymer segment. The preparation of water-soluble conjugated-acidic and conjugated-ionic block copolymers via atom transfer radical polymerization (ATRP) with a polyfluorene-based macroinitiator was reported by Huang's group.<sup>7,8</sup> In recent years, non-covalent bond self-assembly was developed as a facile way to produce

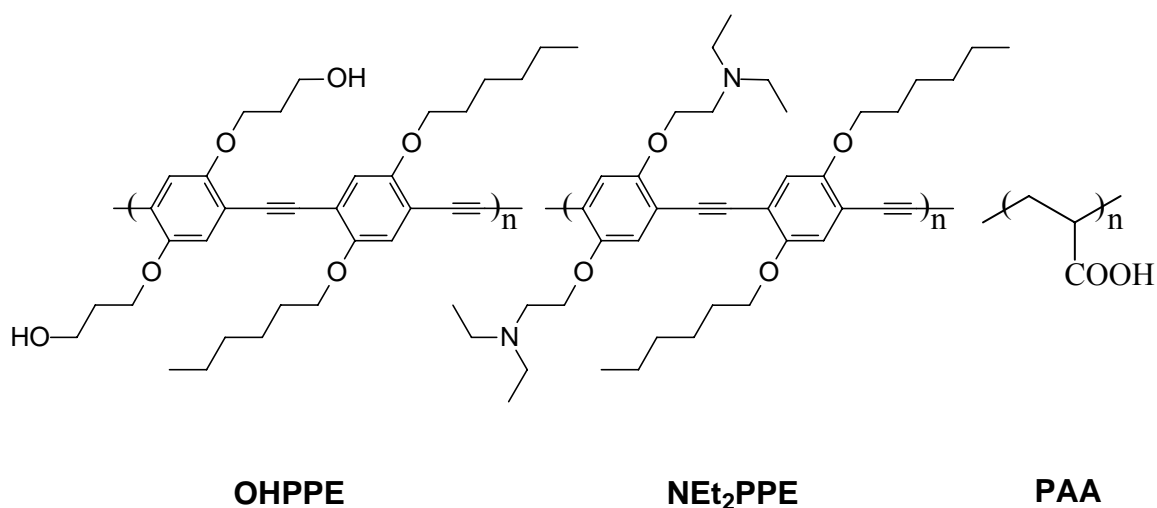
water-soluble micelles and other nanostructures.<sup>9,10</sup> For example, Yoshida et. al. reported the micelle formation of nonamphiphilic diblock copolymer via noncovalent bond cross-linking in 1, 4-dioxane.<sup>10a</sup> Jiang et. al. demonstrated a series of spherical micelles obtained from polyimide (PI) with carboxyl ends, a rigid polymer, and poly(4-vinylpyridine) (PVPy) in a common solvent.<sup>9a</sup> Thus, it is anticipated that the water-solubility of conjugated polymers can also be simply obtained from non-water-soluble conjugated polymers assisted with water-soluble polymers.<sup>10</sup> Recently Huang's group reported the preparation of water-soluble light-emitting materials through hydrogen bond self-assembly of polyfluorene and poly(acrylic acid) (PAA). This phenomenon was attributed to two main factors: the rigid character of PF and the hydrogen bonding between PF and PAA.<sup>11</sup> However, investigation of the influence of non-covalent self-assembly on the conformational change and the related optical behaviors of conjugated polymers in an aqueous environment is more significant and exigent to develop these materials as good biosensors in general.

In this work, hydroxyl-functionalized PPE (OHPPE) and amino-functionalized PPE (NEt<sub>2</sub>PPE) were successfully synthesized. Their nanoparticles (micelles) in aqueous solution were successfully prepared through hydrogen bond assisted self-assembly with poly(acrylic acid). PPE is a conjugated polymer which has been widely used to study optical property-structure relationship because of its good optical response to environmental variations through facial changeable torsion angle and interchain aggregation. Its application as chemosensor has been widely reported by Swager's group.<sup>12-16</sup> Most recently the anionic water-soluble PPEs were utilized to study the

contribution of polymer aggregation on sensitivity of biomolecular detection.<sup>17,18</sup>

Thus, it is reasonable to conceive that PPEs are good candidates for studying the variation of optical properties of nanoparticles by non-covalent self-assembly in aqueous solution. Their water-solubility, optical properties and morphologies were investigated in this work.

## 2.2 Molecular Design



**Scheme 2.1 Functionalized PPEs and the water-soluble polymer for preparing water-soluble nanoparticles**

In order to synthesize functionalized PPEs for non-covalent bond self-assembly systems, hydroxyl and amino groups containing lone electron pair was incorporated into the PPEs which upon forming hydrogen bond with active hydrogen atoms, could afford self-assembly. In addition to the substitutes containing hydroxyl and tertiary amine group, long chains, hexyloxy groups were further substituted into the rest of benzene rings to enhance the solubility of PPEs in common organic solvents. To obtain water-soluble composites by non-covalent bond self-assembly, water-soluble



poly(acrylic acid) (PAA) was used to provide active hydrogen atoms to form hydrogen bond with hydroxyl or amino group on the PPE sidechains. The chemical structures of the desired neutral polymers are illustrated in Scheme 2.1.

## **2.3 Experimental**

### **2.3.1 Materials**

All chemical reagents were purchased from Aldrich Chemical Co. THF was purified by distillation from sodium in the presence of benzophenone. Anisole was distilled from calcium hydride and stored under argon in darkness at 0 °C.

### **2.3.2 Characterization Methods**

The NMR spectra were collected on a Varian Mercury Plus 400 spectrometer with tetramethylsilane as the internal standard. Elemental microanalyses were carried out on a Vario EL III CHNOS Elementar Analyzer. Mass spectra (MS) were obtained by using a micromass VG 7035E mass spectrometer at an ionizing voltage of 70 eV. Thermogravimetric analysis (TGA) was performed on a Shimadzu thermogravimetry and differential thermal analysis DTG-60H at a heating rate of 10 °C/min under N<sub>2</sub>. Differential scanning calorimetry (DSC) measurements were performed under a nitrogen atmosphere at both heating and cooling rates of 10 °C/min, using NETZSCH DSC 200PC apparatus. Gel permeation chromatography (GPC) analysis was conducted with a HP1100 HPLC system equipped with 7911GP-502 and GP NXC

columns using polystyrenes as the standard and tetrahydrofuran (THF) as the eluent at a flow rate of 1.0 mL/min at 35 °C. Ultraviolet-visible (UV-vis) spectra were recorded on a Shimadzu 3150 PC spectrophotometer. Photoluminescence (PL) emission and excitation spectra were carried out on a Shimadzu RF-5301 PC spectrofluorophotometer with a xenon lamp as a light source. The polymer thin films used for these measurements were prepared by spin coating from tetrahydrofuran solution (10 mg/mL) on a quartz plate.

### 2.3.3 Synthesis

#### 1,4-Diiodo-2,5-dimethoxybenzene (1)

13.8 g (0.1 mol) of 1,4-dimethoxybenzene, 8.56 g (0.04 mol) of KIO<sub>3</sub> and 27.94 g (0.11 mol) of I<sub>2</sub> were added into a solution of acetic acid (500 mL), 98% H<sub>2</sub>SO<sub>4</sub> (5 mL), and H<sub>2</sub>O (50 mL). The reaction mixture was stirred at reflux for 24 h and then cooled to room temperature. Aqueous Na<sub>2</sub>SO<sub>4</sub> (20%) was added until the brown color of iodine had disappeared, and the acetic acid was evaporated under reduced pressure. The residue was poured into 200 mL water and the mixture was extracted with ethyl acetate three times, and the obtained organic layer was washed with water two times, and brine once. The combined organic layers were dried over MgSO<sub>4</sub>. After the solvent was evaporated, the crude solid was recrystallized with hexane/chloroform to afford pure product as colorless crystals (29 g, yield 75%). Mp: 172-3 °C. <sup>1</sup>H NMR (CDCl<sub>3</sub>, ppm): δ 7.23 (s, 2H), 3.86 (s, 6H).

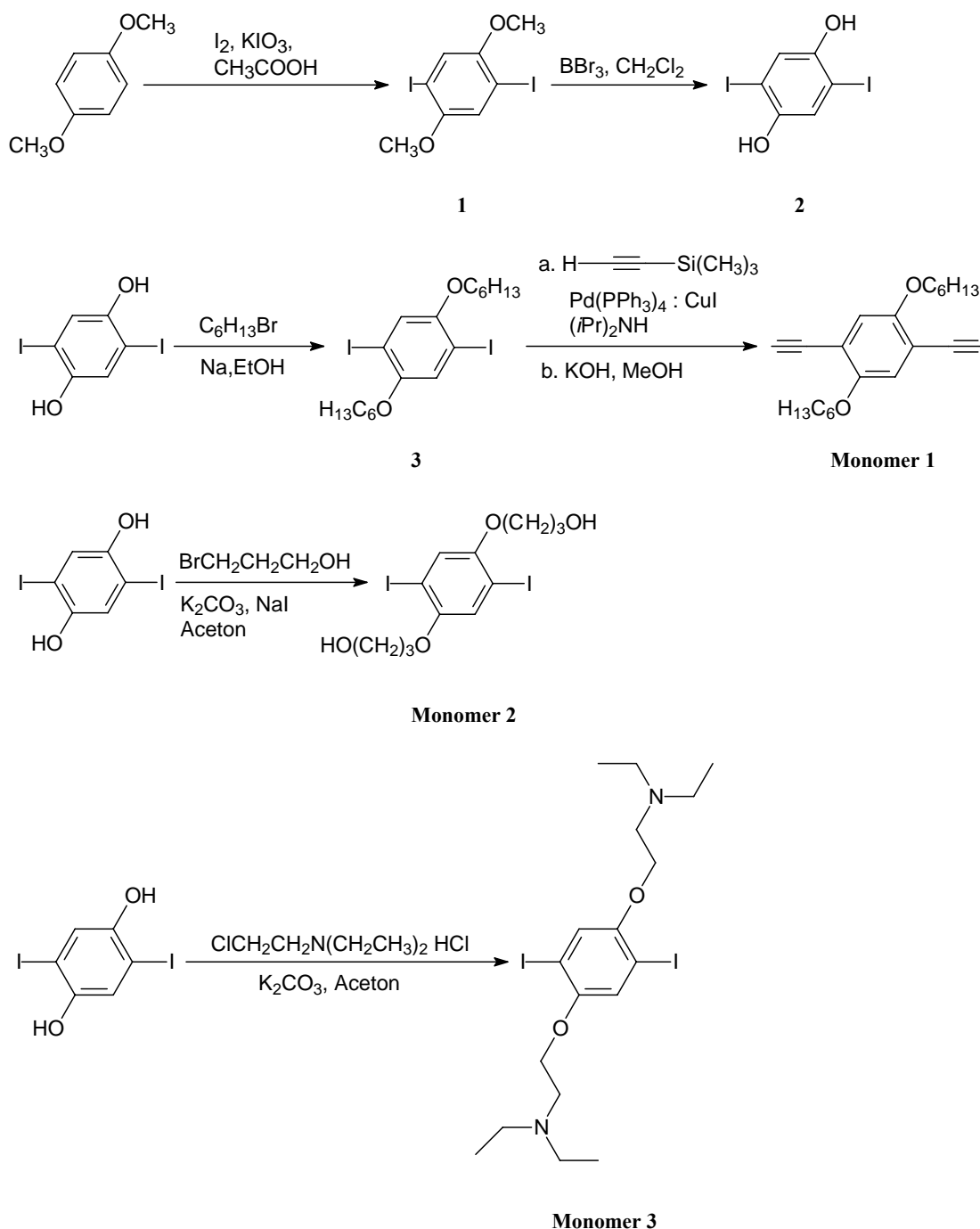
### **1,4-Diiodo-2,5-hydroquinone (2)**

19.5 g (0.05 mol) of 2,5-diiodo-1,4-dimethoxybenzene was dissolved in 250 mL CH<sub>2</sub>Cl<sub>2</sub> in a 500 mL round-bottom flask fitted with a condenser. The reaction mixture was cooled to -80 °C in a dry ice-acetone bath. 26.3 g (0.105 mol) of BBr<sub>3</sub> dissolved in 105 mL CH<sub>2</sub>Cl<sub>2</sub> was added dropwise through the condenser. After the addition, a drying tube was attached on the top of the condenser, and the mixture was allowed to warm to room temperature. The mixture was stirred at room temperature for 12 h and then carefully hydrolyzed with 200 mL of H<sub>2</sub>O. The aqueous layer was separated and extracted with ether three times. The combined organic phases were extracted with NaOH (200 mL, 2 N), the NaOH solution was then neutralized with dilute HCl (1 N) in ice bath. The precipitate was collected and dried, and recrystallized from acetic acid to afford brown crystals (14.5 g, yield 80%). Mp: 198-200 °C. <sup>1</sup>H NMR (DMSO-*d*<sub>6</sub>, ppm): δ 9.82 (s, 2H), 7.15 (s, 2H).

### **1,4-Diiodo-2,5-bis(hexyloxy)benzene (3)**

Sodium ethoxide was prepared by adding 1.52 g (66 mmol) of sodium into 50 mL of anhydrous ethanol. After all the sodium disappeared, 10.86 g (30 mmol) of 1,4-diiodo-2,5-hydroquinone in 10 mL of anhydrous ethanol was added dropwise. To the stirred mixture, 10.89 g (66 mmol) of 1-bromohexane in 10 mL of anhydrous ethanol was added. After stirring for 24 h with refluxing, the ethanol was evaporated at reduced pressure. The brownish residue was added into 300 mL of water, extracted with ethyl acetate, and dried with anhydrous magnesium sulfate. The white product (12.1 g, yield 76%) was obtained by recrystallization in ethanol after most of the

solvent was removed under reduced pressure. Mp: 80-1 °C.  $^1\text{H NMR}$  ( $\text{CDCl}_3$ , ppm):  $\delta$  7.08 (s, 2H), 3.99 (t, 4H,  $J = 4.8$  Hz), 1.82 (m, 4H), 1.52 (m, 4H), 1.37 (m, 8H), 0.94 (t, 6H,  $J = 8.0$  Hz).



**Scheme 2.2** Synthetic routes for functionalized monomers

### 1,4-Bis(ethynyl)-2,5-bis(hexyloxy)benzene (Monomer 1)

To a solution of 1,4-dihexyloxy-2,5-diiodobenzene (3.96 g, 0.0075 mol), CuI (0.07 g, 0.375 mmol), and Pd(PPh<sub>3</sub>)<sub>2</sub>Cl<sub>2</sub> (0.265 g, 0.375 mmol) in 50 mL of diisopropylamine ((iPr)<sub>2</sub>NH) was added (trimethylsilyl)acetylene (1.5 g, 0.015 mol). The mixture was stirred at 70 °C for 2 hours. After cooling, dichloromethane was added, and the white ammonium iodide precipitate was filtered off. The solution was passed through a short silica gel column using hexane as eluent. After the solvent was evaporated under reduced pressure, the white crystals 1,4-bis[(trimethylsilyl)ethynyl]-2,5-bis(hexyloxy)benzene (2.82 g, 85%) were obtained. It was redissolved in THF (20 mL). The mixture of methanol (30 mL) and NaOH (2 mL, 5 N) was added to the stirred THF solution. After 2 hours, the solvent was evaporated, and the residue was poured into 100 mL of water and extracted with hexane twice. The combined hexane layer was washed with distilled water twice, brine once and dried over anhydrous sodium sulfate. The white crystal **1** (1.82 g, 93%) was obtained after recrystallization from ethanol. MS: *m/z* 326.2. <sup>1</sup>H NMR (CDCl<sub>3</sub>), δ (ppm): 6.95 (s, 2H), 3.97 (t, 4H), 3.33 (s, 2H), 1.84-1.75 (m, 4H), 1.50-1.26 (m, 12H), 0.90 (t, 6H). <sup>13</sup>C NMR (CDCl<sub>3</sub>), δ (ppm): 154.43, 118.26, 113.75, 82.75, 80.19, 70.13, 31.90, 29.50, 25.97, 22.96, 14.37. Anal. Calcd for C<sub>22</sub>H<sub>30</sub>O<sub>2</sub>: C, 80.94; H, 9.26. Found: C, 80.88; H, 9.23.

### **2,5-Bis((3-propanol)oxy)-1,4-diiodobenzene (Monomer 2)**

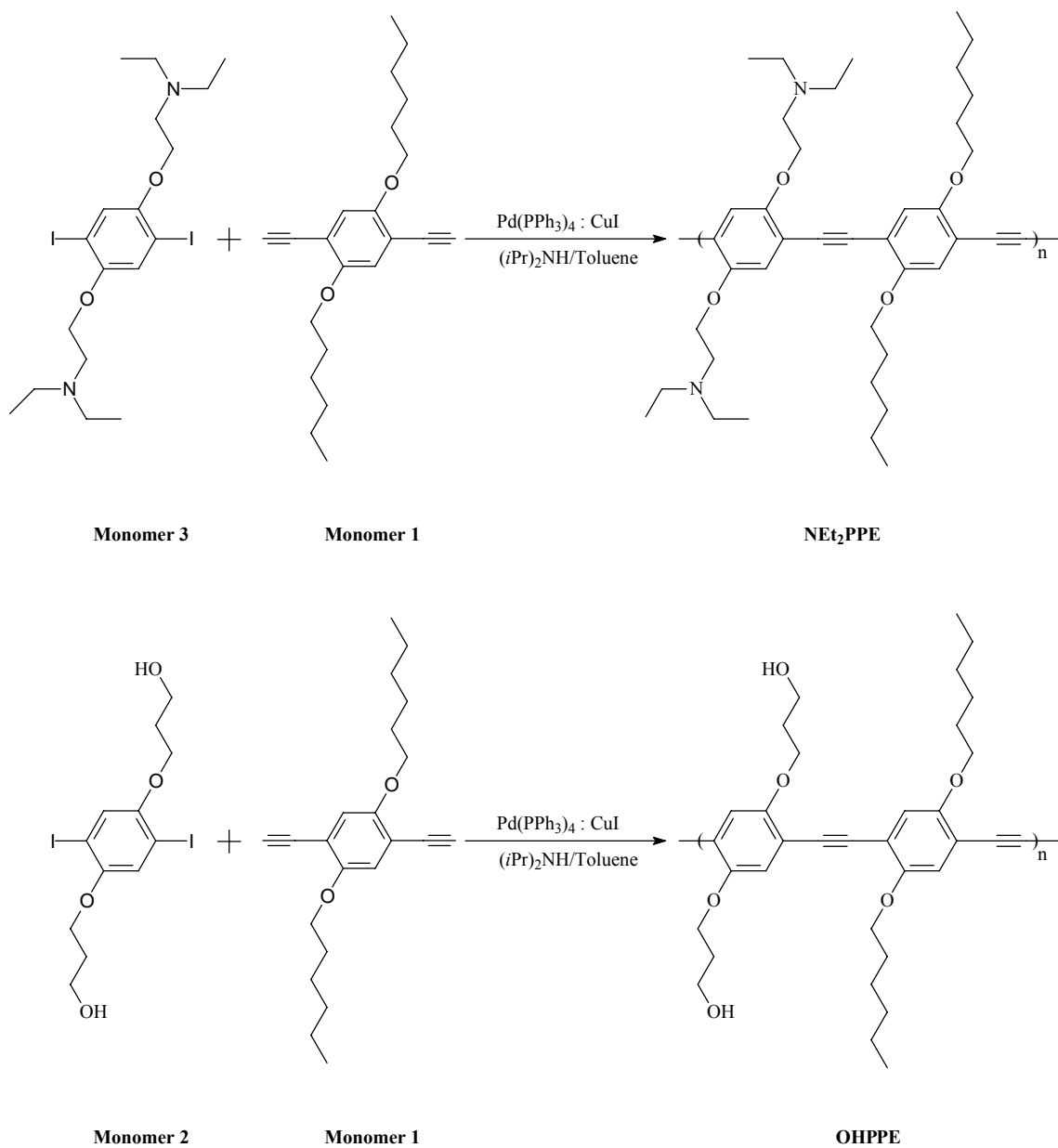
In a round-bottom flask containing acetone (40.0 mL) were combined 2,5-diiodo-1,4-hydroquinone (2.06 g, 5.70 mmol), 3-bromopropanol (1.74 g, 12.5 mmol), K<sub>2</sub>CO<sub>3</sub> (6.32 g, 45.8 mmol), and NaI (0.20 g, 1.29 mmol). The mixture was

heated at 70 °C for 24 hours under nitrogen atmosphere. The reaction mixture was filtered and the salts washed with dichloromethane. The filtrate was washed several times with NaOH solution (0.1 N), followed by distilled water twice, brine once and dried over anhydrous sodium sulfate. The solvent was removed under reduced pressure and the residue was recrystallized from the mixture of dichloromethane/hexane (1:3) to give pure product (1.90g, 70.0%) as white crystal. MS:  $m/z$  477.9.  $^1\text{H}$  NMR ( $\text{CDCl}_3$ ),  $\delta$  (ppm): 7.21 (s, 2 H), 4.11 (t, 4 H), 3.92 (t, 4 H), 2.08 (m, 4 H).  $^{13}\text{C}$  NMR ( $\text{CDCl}_3$ ),  $\delta$  (ppm): 152.93, 122.79, 86.37, 68.61, 60.86, 32.05. Anal. Calcd for  $\text{C}_{12}\text{H}_{16}\text{I}_2\text{O}_4$ : C, 30.15; H, 3.37; I, 53.09. Found: C, 30.10; H, 3.35.

### **2,5-Bis[3-(*N,N*-diethylamino)-1-oxapropyl]-1,4-diiodobenzene (Monomer 3)**

A 250 mL round-bottom flask with magnetic stirring bar was charged with anhydrous potassium carbonate (24.84 g, 0.18 mol), 1,4-diiodo-2,5-hydroquinone (10.86 g, 0.03 mol), and 150 mL of acetone. The stirred mixture was charged with nitrogen for 15 min and then refluxed for about 30 min. 2-chlorotriethylamine hydrochloride (12.38 g, 0.072 mol) was then added into the round-bottom flask and the mixture was refluxed for 3 days. The precipitate mixture was filtered and the filtrate was rotary evaporated. The residue was poured into water and extracted with ether, and the combined organics were washed with 10% aqueous sodium hydroxide twice, water twice, and brine once. The solution was dried over magnesium sulfate, filtered and the solvent was stripped by rotary evaporation to yield a crude solid. The crude product was recrystallized with hexane to afford colorless crystals (12 g, yield 71%). Mp: 76-8 °C. MS:  $m/z$  559.9.  $^1\text{H}$  NMR ( $\text{CDCl}_3$ , ppm):  $\delta$  7.23 (s, 2 H), 4.02 (t, 4 H,  $J = 6.4$  Hz), 2.93

(t, 4 H,  $J = 6.4$  Hz), 2.67 (q, 8 H,  $J = 6.4$  Hz), 1.10 (t, 12 H,  $J = 6.8$  Hz).  $^{13}\text{C}$  NMR (CDCl<sub>3</sub>, ppm)  $\delta$  153.4, 123.4, 86.5, 69.8, 52.0, 48.4, 12.6. Anal. Calcd for C<sub>18</sub>H<sub>30</sub>I<sub>2</sub>N<sub>2</sub>O<sub>2</sub>: C, 38.59; H, 5.40; N, 5.00; I, 45.30. Found: C, 38.99; H, 5.32; N, 4.84.



**Scheme 2.3 Synthetic routes for functionalized PPEs**

### OHPPE

A two-necked flask was charged with **Monomer 2** (348 mg, 0.73 mmol), **Monomer 1** (244 mg, 0.75 mmol), Pd(PPh<sub>3</sub>)<sub>4</sub> (23 mg, 0.02 mmol), and CuI (11 mg, 0.06 mmol). It

was degassed with three vacuum-nitrogen cycles and then diisopropylamine ((iPr)<sub>2</sub>NH) (9 mL) and THF (18 mL) were added at 0 °C. The mixture was vigorously stirred at 65 °C under nitrogen for 1.5 h. To the mixture was added bromobenzene (3.0 mg, 0.02 mmol) and 1-ethynylbenzene (3.0 mg, 0.02 mmol) sequentially, and was stirred for another 12 h. After the mixture was cooled to room temperature, it was subjected to a CHCl<sub>3</sub>/H<sub>2</sub>O workup. The combined organic phase was washed with water NH<sub>4</sub>OH (50%) twice, distilled water twice, and brine once and dried over anhydrous sodium sulfate. The solvent was removed in vacuum, and the residue was dissolved in CHCl<sub>3</sub> and precipitated in hexane twice to afford product as yellow solid. <sup>1</sup>H NMR (CDCl<sub>3</sub>), δ (ppm): 7.13 (s, 2 H), 7.05 (s, 2 H), 4.23 (t, 4 H), 4.06 (t, 4 H), 3.93 (t, 4 H), 2.54 (s, 2 H), 2.11 (m, 4 H), 1.85 (m, 4 H), 1.55-1.34 (12 H), 0.90 (m, 6 H). <sup>13</sup>C NMR (CDCl<sub>3</sub>), δ (ppm): 153.74, 153.48, 131.86, 128.65, 117.32, 116.91, 114.50, 114.10, 92.60, 91.14, 69.80, 61.65, 32.08, 31.87, 29.43, 25.93, 22.90, 14.30. Anal. Calcd for (C<sub>34</sub>H<sub>44</sub>O<sub>6</sub>)<sub>n</sub>: C, 74.42; H, 8.08. Found: C, 73.91; H, 7.91.

### **NEt<sub>2</sub>PPE**

Under argon protection, diisopropylamine/toluene (3:7, 35 mL) was added to a 50 mL round-bottom flask containing a 0.249 g (0.765 mmol) sample of **Monomer 1**, 0.420 g (0.75 mmol) of 1,4-bis[3-(*N,N*-diethylamino)-1-oxapropyl]-2,5-diiodobenzene (**Monomer 3**), 51.9 mg (0.045 mmol) of Pd(PPh<sub>3</sub>)<sub>4</sub> and 42.8 mg (0.225 mmol) of CuI. The mixture was heated at 70 °C for 24 h and then subjected to a CHCl<sub>3</sub>/H<sub>2</sub>O workup. The combined organic phase was washed with water NH<sub>4</sub>OH (50%) twice, water twice, brine once and dried over MgSO<sub>4</sub>. The solvent was removed *in vacuo*, and the



residue was redissolved in 10 mL of  $\text{CHCl}_3$  and reprecipitated in methanol twice, The mixture was filtered to afford 0.42 g of a yellow solid (yield 89%).  $^1\text{H}$  NMR ( $\text{CDCl}_3$ , ppm):  $\delta$  7.06 (s, 2 H), 7.03 (s, 2 H), 4.14 (br, 4 H), 4.06 (br, 4 H), 2.99 (br, 4 H), 2.70 (q, 8 H), 1.88 (br, 4 H), 1.52 (br, 4 H), 1.43-1.22 (br, 8 H), 1.08 (t, 12 H), 0.90 (t, 6 H). FT-IR (KBr pellet,  $\text{cm}^{-1}$ ): 3454 (br), 3057, 2958, 2928, 2865, 2815, 2200, 1510, 1466, 1423, 1383, 1275, 1209, 1038, 950, 858, 803, 717, 509. Anal. Calcd for  $(\text{C}_{40}\text{H}_{58}\text{N}_2\text{O}_4)_n$ : C, 76.15; H, 9.27; N, 4.44. Found: C, 73.22; H, 8.54; N, 3.79.

## 2.4 Results and Discussion

### 2.4.1 Synthesis of Monomers and Polymers

The preparation of monomers was shown in Schemes 2.2. 2,5-dihexyloxy-1,4-diiodobenzene was prepared from 1,4-diiodohydroquinone by a reaction with 1-bromohexane in refluxing ethanol in the presence of sodium ethoxide, while 2,5-bis[3-(*N,N*-diethylamino)-1-oxapropyl]-1,4-diiodobenzene (**Monomer 1**) and 2,5-bis((3-propanol)oxy)-1,4-diiodobenzene (**Monomer 2**) were synthesized by a reaction with 2-(diethylamino) ethyl chloride hydrochloride and 3-bromopropanol in refluxing acetone in the presence of excess anhydrous potassium carbonate respectively. In view of the presence of ammonium groups and hydroxyl groups in the reactants which can form byproducts by reacting with strong base sodium ethoxide, the weak base anhydrous potassium carbonate was chosen to realize the substitution reaction instead of sodium ethoxide. Treating 2,5-dihexyloxy-1,4-diiodobenzene with trimethylsilyl acetylene afforded di(trimethylsilyl)ethynyl compounds which was

further converted to the key **Monomer 3** under base treatment.

Syntheses of the polymers were outlined in Scheme 2.3. The preparation of hydroxyl- and amino-functionalized polymers was accomplished via standard Sonagashira coupling reaction of corresponding diiodide **Monomers 1** and **Monomer 2** with diacetylene **Monomer 3** in the mixture of toluene and diisopropylamine solution in the presence of Pd(PPh<sub>3</sub>)<sub>4</sub>/CuI catalyst at 70 °C for one day.

#### 2.4.2 Solubility and Color Study

OHPPE and NEt<sub>2</sub>PPE were readily soluble in common organic solvents such as chloroform and THF but insoluble in water, methanol, DMSO and DMF, similar to the unfunctionalized PPEs.<sup>19</sup> Both OHPPE and NEt<sub>2</sub>PPE are orange-yellow fibrous solids. Gel permeation chromatography showed reasonably high molecular weight for the neutral polymers (see Table 2.1).

**Table 2.1 GPC and Spectroscopic Data for PPEs**

polymer	GPC			absorbance	emission
	$M_n$	$M_w$	PDI	THF	THF
OHPPE	12 300	25	2.10	443	472
NEt <sub>2</sub> PPE	14 300	32	2.29	444	474
O-OPPE <sup>a</sup>	16 400	—	—	449	474

$M_n$ ,  $M_w$  and PDI of the polymers were determined by gel permeation chromatography using polystyrene standards. <sup>a</sup>  $M_n$  was determined by <sup>1</sup>H NMR spectroscopy.<sup>19</sup>

#### 2.4.3 NMR Spectroscopy

<sup>1</sup>H (see Figure 2.1) and <sup>13</sup>C (see Figure 2.2) NMR spectra confirmed the structures of

NEt<sub>2</sub>PPE and OHPPE polymers. As shown in Figure 2.1, compared to the non splitting signal of the protons on the benzene rings at about 7.1 ppm of unfunctionalized PPEs,<sup>19</sup> the corresponding signals of the functionalized PPEs all split into two peaks with the same relative integrals, which arises from the functionalized and unfunctionalized components. Also, NEt<sub>2</sub>PPE exhibits four characteristic peaks for amino groups. The peaks at 4.14 ppm is the methylene groups linked to the oxygen atoms (-OCH<sub>2</sub>CH<sub>2</sub>N-). The peaks at 2.95 and 2.70 ppm correspond to the methylene groups adjacent to the nitrogen atoms (-OCH<sub>2</sub>CH<sub>2</sub>N- and CH<sub>3</sub>CH<sub>2</sub>N- respectively), and the peak at 1.08 ppm corresponds to the methyl groups (CH<sub>3</sub>CH<sub>2</sub>N-). OHPPE showed two characteristic peaks at 4.23 and 3.93 ppm attributing to the methylene groups adjacent to the oxygen atoms (HOCH<sub>2</sub>CH<sub>2</sub>CH<sub>2</sub>O- and HOCH<sub>2</sub>CH<sub>2</sub>CH<sub>2</sub>O- respectively) and one peak at 2.11 ppm attributing to another methylene group (-OCH<sub>2</sub>CH<sub>2</sub>CH<sub>2</sub>OH).

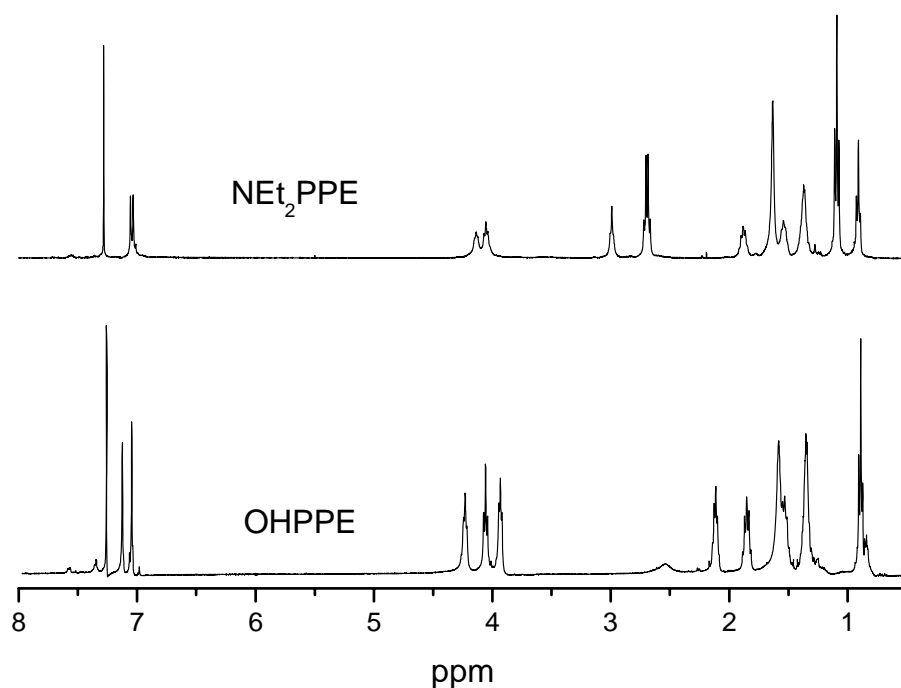


**Figure 2.1** <sup>1</sup>H NMR spectra of the functionalized PPEs

It was found that all the relative integrals of each peak correspond to the theoretically calculated values based on the functionalized PPEs. Thus, the NMR results showed that the functionalized groups have been successfully introduced into the benzene rings of PPEs. It also noted that the peak at 4.06 ppm of OHPPE and  $\text{NEt}_2\text{PPE}$  attributed to the methylene groups adjacent to the oxygen atoms in hexyloxy groups ( $\text{CH}_3\text{CH}_2\text{CH}_2\text{CH}_2\text{CH}_2\text{CH}_2\text{O}-$ ) and one peak at 0.90 ppm of OHPPE and  $\text{NEt}_2\text{PPE}$  attributed to methyl groups in hexyloxy groups ( $\text{CH}_3\text{CH}_2\text{CH}_2\text{CH}_2\text{CH}_2\text{CH}_2\text{O}-$ ). These data indicate that the hexyloxy groups have also been introduced into the benzene rings of PPEs.

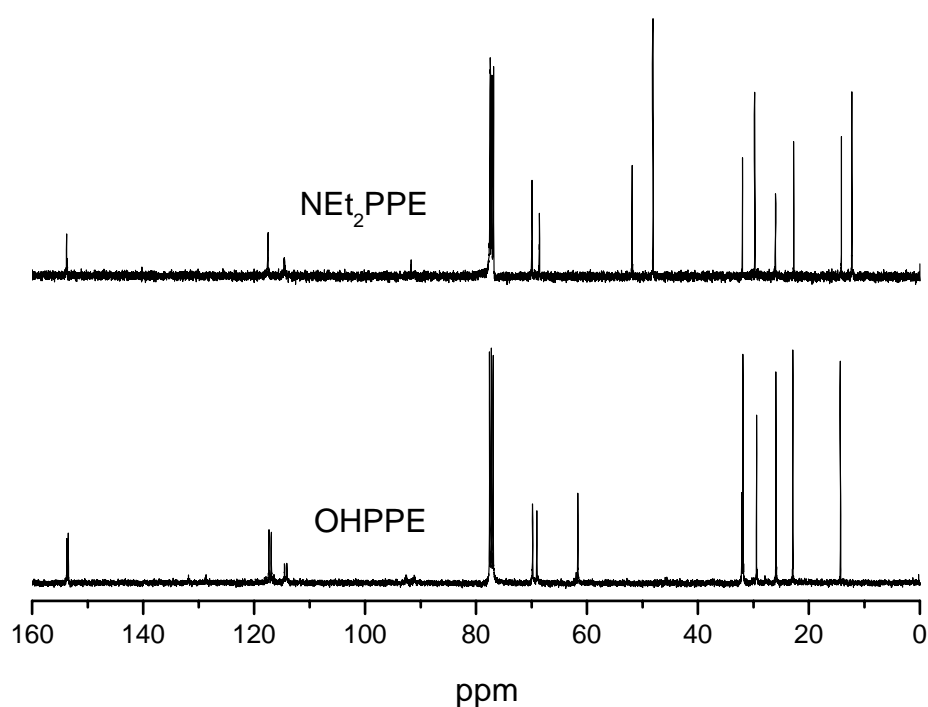


**Figure 2.2**  $^{13}\text{C}$  NMR spectra of the functionalized PPEs

$^{13}\text{C}$  NMR spectrum further confirmed the structure of the two functionalized PPEs. In Figure 2.2,  $\text{NEt}_2\text{PPE}$  exhibits three characteristic peaks. The peaks at 51.8 and 48.2

ppm can be attributed to the methylene groups adjacent to the nitrogen ( $-\text{CH}_2\text{N}-$ ) atoms, and the peak at 12.2 ppm corresponds to the methyl groups ( $-\text{CH}_3\text{CH}_2\text{N}-$ ). OHPPE showed three characteristic peaks at 69.9, 69.0 and 61.6 ppm attributing to the methylene groups adjacent to the oxygen ( $-\text{CH}_2\text{O}-$ ) atoms.

#### 2.4.4 FT-IR Spectroscopy

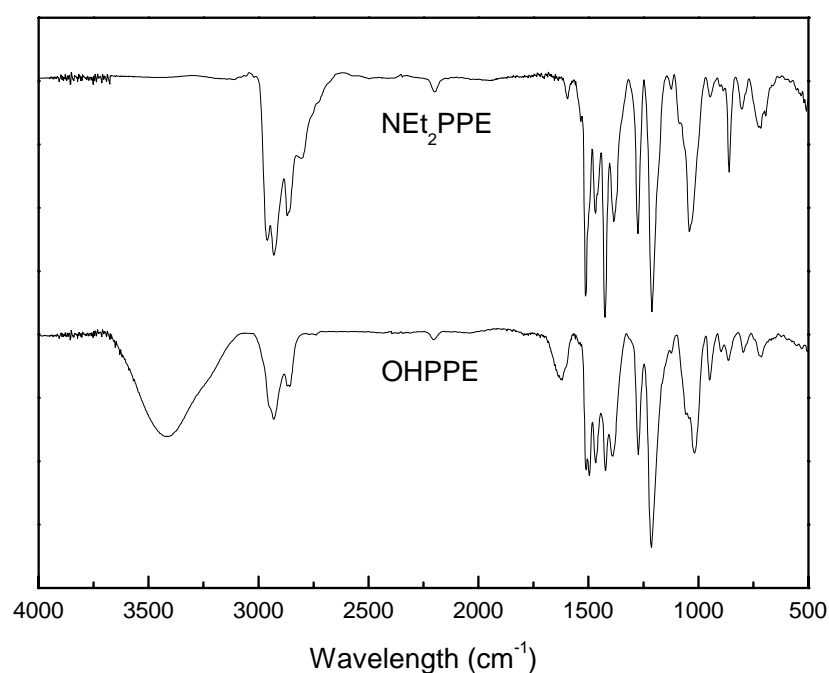


**Figure 2.3 FT-IR spectra of the functionalized PPEs**

Since the difference of OHPPE and NEt<sub>2</sub>PPE only lies in the different functional groups attached to half of the benzene rings, there is no obvious difference between the IR spectra of the two polymers (see Figure 2.3). Almost all the peaks have the same positions except for some difference in the peak intensity. Both polymers have an inherited peak at 2200 cm<sup>-1</sup> which corresponds to the C≡C stretching vibration of

the ethynylene groups. The peaks at about 1600, 1500 and 1460  $\text{cm}^{-1}$  are attributed to the benzene rings. It is note worthy that OHPPE had a broad absorption peak at about 3420  $\text{cm}^{-1}$  while  $\text{NEt}_2\text{PPE}$  exhibited no peak at this position. This can be attributed to the formation of self-associated absorption peak of hydrogen bonds among hydroxyl groups in the OHPPE side chains. All these further demonstrated that the functional groups have been successfully introduced into the molecular structure of PPE.

#### 2.4.5 Thermal Stability

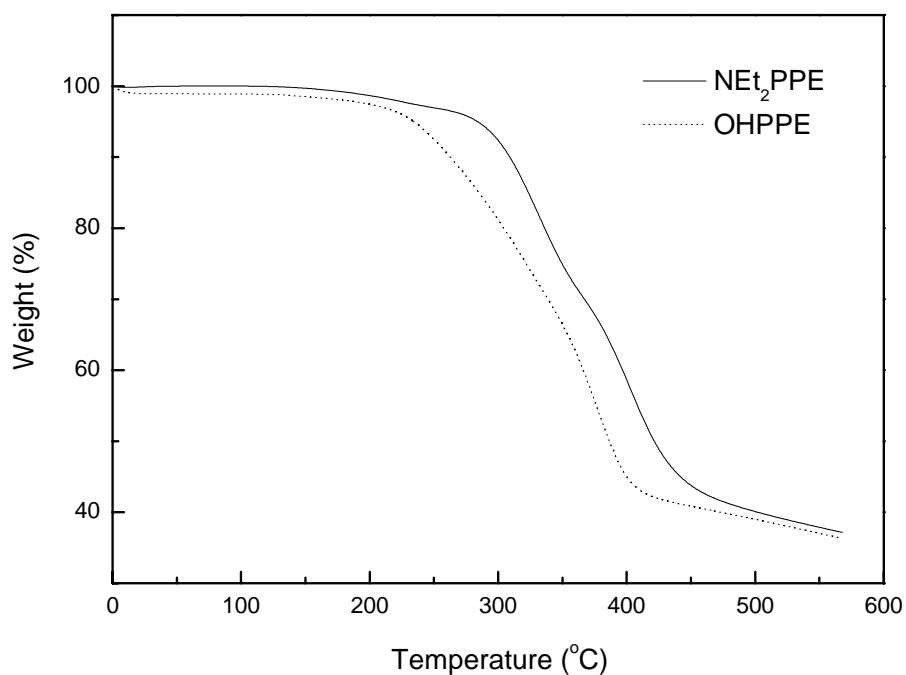


**Figure 2.4 Thermogravimetric analysis of the functionalized PPEs**

The thermal stability of the polymers in nitrogen was evaluated by thermogravimetric analysis (TGA). The thermograms are depicted in Figure 2.4. The onset degradation temperature of all polymers starts at about 250 °C. Both OHPPE and  $\text{NEt}_2\text{PPE}$

suffered two major mass loss steps between 250 °C and 400 °C. This indicates the different side chain cleavage from the aromatic group in the molecular backbone. The first 27% weight loss of OHPPE and 30% weight loss of  $\text{NEt}_2\text{PPE}$  from room temperature to about 350 °C can be attributed to the cleavage of the  $-\text{CH}_2\text{CH}_2\text{CH}_2\text{OH}$  group and the  $-\text{CH}_2\text{CH}_2\text{N}(\text{CH}_2\text{CH}_3)_2$  group respectively. The second 30% weight loss of OHPPE and  $\text{NEt}_2\text{PPE}$  from 350 °C to 400 °C is due to the cleavage of the  $-\text{C}_6\text{H}_{13}$  group. The  $T_d$  at nearly 250 °C for the functionalized polymers made them stable enough as chemo or biosensors even in a hostile environment.

#### 2.4.6 Optical Properties

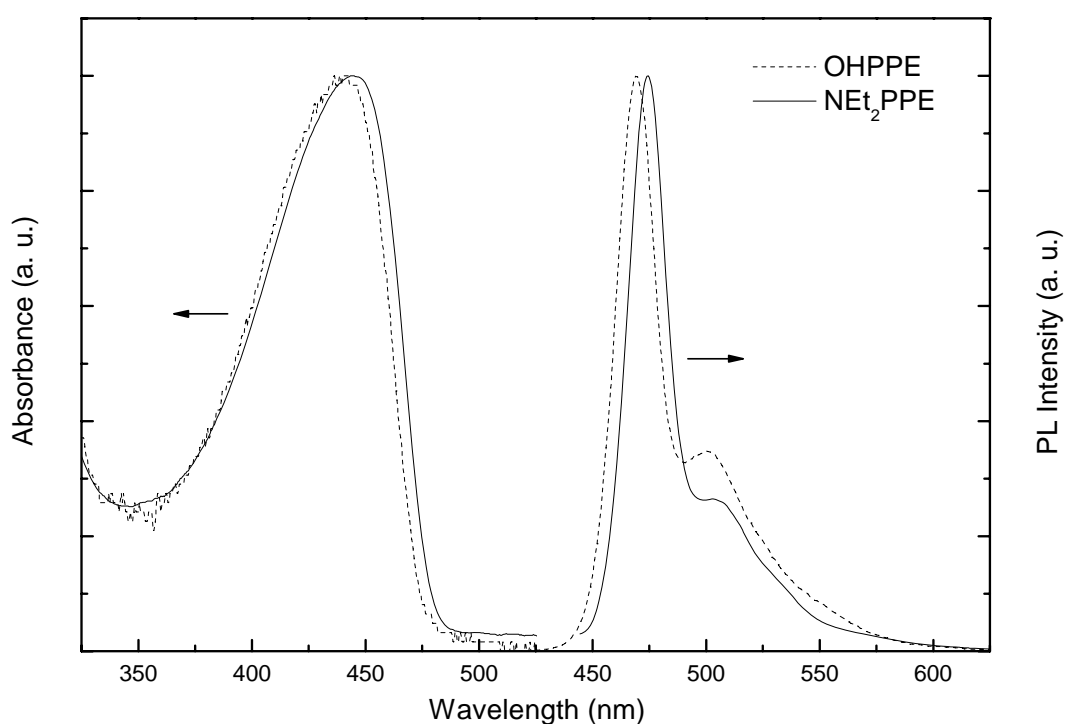


**Figure 2.5** UV-vis and PL spectra of the functionalized polymers in THF

The UV-vis and photoluminescence spectra of the functionalized PPE polymers in

THF are shown in Figure 2.5. Each polymer exhibits a strong absorption peak occurring at 433 nm and 430 nm respectively, while the emission peaks appeared at about 472 nm with a vibronic band shoulder at 506 nm. All these absorption and emission spectra are almost identical to the alkoxy group substituted PPEs reported by Wrighton's group previously,<sup>19</sup> indicating that the electronic properties of these conjugated polymers are predominantly governed by the rigid-rod and highly conjugated polymer backbone and only slightly influenced by the nature of the attached side chains.

#### 2.4.7 Water-Soluble Light-Emitting Nanoparticles

**Table 2.2 DLS Characterization data of the nanoparticles and the preparing proportion of PPE and PAA**

Sample	PPE : PAA (weight ratio, in water)	Diameter (nm)	Polydispersity Index (PI)
OHPPE/PAA-1	1 : 10	353	0.40
OHPPE/PAA-2	1 : 25	312	0.35
OHPPE/PAA-3	1 : 50	289	0.34
OHPPE/PAA-4	1 : 100	234	0.25
NEt <sub>2</sub> PPE/PAA-1	1 : 10	410	0.45
NEt <sub>2</sub> PPE/PAA-2	1 : 25	380	0.41
NEt <sub>2</sub> PPE/PAA-3	1 : 50	373	0.40
NEt <sub>2</sub> PPE/PAA-4	1 : 100	354	0.37

In a typical procedure to prepare the nanoparticles, 2 mL of H<sub>2</sub>O was added to 0.2 mL of PAA (10 mg/mL in water) under ultrasonic for 5 min and 0.2 mL PPE solution(1,



0.4, 0.2 and 0.1 mg/mL in THF) was added dropwise and the nanoparticles formed were measured by DLS (Table 2.2). Ultrasonication is essential because magnetic stirring cannot disperse the added PPEs swiftly enough in aqueous solution which blocks the formation of water-soluble nanoparticles.

It was found that after mixing with PAA in aqueous solution the functionalized OHPPE and  $\text{NEt}_2\text{PPE}$  dissolved well in water to form a clearly yellow solution. This suggests a homogeneous dispersion of OHPPE and  $\text{NEt}_2\text{PPE}$  in water. A bluish yellow tinge was observed in each mixture which suggested the presence of nanoparticles. Besides, each mixture emitted bluish green light under UV lamp 365 nm irradiation. The OHPPE/PAA and  $\text{NEt}_2\text{PPE}$ /PAA mixtures are very stable in aqueous solution and no precipitate was formed after storing in air for four months. However, the unfunctionalized PPEs was unable to form transparent aqueous solution under the same condition and precipitated in water instantly. These observations confirmed the existence of the interaction between OHPPE and PAA or  $\text{NEt}_2\text{PPE}$  and PAA through hydrogen bondings. It is well known that hydrophobic interaction, electrostatic interaction and hydrogen bond are generally the major driving forces to form water-soluble composites through the interaction between hydrophobic components and water-soluble components. Although there may exist the hydrophobic interaction between the unfunctionalized PPE and the hydrophobic portion (the main chain) of PAA, it cannot provide enough interaction between the two polymers to form stable water-soluble nanoparticles and therefore the unfunctionalized PPE precipitated in the aqueous solution. As for the hydroxyl- or amino-functionalized PPEs, because of the

formation of hydrogen bonds of the hydroxyl or amino groups with active hydrogen atoms on the acid groups of PAA, OHPPE/PAA and  $\text{NEt}_2\text{PPE/PAA}$  could form stable nanocomposites in aqueous solution.

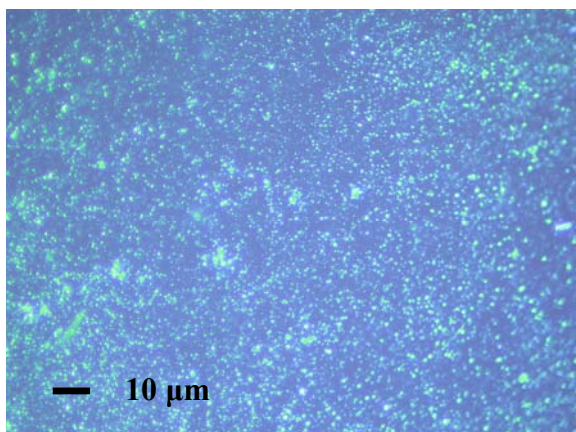


**Figure 2.6** Representative fluorescence micrograph of the OHPPE/PAA (1:25) nanoparticles. The sample was observed in water. The Picture was recorded with 500 times zoom.

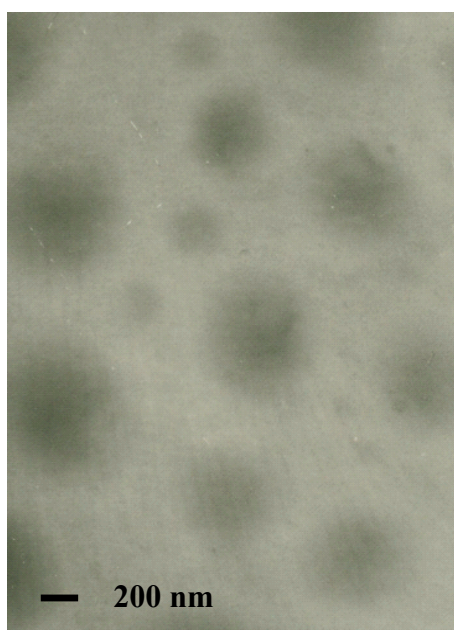


**Figure 2.7** Representative TEM micrographs of the nanoparticles obtained by freeze drying. The picture was recorded with 50,000 times zoom.

Fluorescence microscopy and TEM were used to further investigate the morphology of the composites. Fluorescence microscopy (Figure 2.6) showed that the

nanoparticles which emitted bluish green light dispersed well in aqueous solution. TEM (Figure 2.7) further demonstrated the morphology of the nanoparticles (diameter ranged from 100 - 400 nm mainly in the range 300 - 400 nm), indicating the formation of OHPPE/PAA and NEt<sub>2</sub>PPE/PAA micelles in aqueous solution. It is reasonable to consider that in such nanoparticles, hydrophobic OHPPE and NEt<sub>2</sub>PPE exist as the core and hydrophilic portion (the side chain) of PAA as the shell.

The DLS data are shown in Table 2.2. When the ratio of PAA/OHPPE is at 10:1, the nanoparticle size is 353 nm. When the ratio is increased to 100:1, the nanoparticle size decreased to 234 nm. PAA/NEt<sub>2</sub>PPE nanoparticles also follow the same trend. These results indicate that the nanoparticle size is highly dependant on the ratio of PAA/PPE. The higher the ratio of hydrophilic PAA to hydrophobic PPE, the smaller the particle size obtained. This observation is the same as those reported for inorganic nanoparticles stabilized by surfactants, the particle size of which is determined by the molar ratio of surfactant/inorganic materials.<sup>20</sup> The higher ratio of PAA/OHPPE would reduce the agglomeration of hydrophobic PPE chains in aqueous solution in order to form stable small hydrophobic PPE cores. Thus the nanoparticle size can be conveniently adjusted by controlling the ratio of PAA/PPE. It is noteworthy that the particle size of PAA/NEt<sub>2</sub>PPE composites is larger than that of PAA/OHPPE composites of the same ratio. This may be attributed to the different lengths of hydrophobic conjugated chains and the different capability to form hydrogen bond between PAA and hydroxyl group or amino group. It is well known that the lone electron pair on the hydroxyl group is more active than tertiary amino group, and

hydroxyl group will form stronger hydrogen bond than tertiary amino group. The stronger hydrogen bond will tend to stable the nanoparticles and decrease the agglomeration of hydrophobic PPE chains. Furthermore, the longer hydrophobic conjugated chains are more prone to aggregate in aqueous solution to efficiently decrease their hydrophobicity than the shorter ones. Thus, the OHPPE are more easily to form smaller nanoparticles than  $\text{NEt}_2\text{PPE}$  in the presence of PAA in aqueous solution.

#### 2.4.8 Optical Properties of Nanoparticles

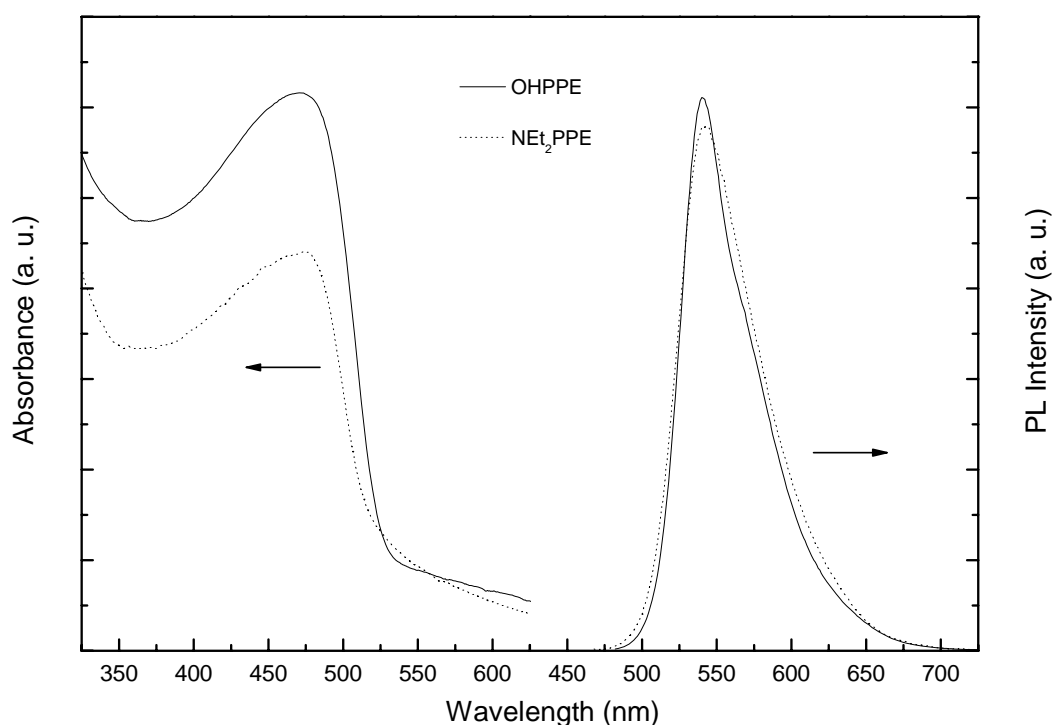


**Figure 2.8 UV-vis and PL spectra of the OHPPE/PAA and  $\text{NEt}_2\text{PPE}$ /PAA nanoparticles in aqueous solution**

It was found that the light blue color of PPE in THF solvent changed into yellow color

after nanoparticles were formed in aqueous solution, indicating the obvious variation of UV-vis absorption of the functionalized PPEs. The UV-Vis absorption and photoluminescence emission spectra of PPE/PAA nanoparticles (solution in water) and their solid films are shown in Figure 2.8 and Figure 2.9 respectively.

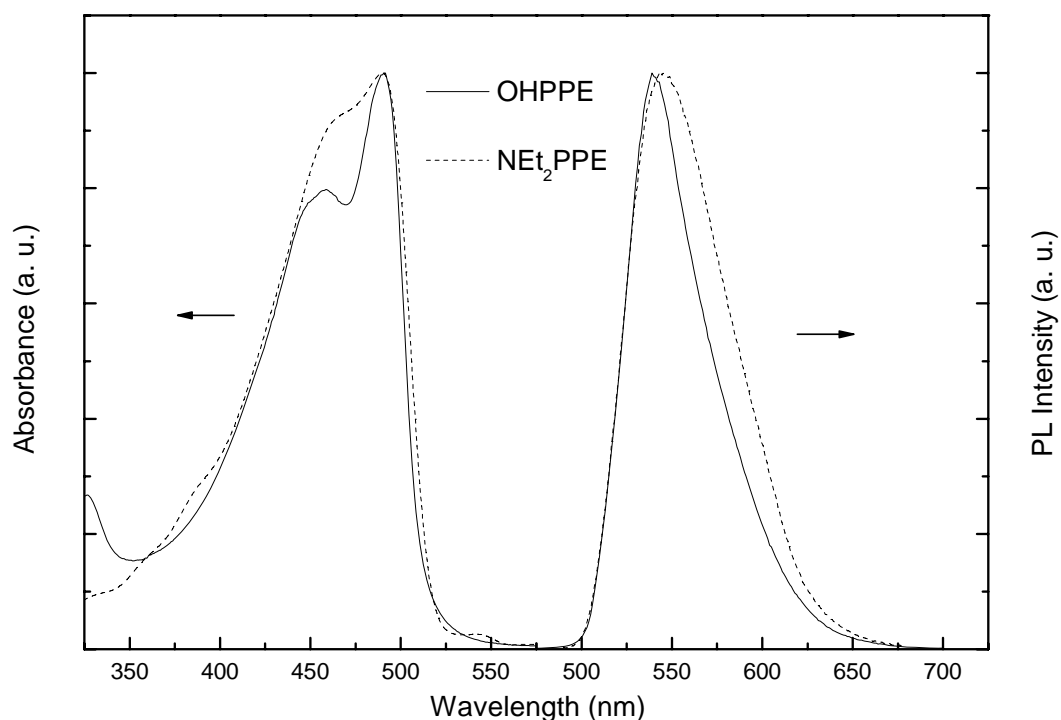


**Figure 2.9** UV-vis and PL spectra of the OHPPE and  $\text{NEt}_2\text{PPE}$  as films

The solid film emission spectra were collected from solid film made by spin-coating PPEs (5 mg/mL) from THF solutions on a glass substrate. Both OHPPE and  $\text{NEt}_2\text{PPE}$  exhibited similar optical properties after the formation of water-soluble nanoparticles. Compared with that of PPEs in THF solution, the absorption maxima of the PPE/PAA nanoparticles was red-shifted about 30 nm from 440 to 475 nm. Such red shifts were also found in PPE films. It is well known that PPE chains are prone to form

$\pi$ -aggregation in solid states based on their rigid rod backbone and result in the red shift of both absorption and emission maxima. Previously similar aggregation absorption at about 470 nm was also reported by Swager et al. in investigating the LB films of a series of PPE derivatives, which is quite close to the value in our system.<sup>21</sup> All these indicate that the  $\pi$ -aggregation of PPE chains were formed in PPE/PAA nanoparticles.

The emission spectra of PPE/PAA further supported the above conclusion. Their photoluminescence spectra were similar to UV spectrum and both red-shifted from 470 to about 540 nm, compared with the PL spectrum of PPEs in THF solution. The deep red shift (about 70 nm) of the nanoparticles is comparable to the reported red-shift (> 70 nm) of PPEs from interchain aggregation, strongly supporting the formation of interchain aggregation.<sup>18</sup>

Time resolved photoluminescent measurements excited at 380 nm were further used to study the optical properties. The PPEs in THF solution revealed a rapid monoexponential decay and showed a fluorescence lifetime at  $\tau \approx 0.50$  ns, which is close to that of those PPEs without any aggregation. After formation of nanoparticles, the fluorescence decay changed into biexponential and can be fitted to two components with  $\tau \approx 0.40$  and 5 ns. This observed new long lifetime emission decay component further confirmed the existence of interchain aggregation. The fluorescence intensity of PPEs is described in Table 2.3. After formation of nanoparticles, the fluorescence quantum yield of **PPE** dramatically decreased from  $\Phi_f \approx 0.60$  of PPE in THF solution to  $\Phi_f = 0.12$ . The reduced fluorescence intensity of

PPE/PAA in aqueous solution can be attributed to the formation of interchain aggregation of PPEs as nanoparticles. Thus, it is reasonable to consider that after formation of nanoparticles, the hydrophobic PPE chains were encapsulated in the cores of nanoparticles and tended to form  $\pi$ -interchain aggregation, just as it did in the solid state.

**Table 2.3 Photophysical properties of functionalized PPEs in THF and their nanoparticles in aqueous solution**

	absorption $\lambda_{\max}/\text{nm}$	emission $\lambda_{\max}/\text{nm}$	$\tau/\text{ns}$ at 475 nm (amplitude/%)	$\tau/\text{ns}$ at 550 nm (amplitude/%)	$\Phi_f$
OHPPE	443	472	0.54 (100)	0.59 (100)	0.64
NEt <sub>2</sub> PPE	444	474	0.55 (100)	0.58 (100)	0.60
OHPPE/PAA-2	472	541	0.44 (15), 5.28 (85)	0.51 (8), 5.80 (92)	0.12
NEt <sub>2</sub> PPE/PAA-2	476	544	0.49 (20), 4.74 (80)	0.55 (5), 5.38 (95)	0.12

The  $\Phi_f$  values of those polymers in solutions were measured using the quinine sulfate solution (ca.  $1.0 \times 10^{-5}$  M) in 0.10 M H<sub>2</sub>SO<sub>4</sub> ( $\Phi_f = 55\%$ ) as a standard.

## 2.5 Conclusion

In this chapter, a series of functionalized PPEs grafted with hydroxyl or amino groups were successfully synthesized by the Sonagashira coupling reaction. Their optoelectronic properties are predominantly governed by the rigid-rod and highly conjugated polymer backbone but little influenced by the nature of the attached side chains. The water-soluble nanoparticles containing functionalized PPEs were successfully prepared through hydrogen bond self-assembly between functionalized PPEs and PAA. It was shown that the nanoparticle size is highly related to the ratio of PAA to functionalized PPEs, i.e., the higher ratio of hydrophilic PAA to hydrophobic

PPE, the smaller the nanoparticle diameter. Furthermore, the particle size of PAA/NEt<sub>2</sub>PPE composites is larger than that of PAA/OHPPE composites under the same ratio. This may result from the different length of hydrophobic conjugated chains and the different degree of hydrogen bond with PAA of hydroxyl group and amino group. Also, it was found that after formation of nanoparticles in aqueous solution, the hydrophobic PPE chains were encapsulated in the cores of nanoparticles and tended to form  $\pi$ -interchain aggregation, just as it did in the solid state.

### References

1. a) Faid, K.; Leclerc, M. *Chem. Commun.* **1996**, 2761; b) Crawford, K. B.; Goldfinger, M. B.; Swager, T. M. *J. Am. Chem. Soc.* **1998**, *120*, 5187; c) Swager, T. M. *Acc. Chem. Res.* **1998**, *31*, 201.
2. a) McQuade, D. T.; Pullen, A. E.; Swager, T. M. *Chem. Rev.* **2000**, *100*, 2537; b) Faid, K.; Leclerc, M. *J. Am. Chem. Soc.* **1998**, *120*, 5274; c) Gaylord, B. S.; Heeger, A. J.; Bazan, G. C. *Proc. Nat. Acad. Sci. USA* **2002**, *99*, 10954; d) Shu, W.; Bazan, G. C. *Adv. Mater.* **2003**, *15*, 1425.
3. Patil, S.; Ikenoue, Y.; Wudl, F.; Heeger, A. J. *J. Am. Chem. Soc.* **1987**, *109*, 1858.
4. a) Thunemann, A. F. *Adv. Mater.* **1999**, *11*, 127; b) Tan, C. Y.; Pinto, M. R.; Schanze, K. S. *Chem. Commun.* **2002**, 446; c) Kuroda, K.; Swager, T. M. *Chem. Commun.* **2003**, 26.
5. a) Shi, S.; Wudl, F. *Macromolecules* **1990**, *23*, 2119; b) Fan, Q. L.; Lu, S.; Lai, Y. H.; Hou, X. Y.; Huang, W. *Macromolecules* **2003**, *36*, 6976.



6. a) Liu, B.; Yu, W. L.; Lai, Y. H.; Huang, W. *Chem. Commun.* **2000**, 551; b) Huang, F.; Wu, H. B.; Wang, D.; Yang, W.; Cao, Y. *Chem. Mater.* **2004**, *16*, 708; c) Stork, M.; Gaylord, B. S.; Heeger, A. J.; Bazan, G. C. *Adv. Mater.* **2002**, *14*, 361.
7. Lu, S.; Fan, Q. L.; Liu, S. Y.; Chua, S. J.; Huang, W. *Macromolecules* **2002**, *35*, 98751.
8. Lu, S.; Fan, Q. L.; Chua, S. J.; Huang, W. *Macromolecules* **2003**, *36*, 304.
9. a) Duan, H. W.; Chen, D. Y.; Jiang, M.; Gan, W. J.; Li, S. J.; Wang M.; Gong, J. *J. Am. Chem. Soc.* **2001**, *123*, 12097; b) Kuang, M.; Duan, H. W.; Wang, J.; Chen, D. Y.; Jiang, M. *Chem. Commun.* **2003**, 496.
10. a) Yoshida, E.; Kunugi, S. *Macromolecules* **2002**, *35*, 6665; b) Wang, M.; Jiang, M.; Ning, F. L.; Chen, D. Y.; Liu, S. Y.; Duan, H. W. *Macromolecules* **2002**, *35*, 5980.
11. Qiang, L. L.; Fan, Q. L.; Ma, Z.; Zheng, Z.; Wang, Y. Y.; Zhang, G. W.; Huang, W. *Chem. Lett.* **2005**, *34*, 1164.
12. Zhou, Q.; Swager, T. M. *J. Am. Chem. Soc.* **1995**, *117*, 7017.
13. Zhou, Q.; Swager, T. M. *J. Am. Chem. Soc.* **1995**, *117*, 12593.
14. Yang, J.-S.; Swager, T. M. *J. Am. Chem. Soc.* **1998**, *120*, 5321.
15. Yang, J.-S.; Swager, T. M. *J. Am. Chem. Soc.* **1998**, *120*, 11864.
16. Kim, J.; McQuade, D. T.; McHugh, S. K.; Swager, T. M. *Angew. Chem. Int. Ed.* **2000**, *39*, 3869.
17. Tan, C.; Mauricio, R. P.; Schanze, K. S. *Chem. Comm.* **2002**, 446.

18. DiCesare, N.; Pinto, M. R.; Schanze, K. S.; Lakowicz, J. R. *Langmuir* **2002**, *18*, 7785.
19. Weder, C.; Wrighton, M. S. *Macromolecules* **1996**, *29*, 5157.
20. Fendler, J. H.; Meldrum, F. C. *Adv. Mater.* **1995**, *7*, 607.
21. Kim, J.; Swager, T. M. *Nature* **2001**, *411*, 1030.

## CHAPTER THREE

### **Water-Soluble Light-Emitting Nanoparticles Prepared by Non-Covalent Bond Self-Assembly of Hydroxyl Group Functionalized Oligo(p-phenyleneethynylene)s with Different Molecular Architectures and Water-Soluble Polymers Containing Different Active Hydrogen Atoms**

#### **3.1 Introduction**

Recently, water-soluble fluorescent  $\pi$ -conjugated polymers have attracted much interest owing to their potential application in the development of highly efficient chemo- or biosensors.<sup>1-4</sup> To prepare water-soluble  $\pi$ -conjugated polymers, the use of conventional synthetic chemistry via covalent bonding interactions is complex, tedious and time-consuming. Recently, the supramolecular assembly via noncovalent bonding interactions offers a simple and convenient method of preparing water-soluble conjugated materials with ordered nanostructures, which will retain the corresponding optical properties of the  $\pi$ -conjugated polymers and consequently can be used in sensors. Even though many publications have appeared in recent years addressing the supramolecular assemblies of conjugated polymers or oligomers,<sup>5-8</sup> only a few reports have been cited on self-assembled  $\pi$ -conjugated systems in water.<sup>9-14</sup>

Noncovalently connected micelles (NCCM) were first reported by Jiang et. al.<sup>15</sup> They used homopolymers, random copolymers, and oligomers as building blocks to construct NCCM, in which the core and shell are connected by hydrogen bonds.<sup>16-21</sup>

Based on this work, we attempted to create new core-shell structured water-soluble conjugated supramolecular assemblies by substituting the components in the core with conjugated polymers, in line with our recent interest in new approaches to macromolecular assembly of  $\pi$ -conjugated polymer systems in water.

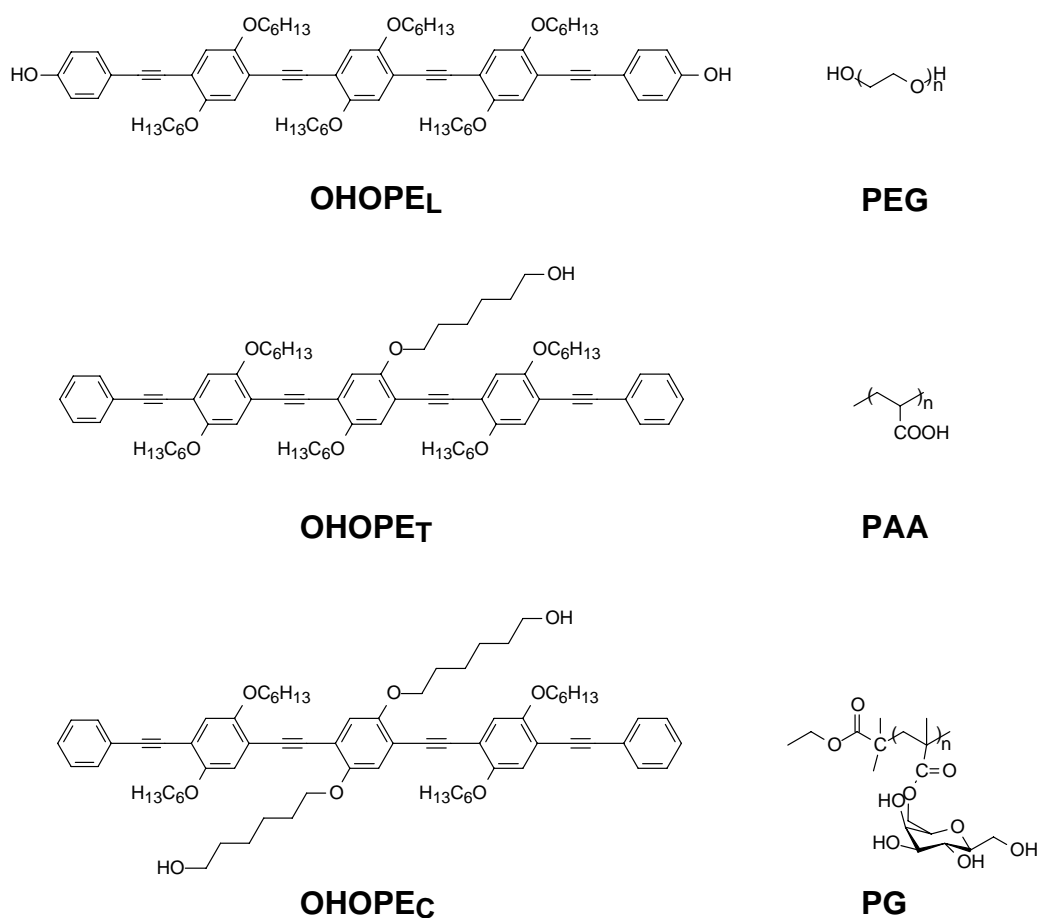
In the previous chapter, we have reported the noncovalently connected water-soluble light-emitting nanoparticles containing hydroxyl- and amino-functionalized poly(*p*-phenyleneethynylene)s (PPEs) and poly(acrylic acid) (PAA).<sup>14</sup> These nanoparticles showed a high degree of size dispersity which may be due to the intrinsic polydispersity of PPE conjugated lengths. However, nanoparticles with monodispersity are highly desired for bioapplication. To prepare nanoparticles with a low degree of dispersity, it is important to understand the influences on the physical properties of the NCCMs exerted by the structures of the conjugated oligomers (with the monodispersed conjugated length). On the other hand, the influence of the strength of hydrogen bonds formed between conjugated oligomers and water-soluble polymers on the size and dispersity of NCCMs is also important and will be investigated.

In this work, we report the preparation of water-soluble light-emitting nanoparticles prepared from oligomers by non-covalent bond self-assembly. First, a series of hydroxyl group functionalized oligo(*p*-phenyleneethynylene)s (OPEs) with different molecular architectures were successfully synthesized. We also use different water-soluble polymers, which have different active hydrogen containing groups, to realize different strength of hydrogen bonds. The properties of the water-soluble

light-emitting nanoparticles prepared from the OPEs and a number of water soluble polymers are also studied.

### 3.2 Molecular Design

We envisage that the size and the polydispersity of the nanoparticles are influenced by both the structure of the conjugated oligomers and activity of hydrogen atoms on the water-soluble polymers. In this work, oligo(*p*-phenyleneethynylene)s with the same conjugated length incorporated with hydroxyl group at different sites, i.e., linear, cross-shaped and T-shaped structures were designed and synthesized.



**Scheme 3.1** Functionalized OPEs and water-soluble polymers for the preparation of water-soluble nanoparticles

In addition, different water-soluble polymers with functionalized groups, i.e., poly(ethylene glycol) (PEG), poly(galactose) (PG) and poly(acrylic acid) (PAA) were used to provide different active hydrogen atoms to form hydrogen bonds with different strengths. The chemical structures of the conjugated oligomers and water-soluble polymers are illustrated in Scheme 3.1.

### **3.3 Experimental**

#### **3.3.1 Materials**

All chemical reagents were purchased from Aldrich Chemical Co. THF was purified by distillation from sodium in the presence of benzophenone. Poly(ethylene glycol) (PEG,  $M_n = 3400$ ) was purchased from Aldrich Chemical Co. Poly(galactose) (PG,  $M_n = 3200$ , PDI = 1.12) and poly(acrylic acid) (PAA,  $M_n = 3800$ , PDI = 1.21) were afforded by Institute of Advanced Materials of Fudan University.

#### **3.3.2 Characterization Methods**

The NMR spectra were collected on a Varian Mercury Plus 400 spectrometer with tetramethylsilane as the internal standard. Elemental microanalyses were carried out on a Vario EL III CHNOS Elementar Analyzer. Mass spectra (MS) were obtained by using a micromass VG 7035E mass spectrometer at an ionizing voltage of 70 eV. MALDI experiments were carried out using a Shimadzu AXIMA-CFRTM plus time-of-flight mass spectrometer (Kratos Analytical, Manchester, U. K.). The

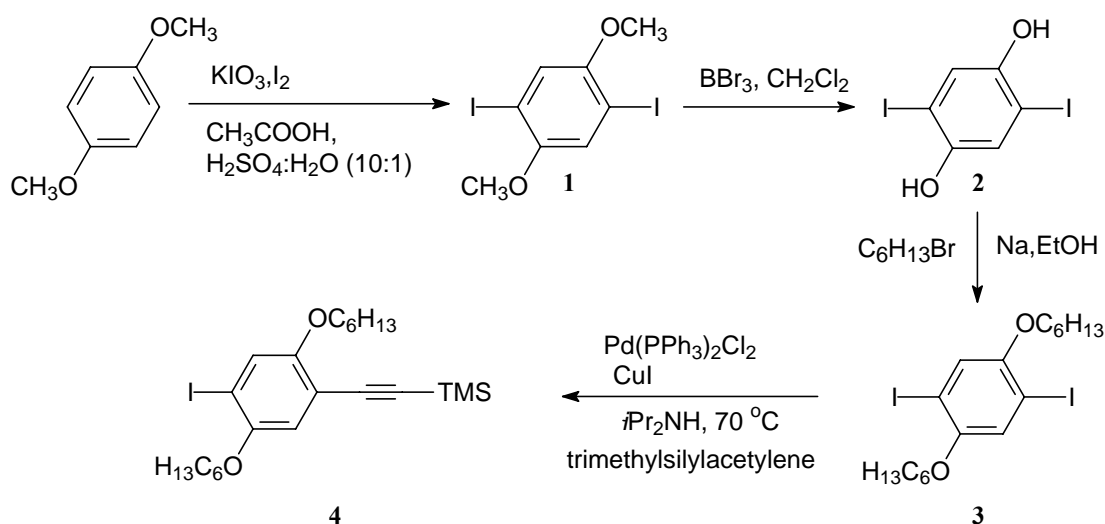
instrument is equipped with a nitrogen laser emitting at 377 nm, a 2 GHz sampling rate digitizer, a pulsed ion extraction source, and an electrostatic reflectron. Spectra were acquired in the positive ion mode using the reflectron. DSC measurements were performed under a nitrogen atmosphere at both heating and cooling rates of 10 °C/min, using NETZSCH DSC 200PC apparatus. GPC analysis was conducted with a HP1100 HPLC system equipped with 7911GP-502 and GP NXC columns using polystyrenes as the standard and tetrahydrofuran as the eluent at a flow rate of 1.0 mL/min at 35 °C. UV-vis spectra were recorded on a Shimadzu 3150 PC spectrophotometer. Fluorescence measurement was carried out on a Shimadzu RF-5301 PC spectrofluorophotometer with a xenon lamp as a light source. Time-correlated single photon fluorescence studies were performed using an Edinburgh Instruments LifeSpec-PS spectrometer. The LifeSpec-PS comprises a 371 nm picosecond laser (PicoQuant PDL 800B) operated at 2.5 MHz and a Peltier-cooled Hamamatsu microchannel plate photomultiplier (R3809U-50). Lifetimes were determined from the data using the Edinburgh Instruments software package.

### **3.3.3 Synthesis**

#### **2,5-Diiodo-1,4-dimethoxybenzene (1)**

13.8 g (0.1 mol) of 1,4-dimethoxybenzene, 8.56 g (0.04 mol) of KIO<sub>3</sub> and 27.94 g (0.11 mol) of I<sub>2</sub> were added into a solution of acetic acid (500 mL), 98% H<sub>2</sub>SO<sub>4</sub> (5 mL), and H<sub>2</sub>O (50 mL). The reaction mixture was stirred at reflux for 24 h and then cooled to room temperature. Aqueous Na<sub>2</sub>SO<sub>4</sub> (20%) was added until the brown color

of iodine had disappeared, and the acetic acid was evaporated under reduced pressure. The residue was poured into 200 mL of water and the mixture was extracted with ethyl acetate three times, and the obtained organic layer was washed with water two times, and brine once. The combined organic layers were dried over  $\text{MgSO}_4$ . After the solvent was evaporated, the crude solid was recrystallized with hexane/chloroform to afford pure product as colorless crystals (29 g, yield 75%). Mp: 172-3 °C.  $^1\text{H}$  NMR ( $\text{CDCl}_3$ , ppm):  $\delta$  7.23 (s, 2H), 3.86 (s, 6H).



**Scheme 3.2.1 Synthetic routes for compound 1-4**

### 1,4-Diiodo-2,5-hydroquinone (2)

19.5 g (0.05 mol) of 2,5-diiodo-1,4-dimethoxybenzene was dissolved in 250 mL  $\text{CH}_2\text{Cl}_2$  in a 500 mL round-bottom flask fitted with a condenser. The reaction mixture was cooled to  $-80$  °C in a dry ice-acetone bath. 26.3 g (0.105 mol) of  $\text{BBr}_3$  dissolved in 105 mL  $\text{CH}_2\text{Cl}_2$  was added dropwise through the condenser. After the addition, a drying tube was attached on the top of the condenser, and the mixture was allowed to warm to room temperature. The mixture was stirred at room temperature for 12 h and



then carefully hydrolyzed with 200 mL of H<sub>2</sub>O. The aqueous layer was separated and extracted with ether three times. The combined organic phases were extracted with NaOH (200 mL, 2 N), and then the NaOH solution was neutralized with dilute HCl (1 N) in ice bath. The precipitate was collected and dried, and recrystallized from acetic acid to afford brown crystals (14.5 g, yield 80%). Mp: 198-200 °C. <sup>1</sup>H NMR (DMSO-*d*<sub>6</sub>, ppm): δ 9.82 (s, 2H), 7.15 (s, 2H).

### **1,4-Diiodo-2,5-bis(hexyloxy)benzene (3)**

Sodium ethoxide was prepared by adding 1.52 g (66 mmol) of sodium into 50 mL of anhydrous ethanol. After all the sodium disappeared, 10.86 g (30 mmol) of 1,4-diiodo-2,5-hydroquinone in 10 mL of anhydrous ethanol was added dropwise. To the stirred mixture, 10.89 g (66 mmol) of 1-bromohexane in 10 mL of anhydrous ethanol was added. After stirring for 24 h with refluxing, the ethanol was evaporated at reduced pressure. The brownish residue was added into 300 mL of water, extracted with ethyl acetate, and dried with anhydrous magnesium sulfate. The white product (12.1 g, yield 76%) was obtained by recrystallization in ethanol after most of the solvent was removed under reduced pressure. Mp: 80-1 °C. MS: *m/z* 530.0. <sup>1</sup>H NMR (CDCl<sub>3</sub>, ppm): δ 7.08 (s, 2H), 3.99 (t, 4H, *J* = 4.8 Hz), 1.82 (m, 4H), 1.52 (m, 4H), 1.37 (m, 8H), 0.94 (t, 6H, *J* = 8.0 Hz). Anal. Calcd for C<sub>18</sub>H<sub>28</sub>I<sub>2</sub>O<sub>2</sub>: C, 40.77; H, 5.32; I, 47.87. Found: C, 40.70; H, 5.32.

### **2,5-Bis(hexyloxy)-4-[(trimethylsilyl)ethynyl]iodobenzene (4)**

To a solution of 1,4-diiodo-2,5-bis(hexyloxy)benzene (15.9 g, 0.03 mol), CuI (0.28 g,

1.5 mmol), and Pd(PPh<sub>3</sub>)<sub>2</sub>Cl<sub>2</sub> (1.06 g, 1.5 mmol) in 200 mL of diisopropylamine was added (trimethylsilyl)acetylene (2.94 g, 0.03 mol). The mixture was stirred at room temperature for 15 h. After removal of the solvent under reduced pressure, a light yellow oil (6.60 g, 44%) was separated from starting material and byproduct by column chromatography using silica gel with hexane/CH<sub>2</sub>Cl<sub>2</sub> (20:1) as eluent.

### **2-(4-Iodophenoxy)-tetrahydro-2H-pyran (5)**

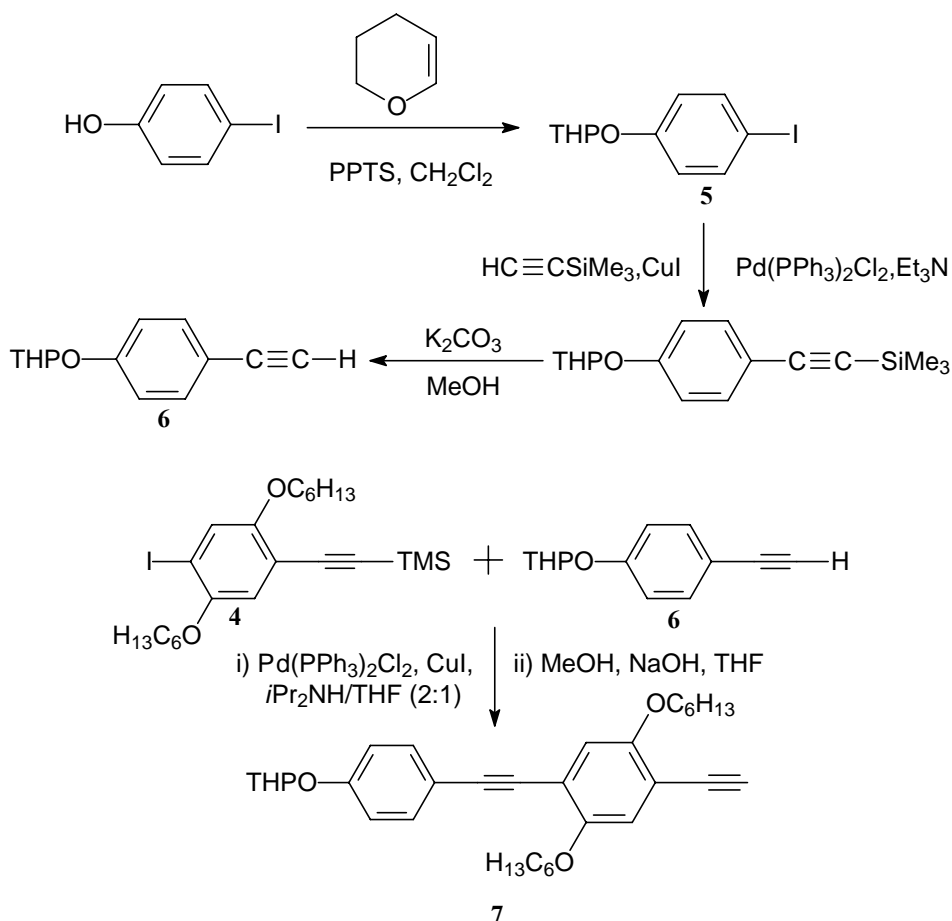
A solution of 4-iodophenol (11.2 g, 0.05 mol) and 3,4-dihydro-2H-pyran (12.6 g, 0.15 mol) in 800 mL of dry methylene chloride containing pyridinium *p*-toluenesulfonate, PPTS (1.75 g, 7 mmol), was stirred at room temperature for 5 h. Then the solution was diluted with ether and washed several times with half-saturated brine to remove the catalyst. Upon evaporation of the solvent, recrystallization from ethanol was accomplished to yield white chunky crystals (12.9 g, 84%).

### **2-(4-Ethynylphenoxy)-tetrahydro-2H-pyran (6)**

2-(4-iodophenoxy)-tetrahydro-2H-pyran (10.0 g, 0.0328 mol), (trimethylsilyl)acetylene (4.8 g, 0.0490 mol), bis(triphenylphosphine)palladium(II) dichloride (1 g), and copper(I) iodide (0.133 g) were added into 300 mL of triethylamine. The reaction mixture was stirred under nitrogen at room temperature for 3 h before the solvent was removed under reduced pressure. The residue was extracted with 500 mL of petroleum ether, and the solution was filtered, washed with water, and then dried over anhydrous MgSO<sub>4</sub>. Upon evaporating the solvent, the brown crude product was purified by flash chromatography on silica gel using 1:15

diethyl ether/petroleum ether as the eluent. The pale yellowish product was recrystallized to yield white chunky crystals (7.0 g, 78%).

The product obtained (5.0 g, 0.018 mol) and anhydrous potassium carbonate (1.0 g) were dissolved in 100 mL of methanol, and the solution was stirred for 2 h. The solvent was then evaporated, and the residue was dissolved in 200 mL of petroleum ether followed by washing with water and drying over anhydrous  $\text{MgSO}_4$ . Recrystallization from ethanol gave white chunky crystals (3.4 g, 94%).



**Scheme 3.2.2 Synthetic routes for compound 5-7**

**2-(4-(2-(4-Ethynyl-2,5-bis(hexyloxy)phenyl)ethynyl)phenoxy)-tetrahydro-2H-pyran (7)**

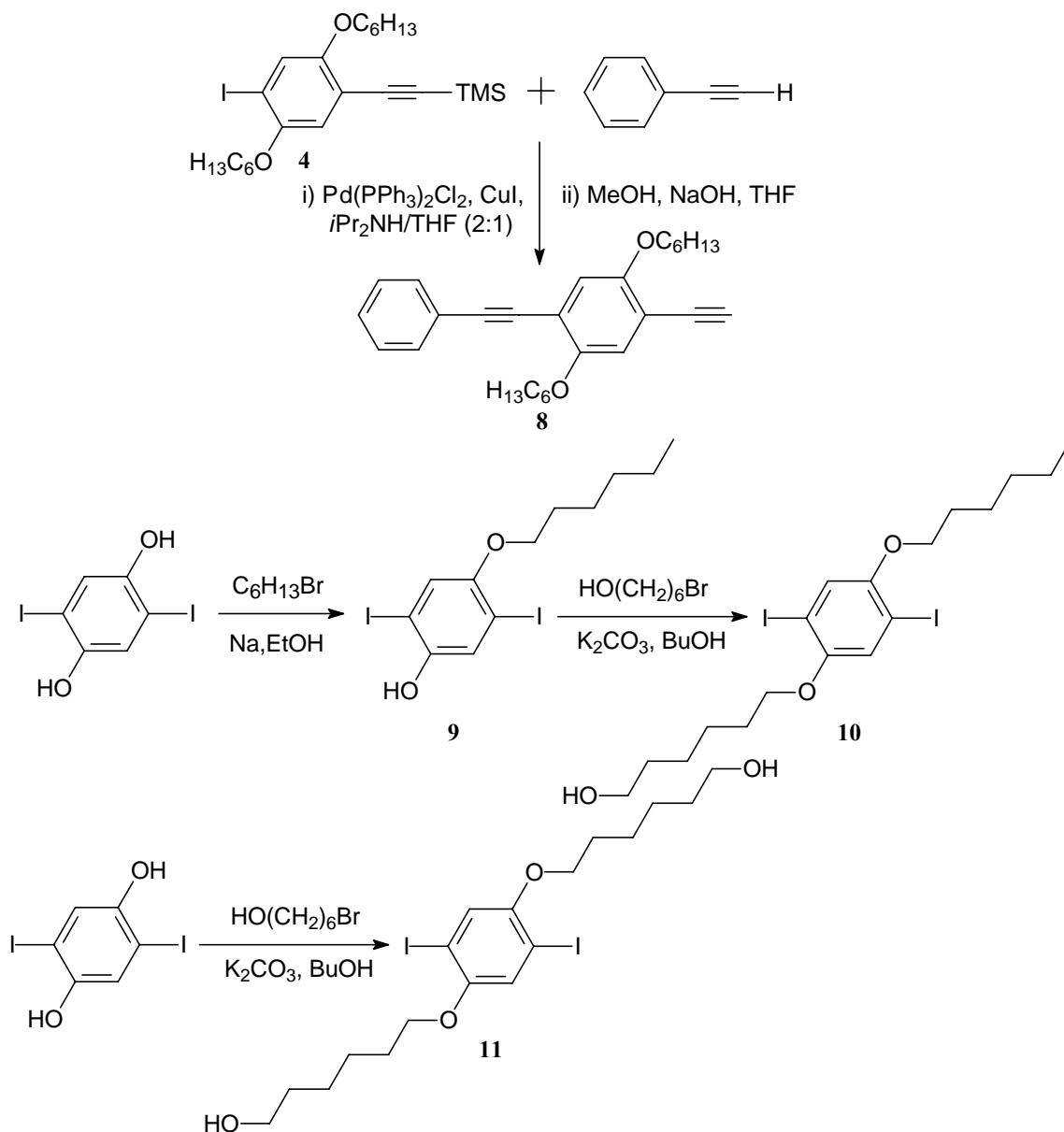
A two-neck flask was charged with 2,5-dihexyloxy-4-[(trimethylsilyl)ethynyl]iodobenzene (3.50 g, 7.00 mmol), 2-(4-ethynylphenoxy)-tetrahydro-2H-pyran (1.42 g, 7.00 mmol), CuI (0.133 g, 0.700 mmol), and Pd(PPh<sub>3</sub>)<sub>2</sub>Cl<sub>2</sub> (0.491 g, 0.500 mmol). It was degassed with three vacuum-nitrogen cycles and diisopropylamine ((iPr)<sub>2</sub>NH) (50.0 mL) and THF (25.0 mL) were added at 0 °C. The reaction mixture was stirred at room temperature for 12 hours, and then it was added into water and extracted with dichloromethane. The combined organic solution was washed with water NH<sub>4</sub>OH (50%) twice, distilled water twice and brine twice and dried over anhydrous sodium sulfate. After removal of the solvent under reduced pressure, the residue was purified using a flash silica gel chromatograph with hexane/dichloromethane (5:1) as eluent. Thus, the intermediate product, (2-(2,5-bis(hexyloxy)-4-(2-(4-(tetrahydro-2H-pyran-2-yloxy)phenyl)ethynyl)phenyl)ethynyl)trimethylsilane (3.45 g, 90.0%), was obtained, and it was dissolved in THF (30 mL). A mixture of methanol (40 ml) and NaOH solution (3 mL, 5 N) was added to the THF solution slowly. After the reaction mixture was stirred at room temperature for 1 hour, the solvents were evaporated and the resulting residue was purified using a silica gel chromatograph with dichloromethane/hexane (1:5) as eluent to afford **7** (3.01 g, 95.0% ) as white crystal. MS: *m/z* 502.3. <sup>1</sup>H NMR (CDCl<sub>3</sub>), δ (ppm): 7.45 (m, 2 H), 7.02 (m, 2 H), 6.96 (m, 2 H), 5.44 (t, 1 H), 4.01 (m, 4 H), 3.91 (m, 1 H), 3.64 (m, 1 H), 3.33 (s, 1H), 2.03 (m, 1 H), 1.97-1.78 (m, 17 H), 1.33 (m, 4 H), 0.90 (m, 6 H). <sup>13</sup>C NMR (CDCl<sub>3</sub>), δ (ppm): 157.41, 154.38, 153.49, 133.17, 118.00, 116.91, 116.57, 116.52, 115.73, 112.29, 96.44, 95.31, 84.69, 82.34, 80.31,

69.86, 69.81, 62.27, 31.83, 31.76, 30.47, 29.52, 29.35, 25.96, 25.83, 25.36, 22.87, 22.83, 18.89, 14.28. Anal. Calcd for C<sub>33</sub>H<sub>42</sub>O<sub>4</sub>: C, 78.85; H, 8.42. Found: C, 78.74; H, 8.36.

### **1-Ethynyl-2,5-bis(hexyloxy)-4-(2-phenylethynyl)benzene (8)**

A two-neck flask was charged with 2,5-dihexyloxy-4-[(trimethylsilyl)ethynyl]iodobenzene (3.50 g, 7.00 mmol), 1-ethynylbenzene (0.715 g, 7.00 mmol), CuI (0.133 g, 0.700 mmol), and Pd(PPh<sub>3</sub>)<sub>2</sub>Cl<sub>2</sub> (0.491 g, 0.500 mmol). It was degassed with three vacuum-nitrogen cycles and diisopropylamine ((*i*Pr)<sub>2</sub>NH) (50.0 mL) and THF (25.0 mL) were added at 0 °C. The reaction mixture was stirred at room temperature for 12 hours, and then it was added into water and extracted with dichloromethane. The combined organic solution was washed with water NH<sub>4</sub>OH (50%) twice, distilled water twice and brine twice and dried over anhydrous sodium sulfate. After removal of the solvent under reduced pressure, the residue was purified using a flash silica gel chromatograph with hexane/dichloromethane (6:1) as eluent. The intermediate product, (2-(2,5-bis(hexyloxy)-4-(2-phenylethynyl)phenyl)ethynyl)-trimethylsilane (3.90 g, 92.8%), was dissolved in THF (30.0 mL). A mixture of methanol (40.0 ml) and NaOH solution (3.00 mL, 5 N) was added to the stirred THF solution slowly. After the reaction mixture was stirred at room temperature for 1 hour, the solvents were evaporated and the resulting residue was purified using a silica gel chromatograph with dichloromethane/hexane (1:6) as eluent to afford **8** (3.14 g, 95.0% ) as white crystal. MS: *m/z* 402.2. <sup>1</sup>H NMR (CDCl<sub>3</sub>), δ (ppm): 7.53 (m, 2 H),

7.34 (m, 3 H), 6.99 (m, 2 H), 4.01 (m, 4 H), 3.33 (s, 1 H), 1.82 (m, 4 H), 1.58 (m, 8 H), 1.33 (m, 4 H), 0.90 (m, 6 H).  $^{13}\text{C}$  NMR ( $\text{CDCl}_3$ ),  $\delta$  (ppm): 154.36, 153.66, 131.81, 128.53, 123.58, 117.98, 117.04, 114.86, 112.72, 95.15, 85.92, 82.50, 80.24, 31.83, 31.77, 29.51, 29.35, 25.96, 25.83, 22.87, 22.83, 14.27. Anal. Calcd for  $\text{C}_{28}\text{H}_{34}\text{O}_2$ : C, 83.54; H, 8.51. Found: C, 83.39; H, 8.47.



**Scheme 3.2.3** Synthetic routes for compound 8-11

#### 4-(Hexyloxy)-2,5-diiodophenol (9)

A two-neck flask was charged with 1,4-diiodo-2,5-hydroquinone (3.37 g, 9.32 mmol) and degassed. A solution of sodium hydroxide (573 mg, 14.3 mmol) in absolute ethanol (90.0 mL) was added to the flask at room temperature under a nitrogen atmosphere. The mixture solution was warmed to 60 °C with constant stirring, followed by the dropwise addition of 1-bromohexane (1.54g, 9.32 mmol). After 10 hour of stirring under nitrogen atmosphere, the reaction mixture was cooled and filtered, and the precipitate was washed with methanol. The filtrate was concentrated to remove the solvents. Distilled water was added to the residue, and the mixture was acidified with concentrated HCl, boiled gently for 1 hour, and cooled. The resulting precipitate was collected by filtration, washed with water. The crude product was purified by column chromatography on silica gel using dichloromethane/hexane (1:5) as eluent to get the pure product **9** (2.50 g, 60.0%). <sup>1</sup>H NMR (CDCl<sub>3</sub>), δ (ppm): 7.40 (s, 1 H), 7.02 (s, 1 H), 4.91 (s, 1 H), 3.92 (t, 2 H), 0.93 (m, 3 H), 1.81 (m, 2 H), 1.52-1.34 (m, 6 H).

#### **6-(4-(Hexyloxy)-2,5-diiodophenoxy)hexanol (10)**

Compound **9** (2.54 g, 5.70 mmol), 6-bromohexanol (1.14 g, 6.25 mmol), K<sub>2</sub>CO<sub>3</sub> (3.16 g, 22.9 mmol), and NaI (0.100 g, 0.645 mmol) were added to a round-bottom flask containing 2-butanone (40.0 mL). The mixture was heated 70 °C for 24 hours under nitrogen atmosphere. The reaction mixture was filtered and the salts washed with dichloromethane. The filtrate was washed several times with NaOH solution (0.1 N), followed by distilled water, and dried over anhydrous sodium sulfate. The solvent was

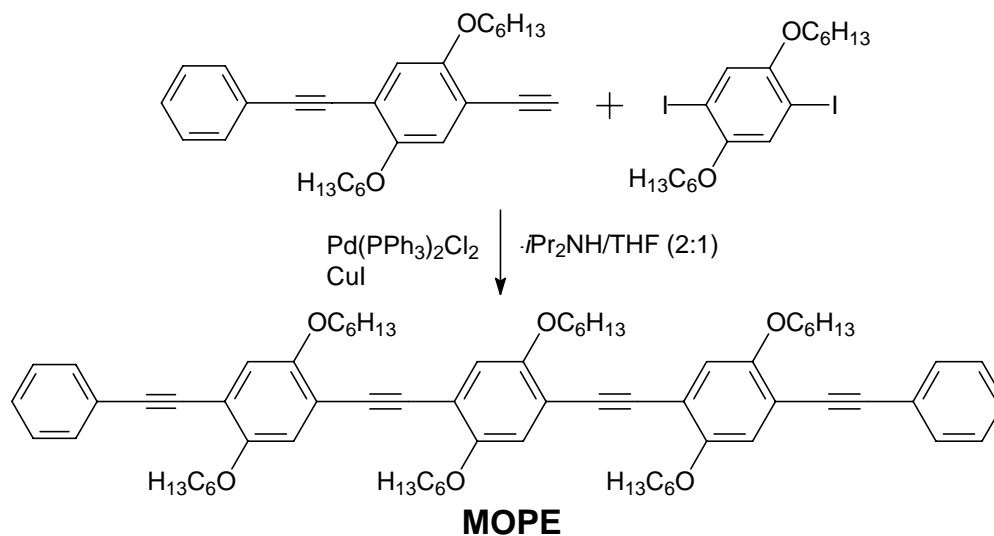
removed under reduced pressure and the residue was purified by column chromatography on silica gel using dichloromethane/hexane (1:2) **10** (2.34g, 75.0%) as white liquid. MS:  $m/z$  546.0.  $^1\text{H}$  NMR ( $\text{CDCl}_3$ ),  $\delta$  (ppm): 7.16 (s, 2 H), 3.94 (m, 4 H), 3.67 (m, 2 H), 2.18 (s, 1 H), 1.82-1.30 (m, 16 H), 0.90 (m, 3 H).  $^{13}\text{C}$  NMR ( $\text{CDCl}_3$ ),  $\delta$  (ppm): 153.09, 152.96, 122.97, 122.94, 86.53, 86.50, 70.56, 70.36, 63.11, 63.00, 34.11, 33.62, 29.92, 29.31, 26.12, 25.93, 22.82, 14.28. Anal. Calcd for  $\text{C}_{18}\text{H}_{28}\text{I}_2\text{O}_3$ : C, 39.58; H, 5.17; I, 46.47. Found: C, 39.54; H, 5.10.

#### **1,4-Bis((6-hexanol)oxy)-2,5-diiodobenzene (11)**

1,4-diiodo-2,5-hydroquinone (2.06 g, 5.70 mmol), 6-bromohexanol (2.27 g, 12.5 mmol),  $\text{K}_2\text{CO}_3$  (6.32 g, 45.8 mmol), and NaI (0.20 g, 1.29 mmol) were added to a round-bottom flask containing 2-butanone (40.0 mL). The mixture was heated at 70 °C for 24 hours under nitrogen atmosphere. The reaction mixture was filtered and the salts washed with dichloromethane. The filtrate was washed several times with NaOH solution (0.1 N), followed by distilled water, and dried over anhydrous sodium sulfate. The solvent was removed under reduced pressure and the residue was recrystallized from the mixture of dichloromethane/hexane (1:3) to give pure product **11** (2.34g, 73.0%) as white powder. MS:  $m/z$  562.0.  $^1\text{H}$  NMR ( $\text{CDCl}_3$ ),  $\delta$  (ppm): 7.16 (s, 2 H), 3.95 (m, 4 H), 3.68 (m, 4 H), 2.17 (s, 2 H), 1.82 (m, 4 H), 1.46-1.30 (m, 12H).  $^{13}\text{C}$  NMR ( $\text{CDCl}_3$ ),  $\delta$  (ppm): 153.02, 122.97, 86.51, 70.36, 63.14, 32.89, 29.31, 26.12, 25.64. Anal. Calcd for  $\text{C}_{18}\text{H}_{28}\text{I}_2\text{O}_4$ : C, 38.45; H, 5.02; I, 45.14. Found: C, 38.35; H, 4.90.



### Oligo(2,5-dihexyloxy-1,4-phenyleneethynylene (MOPE))



**Scheme 3.2.4** Synthetic routes for MOPE

A two-neck flask was charged with **8** (402 mg, 1 mmol), 1,4-dihexyloxy-2,5-diiodobenzene (265 mg, 0.500 mmol), CuI (19.0 mg, 0.100 mmol) and Pd(PPh<sub>3</sub>)<sub>2</sub>Cl<sub>2</sub> (70.2 mg, 0.100 mmol). It was degassed with three vacuum-nitrogen cycles and (iPr)<sub>2</sub>NH (26.0 mL) and THF (13.0 mL) were added at 0 °C. The reaction mixture was stirred at room temperature for 12 hours, and then it was subjected to water and extracted with dichloromethane. The combined organic solution was washed with water NH<sub>4</sub>OH (50%) twice, distilled water twice and brine twice and dried over anhydrous sodium sulfate. After removal of the solvent under reduced pressure, the residue was purified using a silica gel chromatograph with dichloromethane/hexane (1:2) as eluent to afford **MOPE** (421 mg, 78.0%) as light yellow crystal. MS: *m/z* 1078.6. <sup>1</sup>H NMR (CDCl<sub>3</sub>), δ (ppm): 7.53 (m, 4 H), 7.33 (m, 6), 7.01 (m, 6 H), 4.04 (m, 12 H), 1.85 (m, 12 H), 1.52 -1.34 (m, 36 H), 0.89 (m, 18 H). <sup>13</sup>C NMR (CDCl<sub>3</sub>), δ (ppm): 153.85, 153.71, 131.79, 128.5, 128.47, 123.69,

117.44, 117.33, 117.28, 114.49, 114.20, 95.11, 91.75, 86.23, 69.93, 69.88, 69.81, 31.85, 29.57, 29.51, 25.99, 25.91, 22.88, 14.28. Anal. Calcd for C<sub>74</sub>H<sub>94</sub>O<sub>6</sub>: C, 82.33; H, 8.78. Found: C, 82.24; H, 8.72.

### **Linear-shaped OH-functionalized OPE (OHOPE<sub>L</sub>)**

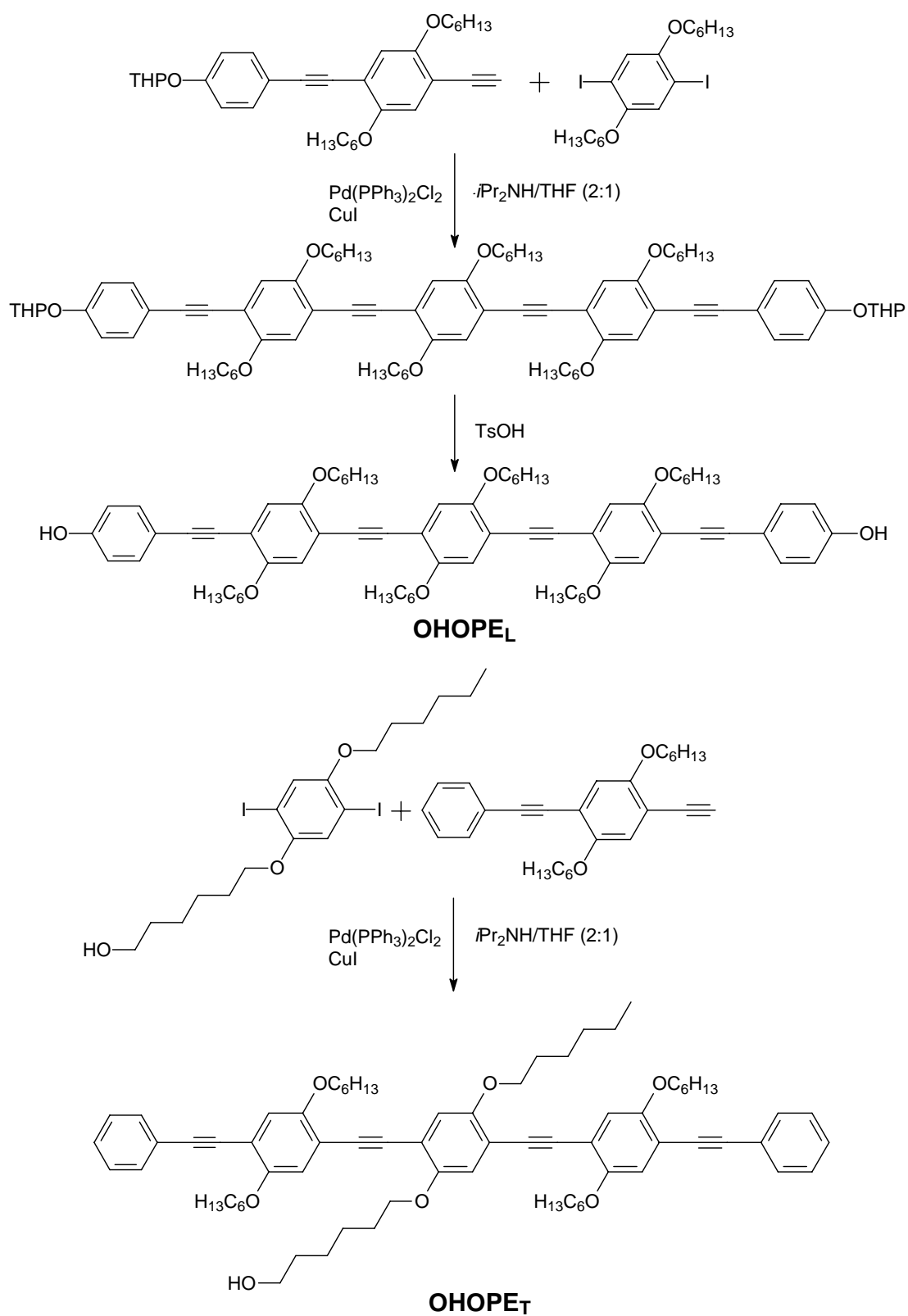
A two-neck flask was charged with **7** (502 mg, 1.00 mmol), 1,4-dihexyloxy-2,5-diiodobenzene (265 mg, 0.500 mmol), CuI (19.0 mg, 0.100 mmol) and Pd(PPh<sub>3</sub>)<sub>2</sub>Cl<sub>2</sub> (70.2 mg, 0.100 mmol). It was degassed with three vacuum-nitrogen cycles and (*i*Pr)<sub>2</sub>NH (26.0 mL) and THF (13.0 mL) were added at 0 °C. The reaction mixture was stirred at room temperature for 12 hours and it was then added into water and extracted with dichloromethane. The combined organic solution was washed with water NH<sub>4</sub>OH (50%) twice, distilled water twice and brine twice and dried over anhydrous sodium sulfate. After removal of the solvent under reduced pressure, the residue (about 600 mg) was obtained and dissolved in the mixture of THF (25.0 mL) and methanol (3.00 mL). *p*-Toluenesulfonic acid (0.490 g, 4.45 mmol) was added to the combined solution and stirred at 60 °C for 6 hours. After cooling, the solution was diluted with dichloromethane and washed twice with water and with once half-saturated brine to remove the catalyst, and dried over anhydrous sodium sulfate. After removal of the solvent under reduced pressure, the residue was purified using a silica gel chromatograph with dichloromethane/ethyl acetate (15:1) as eluent to afford **OHOPE<sub>L</sub>** (350mg, 63.0%) as yellow crystal. MS: *m/z* 1110.7. <sup>1</sup>H NMR (CDCl<sub>3</sub>), δ (ppm): 7.44 (d, 4 H), 7.00 (d, 4 H), 6.82 (s, 4 H), 5.00 (s, 2 H), 4.05 (m, 12

H), 1.85 (m, 12 H), 1.55-1.33 (m, 36 H), 0.90 (m, 18 H).  $^{13}\text{C}$  NMR ( $\text{CDCl}_3$ ),  $\delta$  (ppm): 153.86, 153.70, 150.71, 132.98, 121.79, 121.42, 117.43, 117.26, 114.66, 114.48, 113.88, 94.10, 91.83, 91.73, 86.21, 69.91, 69.87, 69.78, 31.83, 29.53, 29.50, 25.96, 25.91, 22.86, 14.26. Anal. Calcd for  $\text{C}_{74}\text{H}_{94}\text{O}_8$ : C, 79.96; H, 8.52. Found: C, 79.82; H, 8.50.

### **T-shaped OH-functionalized OPE (OHOPE<sub>T</sub>)**

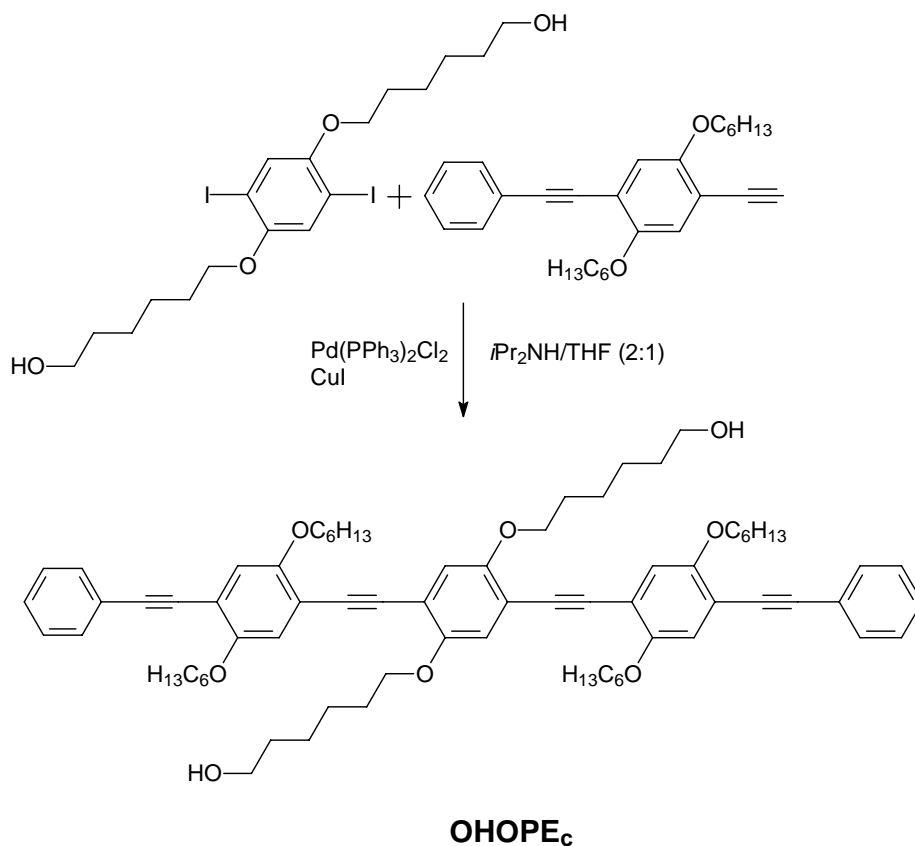
A two-neck flask was charged with **8** (402 mg, 1 mmol), **10** (273 mg, 0.500 mmol), CuI (19.0 mg, 0.100 mmol) and Pd(PPh<sub>3</sub>)<sub>2</sub>Cl<sub>2</sub> (70.2 mg, 0.100 mmol). It was degassed with three vacuum-nitrogen cycles and (*i*Pr)<sub>2</sub>NH (26.0 mL) and THF (13.0 mL) were added at 0 °C. The reaction mixture was stirred at room temperature for 12 hours and it was then added into water and extracted with dichloromethane. The combined organic solution was washed with water NH<sub>4</sub>OH (50%) twice, distilled water twice and brine twice and dried over anhydrous sodium sulfate. After removal of the solvent under reduced pressure, the residue was purified using a silica gel chromatograph with dichloromethane/ethyl acetate (10:1) as eluent to afford **OHOPE<sub>T</sub>** (329 mg, 60.0%) as yellow crystal. MS: *m/z* 1094.7.  $^1\text{H}$  NMR ( $\text{CDCl}_3$ ),  $\delta$  (ppm): 7.51 (m, 4 H), 7.32 (d, 6 H), 7.01 (s, 6 H), 4.05 (m, 12 H), 3.66(m, 2 H), 2.12(s, 1 H), 1.85 (m, 12 H), 1.70-1.35 (m, 36 H), 0.90 (m, 15 H).  $^{13}\text{C}$  NMR ( $\text{CDCl}_3$ ),  $\delta$  (ppm): 153.78, 153.68, 153.65, 131.80, 128.58, 128.45, 123.67, 117.62, 117.35, 117.279, 114.50, 114.42, 95.18, 91.74, 91.61, 86.22, 69.86, 69.78, 66.20, 31.89, 30.95, 30.78, 29.61, 29.54, 29.38, 25.95, 25.85, 25.82, 22.84, 14.32. Anal. Calcd for  $\text{C}_{74}\text{H}_{94}\text{O}_7$ : C, 81.13; H, 8.65.

Found: C, 81.09; H, 8.60.



Scheme 3.2.5 Synthetic routes for OHOPE<sub>L</sub> and OHOPE<sub>T</sub>

### Cross-shaped OH-functionalized OPE (**OHOPE<sub>C</sub>**)



**Scheme 3.2.6** Synthetic route for **OHOPE<sub>C</sub>**

A two-neck flask was charged with **8** (402 mg, 1 mmol), **11** (281 mg, 0.500 mmol), CuI (19.0 mg, 0.100 mmol) and Pd(PPh<sub>3</sub>)<sub>2</sub>Cl<sub>2</sub> (70.2 mg, 0.100 mmol). It was degassed with three vacuum-nitrogen cycles and then (iPr)<sub>2</sub>NH (26.0 mL) and THF (13.0 mL) were added at 0 °C. The reaction mixture was stirred at room temperature for 12 hours and it was then added into water and extracted with CH<sub>2</sub>Cl<sub>2</sub>. The combined organic solution was washed with water NH<sub>4</sub>OH (50%) twice, water twice and brine twice and dried over anhydrous sodium sulfate. After removal of the solvent under reduced pressure, the residue was purified using a silica gel chromatograph with dichloromethane/ethyl acetate (8:1) as eluent to afford **OHOPE<sub>C</sub>** (322 mg, 58%) as

yellow crystal. MS:  $m/z$  1110.7.  $^1\text{H}$  NMR ( $\text{CDCl}_3$ ),  $\delta$  (ppm): 7.54 (m, 4 H), 7.35 (m, 6 H), 7.01 (s, 6 H), 4.15 (t, 12 H), 3.68 (m, 4 H), 2.15 (s, 2 H), 1.85-1.35 (m, 48 H), 0.90 (m, 12 H).  $^{13}\text{C}$  NMR ( $\text{CDCl}_3$ ),  $\delta$  (ppm): 153.83, 153.72, 153.67, 131.78, 128.52, 128.46, 123.65, 117.63, 117.37, 117.32, 114.59, 114.36, 95.18, 91.77, 91.57, 86.18, 69.89, 69.82, 66.13, 31.85, 31.76, 30.78, 29.58, 29.50, 29.38, 26.10, 25.99, 25.92, 22.87, 14.30. Anal. Calcd for  $\text{C}_{74}\text{H}_{94}\text{O}_8$ : C, 79.96; H, 8.52. Found: C, 79.89; H, 8.46.

### 3.4 Results and Discussion

#### 3.4.1 Synthesis of Oligomers

The synthetic procedure for the hydroxyl-functionalized OPEs is depicted in Scheme 3.2.1-6. The procedure involves only two types of reaction: desilylation and Pd/Cu-catalyzed coupling reaction. The initial diiodobenzene derivatives were obtained from 1,4-diiodo-2,5-hydroquinone by Williamson ether reaction. Treatment of 2,5-dihexyloxy-1,4-diiodobenzene with one molar amount of (trimethylsilyl)acetylene gave 2,5-dihexyloxy-4-[(trimethylsilyl)ethynyl]-iodobenzene (**4**). Pd/Cu-catalyzed coupling of **4** with **6** and **4** with 1-ethynylbenzene and then removal of the protection group with base generated the desilylated dimer **7** and **8** respectively. Thus, after using a convergent method via a series of well-known organic reactions such as Sonogashira coupling reaction and Williamson ether reaction, the hydroxyl groups were integrated into the different positions of OPE. And the OPEs with different architectures were successfully

synthesized in satisfactory yields and denoted as **OHOPE<sub>L</sub>**, **OHOPE<sub>T</sub>**, and **OHOPE<sub>C</sub>**, respectively. Meanwhile, the model compound, oligo(2,5-dihexyloxy-1,4-phenyleneethynylene) (**MOPE**) to be used for comparison, was also prepared by a similar procedure. All of the hydroxyl functionalized oligomers possess very good solubility in common organic solvents such as chloroform and THF but insoluble in methanol, DMSO and DMF, just the same as PPEs. All OPEs are yellow powders.

### 3.4.2 NMR Spectroscopy

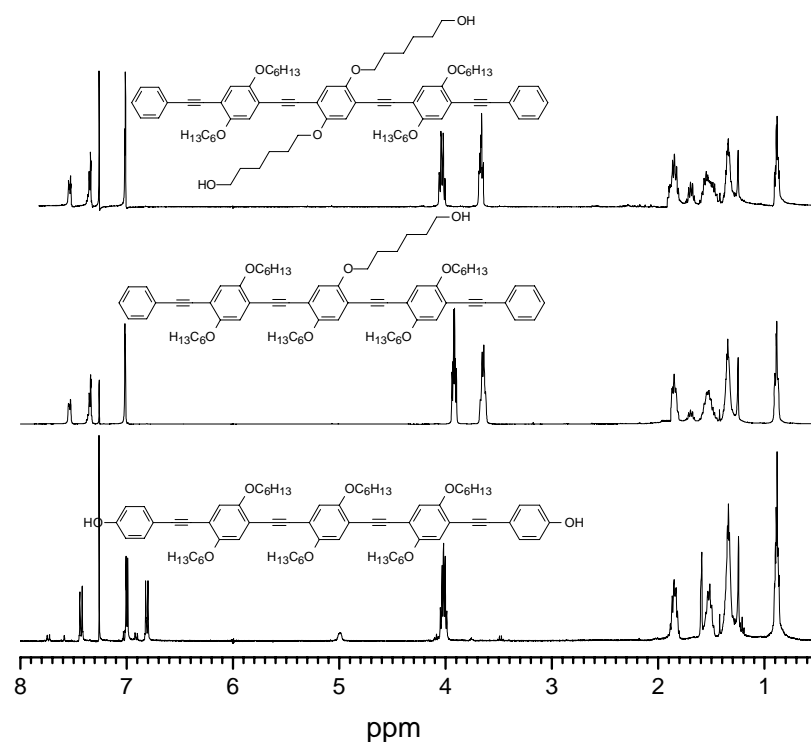


**Figure 3.1** <sup>1</sup>H NMR spectra of the functionalized OPEs

The chemical structures of these polymers were confirmed by <sup>1</sup>H and <sup>13</sup>C NMR. The <sup>1</sup>H and <sup>13</sup>C NMR spectra of oligomers coupled with hydroxyl groups are represented

in Figure 3.1 and Figure 3.2 respectively. In all  $^1\text{H}$  NMR spectra, the peak at 7.00 ppm corresponds to the hydrogen atoms on the benzene rings with alkoxy groups. The existence of the peak at 7.44 ppm and 6.80 assigned to the hydrogen atoms of the end phenol groups ( $-\text{CH}_2-$ ) of **OHOPE<sub>L</sub>** shows the successful incorporation of phenol groups into the linear oligomer. While for **OHOPE<sub>T</sub>** and **OHOPE<sub>C</sub>**, the peaks at 7.54 and 7.34 ppm attributing to the hydrogen atoms on benzene rings appeared, indicating that the molecular structure of **OHOPE<sub>T</sub>** and **OHOPE<sub>C</sub>** were ended with benzene rings. It was also shown that there only exists one peak of **OHOPE<sub>L</sub>** at 4.02 ppm assigned to the alkoxy group ( $-\text{CH}_2\text{OPh}$ ) attached to the benzene rings, while another peak at 3.65 ppm which is attributed to the hydrogen atoms near the hydroxyl group ( $-\text{CH}_2\text{OH}$ ) existed in **OHOPE<sub>T</sub>** and **OHOPE<sub>C</sub>**. This demonstrates that the hydroxyl groups were successfully introduced into the side chains of OPEs.

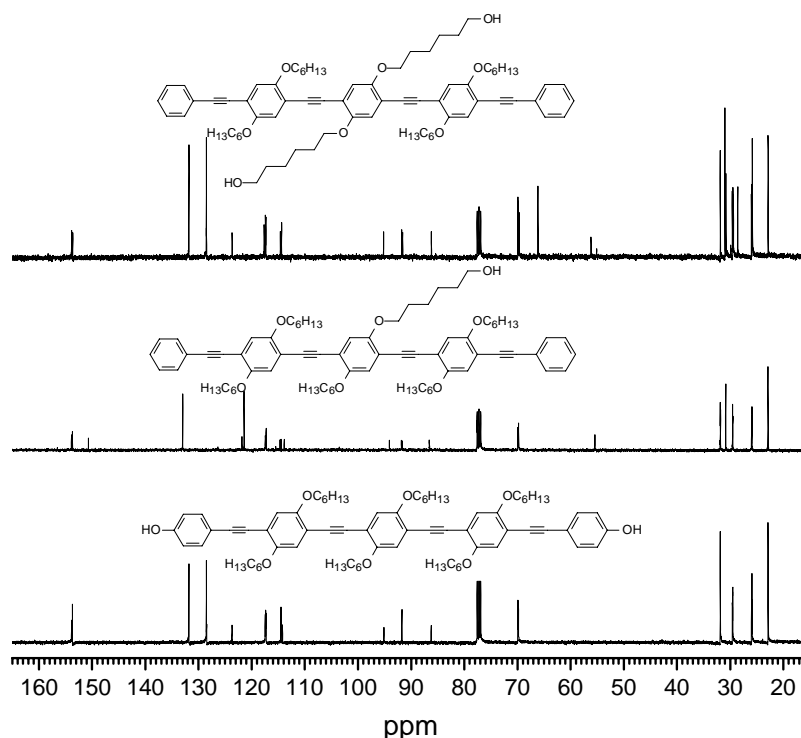


**Figure 3.2**  $^{13}\text{C}$  NMR spectra of the functionalized OPEs



Furthermore, the successful synthesis of OPEs can also be inferred from their  $^{13}\text{C}$  NMR spectra. In Figure 3.2, all OPEs exhibit the characteristic peaks at about 50 ppm which can be attributed to the methylene groups adjacent to the oxygen ( $-\text{CH}_2\text{O}-$ ) atoms, and three peaks at 95.2, 91.8 and 86.2 ppm corresponding to the ethynyl groups ( $-\text{C}\equiv\text{C}-$ ).

### 3.4.3 Water-Soluble Light-Emitting Nanoparticles

In a typical procedure to prepare the nanoparticles, 2 mL of  $\text{H}_2\text{O}$  was firstly added to 8mg and 40 mg of water-soluble polymers (PEG, PG, and PAA) under ultrasonic for 5 min respectively. 0.2 mL of OPEs (0.4 mg/ml in THF) was then added dropwise in those aqueous solutions with different polymer (PEG, PG and PAA) concentrations and the size of the nanoparticles so formed was measured by DLS (Table 3.1).

**Table 3.1 DLS Characterization data of the nanoparticles and the preparing proportion of OPEs and PAA**

Sample	Diameter (nm)	Polydispersity Index (PI)	OPE : PAA (weight ratio, in water)
OHOPE <sub>I</sub> /PAA-1	160	0.24	1 : 10
OHOPE <sub>I</sub> /PAA-2	112	0.18	1 : 50
OHOPE <sub>T</sub> /PAA-1	183	0.28	1 : 10
OHOPE <sub>T</sub> /PAA-2	120	0.16	1 : 50
OHOPE <sub>C</sub> /PAA-1	176	0.30	1 : 10
OHOPE <sub>C</sub> /PAA-2	126	0.20	1 : 50

It was found that after mixing with PAA in aqueous solution all the hydroxyl group functionalized OPEs dissolved in water to form a clear yellow aqueous solution. Also

the OHOPE/PAA micelles were very stable in aqueous solution and no precipitation was observed after three months in air. However, the control compound OPE (**MOPE**) without any functionalization precipitated in water instantly. These observations confirmed the existence of the interaction between OHOPEs and PAA through hydrogen bonds. It was also found that all the OHOPEs with different molecular architectures formed the water-soluble nanoparticles with similar sizes and polydispersity (see Table 3.1), which indicate that the formation of water-soluble OHOPE/PAA micelles in this work showed little connection with the molecular architecture and the position of hydroxyl group on the OHOPEs molecules. Furthermore, all of the micelles prepared from conjugated oligomers showed a smaller size and a lower polydispersity than those micelles prepared from conjugated polymers reported in Chapter 2. This can be attributed to the more regular molecular structure (monodispersity of conjugated backbone) and shorter conjugated length of OPEs than PPEs which will favor the formation of smaller self-assemble nanoparticles with a more regular structure.

**Table 3.2 DLS data of the nanoparticles and the prepared by OHOPE<sub>L</sub> and water-soluble polymers (PEG, PG or PAA)**

Sample	Diameter (nm)	Polydispersity Index (PI)	OPE : Water-soluble polymer (weight ratio, in water)
OHOPE <sub>L</sub> /PEG-1	1200	0.42	1 : 50
OHOPE <sub>L</sub> /PG-1	150	0.22	1 : 50
OHOPE <sub>L</sub> /PAA-1	112	0.18	1 : 50

The DLS data of water-soluble light-emitting nanoparticles prepared from **OHOPE<sub>L</sub>**

and different water-soluble polymers (PEG, PG, and PAA) are shown in Table 3.2. The **OHOPE<sub>L</sub>**/PEG system did not appear transparent and precipitated in water instantly. In comparison, both **OHOPE<sub>L</sub>**/PG and **OHOPE<sub>L</sub>**/PAA systems gave clear yellow aqueous solutions. From the DLS results, we observed that the **OHOPE<sub>L</sub>**/PEG system produced larger particles and higher polydispersity (1200 nm, PI = 0.42) compared to **OHOPE<sub>L</sub>**/PG (150 nm, PI = 0.22) and **OHOPE<sub>L</sub>**/PAA (112 nm, PI = 0.18) systems. Previously it was reported<sup>15-21</sup> that hydrogen bonds are generally the major driving force to form water-soluble micelles through the interaction between hydrophobic components and water-soluble components. Although there exists the hydrogen bonds in **OHOPE<sub>L</sub>**/PEG mixture from the interaction between the hydroxyl groups of **OHOPE<sub>L</sub>** and PEG, the lower content of hydroxyl groups in PEG (two hydroxyl groups per PEG chain) cannot provide a strong enough interaction between the two polymers which resulted in precipitation. Unlike PEG, PG has polyhydroxyl groups in each units that can provide relatively strong hydrogen bonds to form stable micelles with smaller size and lower polydispersity. Similarly, the stable **OHOPE<sub>L</sub>**/PAA micelles are also formed due to the strong hydrogen bonds between the carboxyl groups of PAA and the hydroxyl groups of **OHOPE<sub>L</sub>**. Thus, the micelle size and polydispersity are highly related to the activity of hydrogen atoms provided by the water-soluble polymers.

Fluorescence microscopy (Figure 3.3) and TEM (Figure 3.4) were used to further investigate the morphology of the nanoparticles. Fluorescence microscopy showed that the nanoparticles which emitted bluish green light are well dispersed in aqueous

solution. TEM photos show that the **OHOPE<sub>L</sub>/PAA** system forms nanoparticles in aqueous solution (diameter ranged from 100-200 nm).

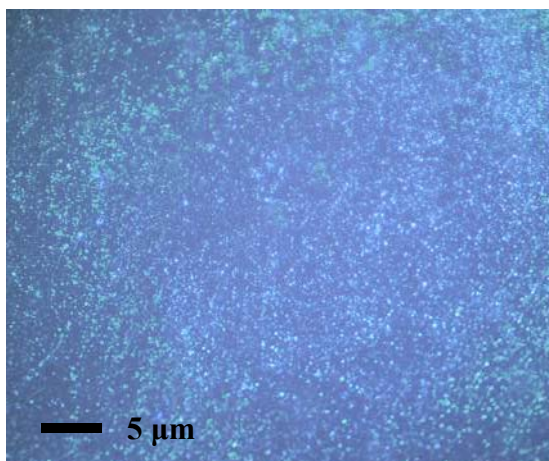


**Figure 3.3** Representative fluorescence micrograph of the **OHOPE<sub>L</sub>/PAA (1:50)** nanoparticles. The sample was observed in water.

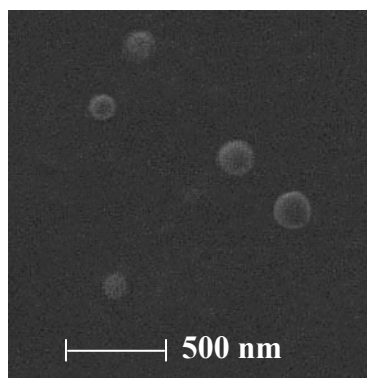


**Figure 3.4** Representative TEM micrographs of the **OHOPE<sub>L</sub>/PAA** nanoparticles obtained by freeze drying.

### 3.4.4 Optical Properties

#### 3.4.4.1 Solution-state Photophysics.

The UV-Vis and PL Spectra of all OPEs in dilute solution ( $10^{-6}$  mg/mL) are shown in Figure 3.5. In dilute solution ( $< 10^{-5}$  M) where interchain interaction is assumed to be

negligible, all OPEs exhibit the optical properties as single molecules do which are determined by the conjugated backbones only.<sup>22</sup> The nearly identical absorption and emission behaviors confirmed the same efficient conjugation length and the similar chain conformation in dilute solutions.<sup>23</sup> These OPEs in dilute solution showed an absorption maxima at 405 nm and a maximal emission peak at 446 nm. For sake of convenience, only **OHOPE<sub>L</sub>** will be used for the discussion in the following sections.

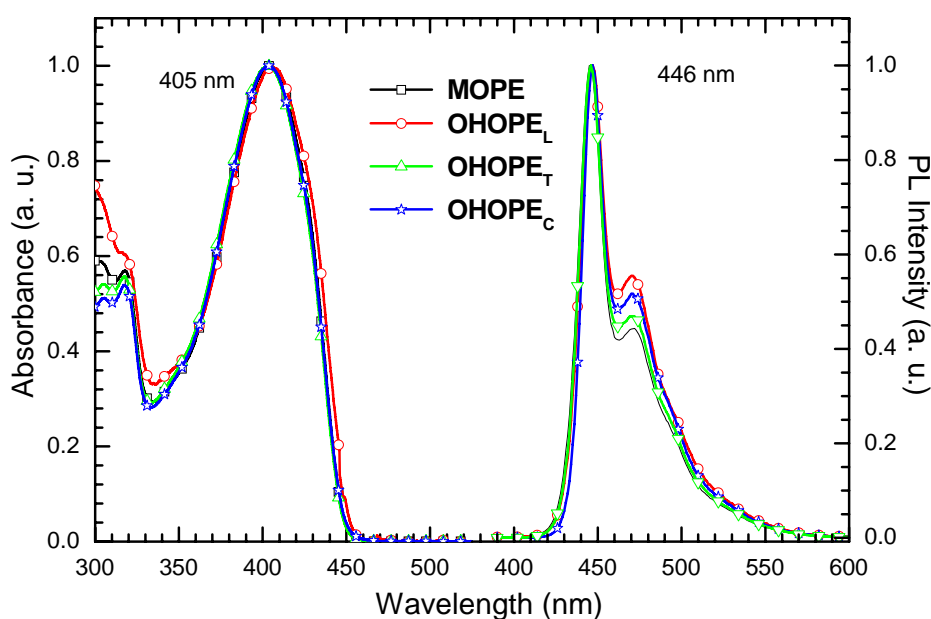


**Figure 3.5** UV-vis and PL spectra of those OPEs in THF ( $10^{-6}$  mg/mL)

In order to study the effect of solution concentration on the emission behavior of **OHOPE<sub>L</sub>**, the emission spectra of **OHOPE<sub>L</sub>** with a concentration of  $10^{-6}$  and 1 mg/mL are shown in Figure 3.6 respectively. Unlike in dilute solution, the molecular conformation is subjected to changes in concentrated solution which in turn will lead to shifts in the absorption and emission spectra.<sup>24</sup> The emission spectrum of **OHOPE<sub>L</sub>** at the concentrated solution (1 mg/mL) changes drastically in contrast to that of the

dilute solution ( $10^{-6}$  mg/mL). In the dilute solution, where unimolecular OPE chromophores are responsible, the maximal emission peak is formed at 446 nm. In the concentrated solution, it slightly red shifted to 452 nm by 6 nm, indicating the adoption of a more planar conformation in the concentrated solution. Furthermore, the relative intensity of emission peak at the long-wavelength side (470 nm) increases for the concentrated solution, which is consistent with the similar OPE compounds in the previous report and could be attributed to the formation of low energy sites,<sup>25</sup> a result from the enhanced efficient conjugated length derived from the more planar conformation.

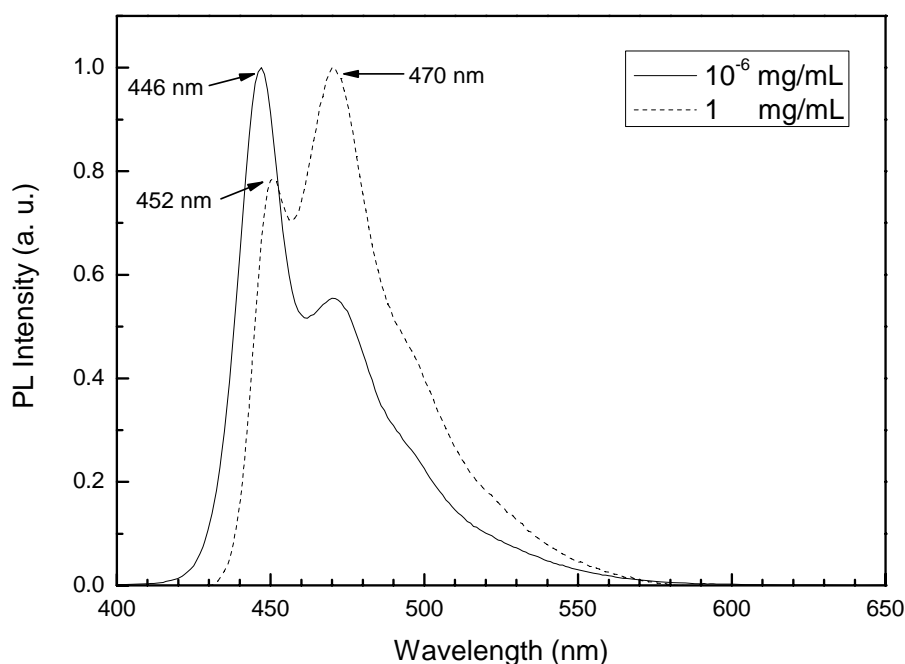


**Figure 3.6 Normalized PL emission spectra of OHOPE<sub>L</sub> in the dilute and concentrated solutions**

#### 3.4.4.2 Solid-state Photophysics

The solid-state absorption and emission spectra of OHOPE<sub>L</sub> are illustrated in Figure

3.7. The solid-state absorption spectrum of **OHOPE<sub>L</sub>** is complicated, featuring three peaks at 412, 423 nm and 450 nm, and all of them are red-shifted compared to the data in dilute solution at 405 nm. The solid-state emission spectrum of **OHOPE<sub>L</sub>** shows a maximal peak located at 492 nm with a 46 nm red-shift compared to the dilute solution state at 446 nm.

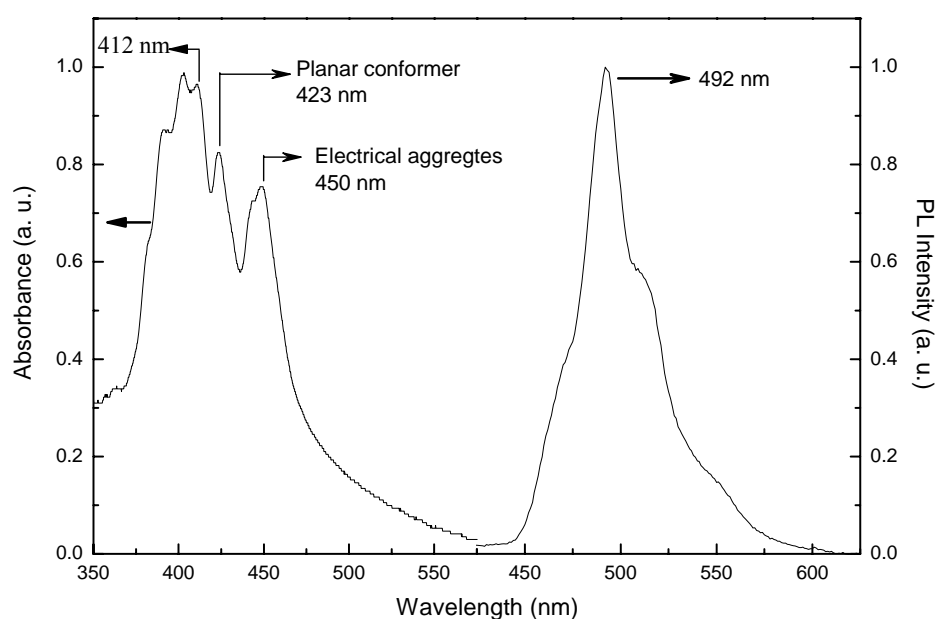


**Figure 3.7** Normalized UV and PL spectra of **OHOPE<sub>L</sub>** in the solid state

PPE systems in general show a significant conformation-dependent photophysical properties due to the relatively free rotation of the alkyne-ary single bonds along the backbone.<sup>26</sup> When transforming from the solution state into the solid state, the chain conformation will transfer from a twisted one into a more planar one. This increased planarity of the backbone will cause the slight red shift in absorption and emission spectra.<sup>27</sup> The pronounced red-shifted absorption peak at around 450 nm can be attributed to the interchain  $\pi$ -aggregation, which are the new ground-state species

formed by extending the delocalization of  $\pi$ -electrons over those chromophores.<sup>28</sup>

As for the PL spectrum, the decay dynamics of the emission peak at 492 nm is well fitted by a double-exponential with lifetimes of 0.62 ns (30%) and 2.0 ns (70%) (see Table 3.3).

This suggests that the two emission species, i.e., the unimolecule and the interchain  $\pi$ -aggregation, are responsible for the emission at 492 nm. According to the double-exponential decay dynamics, the domination of the longer lifetime (2.0 ns / 70%), confirms the formation of interchain  $\pi$ -aggregation.<sup>29</sup> Although this also confirmed the existence of unimolecule emission, the emission peak at 446nm was however not observed. This could be explained by the efficient energy transfer from unimolecules to the interchain  $\pi$ -aggregates in the solid state.<sup>23</sup>

#### **3.4.4.3 Optical Properties of Nanoparticles**

The UV-Vis absorption and photoluminescence emission spectra of OPE/PAA nanoparticles in aqueous solution are shown in Figure 3.8. All the nanoparticles showed similar absorption and emission spectra. Their absorption peaks are broad ranging from 375 to 475 nm, which contained all the three absorption peaks (412, 423 and 450 nm) observed for OHOPE films. The emission maxima of nanoparticles at around 490 nm is the same as that found in OHOPE films. This suggests that the interchain  $\pi$ -aggregation of OPEs existed in the nanoparticles just as it did in films. However, the nanoparticles exhibit broader absorption peaks without the fine features found in OHOPE films. This may be attributed to the complicated conformational



changes of OPE chains in the nanoparticles. We also found that the UV-Vis absorption and photoluminescence emission spectra of **OHOPE<sub>L</sub>/PEG**, **OHOPE<sub>L</sub>/PAA** and **OHOPE<sub>L</sub>/PG** nanoparticles in aqueous solution are alike, indicating the similar state of aggregation of OPEs in the corresponding nanoparticles.

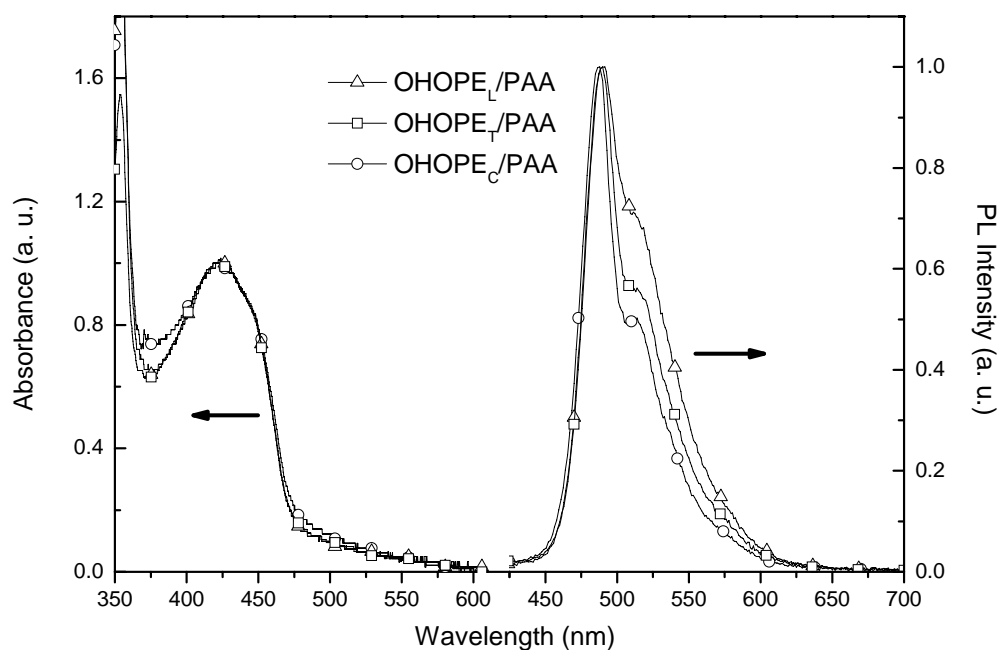


**Figure 3.8 UV-vis and PL spectra of the functionalized OPE/PAA nanoparticles in aqueous solution**

Time resolved photoluminescent measurements excited at 380 nm were used to study the optical properties (see Table 3.3). The OPEs in THF solution revealed a rapidly monoexponential decay and showed a fluorescence lifetime at  $\tau \approx 0.50$  ns, which is close to that of reported PPEs exhibiting unimolecular properties.<sup>29</sup> After formation of nanoparticles, the fluorescence decay changed into biexponential and can be fitted to two components with  $\tau \approx 0.50$  and 2 ns respectively. This biexponential decay in the nanoparticles is similar to that obtained in the solid state. As we have discussed

previously, the observed new long lifetime emission decay component confirmed the existence of OPEs interchain  $\pi$ -aggregation, and by the same token this aggregation also exists in the nanoparticles. It is reasonable to consider that after formation of nanoparticles, the hydrophobic OPE chains were encapsulated in the cores of the nanoparticles to form  $\pi$ -interchain aggregation, just as it did in the film state.

**Table 3.3 Photophysical properties of functionalized OPEs in THF, OPEs as films and OPE/PAA nanoparticles in aqueous solution**

	Solution		$\tau$ /ns at 492 nm (amplitude/%)	$\Phi_f$
	absorption $\lambda_{\max}$ /nm	emission $\lambda_{\max}$ /nm		
OHOPE <sub>L</sub> (in THF)	405	446	0.55 (100)	0.72
OHOPE <sub>T</sub> (in THF)	405	446	0.52 (100)	0.74
OHOPE <sub>C</sub> (in THF)	405	446	0.52 (100)	0.70
OHOPE <sub>L</sub> (as film)	412,423,450	492	0.62 (30),2.00 (70)	0.13
OHOPE <sub>T</sub> (as film)	412,423,450	492	0.59 (36),2.44 (64)	0.11
OHOPE <sub>C</sub> (as film)	412,423,450	492	0.55 (40),2.40 (60)	0.09
OHOPE <sub>L</sub> /PAA(micelle)	422	491	0.53 (25),2.60 (75)	0.12
OHOPE <sub>T</sub> /PAA(micelle)	422	489	0.49 (20),2.40 (80)	0.12
OHOPE <sub>C</sub> /PAA(micelle)	422	487	0.53 (28),2.88 (72)	0.11
OHOPE <sub>L</sub> /PEG(micelle)	422	491	0.57 (34),2.29 (66)	0.08
OHOPE <sub>L</sub> /PG(micelle)	422	489	0.53 (24),2.57 (76)	0.10

The  $\Phi_f$  values of those polymers in solutions were measured using the quinine sulfate solution (ca.  $1.0 \times 10^{-5}$  M) in 0.10 M H<sub>2</sub>SO<sub>4</sub> ( $\Phi_f = 55\%$ ) as a standard. The  $\Phi_f$  values of those polymers as films were measured using diphenylanthracene (dispersed in PMMA film with a concentration less than  $10^{-3}$  M, assuming  $\Phi_f = 81\%$ ) as a standard.

The fluorescence intensities of all OPEs are described in Table 3.3. After formation of nanoparticles, the fluorescence intensity of OPEs dramatically decreased from  $\Phi_f \approx$

0.70 in THF solution to  $\Phi_f \approx 0.10$ . The reduced fluorescence intensity of OPEs can also be attributed to the formation of interchain  $\pi$ -aggregation in nanoparticles.

### 3.5 Conclusion

In this chapter, we report the successful synthesis of hydroxyl group functionalized OPEs with the same conjugated length but of different molecular architectures, i.e., linear (**OHOPE<sub>L</sub>**), cross-shaped (**OHOPE<sub>C</sub>**) and T-shaped structure (**OHOPE<sub>T</sub>**). The interaction between these non-covalent bond self-assemblies with water-soluble polymers was investigated. The underlying photophysics of these OPEs was systematically studied by UV-vis, PL and time resolved photoluminescent analysis. In dilute solutions, all the OPEs exhibit almost identical absorption and emission characteristics due to the similar intrinsic photophysical properties where the unimolecular OPE chromophores are responsible. However, in the solid state, the absorption and emission spectra of OPEs are largely red-shifted owing to the formation of the interchain  $\pi$ -aggregation. The optical properties of OPE-based water-soluble nanoparticles exhibited the same properties as that found in OPE films, indicating the existence of interchain  $\pi$ -aggregation of OPEs in the nanoparticles. It was also found that the OPEs with different molecular architectures provided water-soluble nanoparticles with very similar size and dispersity, indicating that the formation of the nanoparticles was little influenced by the molecular architecture and the position of the hydroxyl groups. Furthermore, compared with the PPE-based nanoparticles discussed in Chapter 2, OPE-based nanoparticles exhibit smaller size and

lower dispersity, indicating that the structures of water-soluble nanoparticles are linked to the conjugated length. To investigate the effect of strength of hydrogen bonds between the OPEs and the water-soluble polymers, water-soluble polymers such as PEG, PG and PAA containing different active hydrogen were used to prepare the corresponding nanoparticles. The **OHOPE<sub>L</sub>/PG** and **OHOPE<sub>L</sub>/PAA** systems produced smaller particles and lower polydispersity than **OHOPE<sub>L</sub>/PEG** system. These results show a strong correlation between strength of hydrogen bonds and size and degree of dispersity of the nanoparticles so formed.

### References

1. Gaylord, B. S.; Massie, M. R.; Feinstein, S. C.; Bazan, G. C. *Proceedings of the National Academy of Sciences of the United States of America* **2005**, *102*, 34.
2. He, F.; Tang, Y. L.; Wang, S.; Li, Y. L.; Zhu, D. B. *Journal of the American Chemical Society* **2005**, *127*, 12343.
3. Ho, H. A.; Bera-Aberem, M.; Leclerc, M. *Chemistry-A European Journal* **2005**, *11*, 1718.
4. Ramey, M. B.; Hiller, J. A.; Rubner, M. F.; Tan, C. Y.; Schanze, K. S.; Reynolds, J. R. *Macromolecules* **2005**, *38*, 234.
5. Liang, Z.; Cabarcos, O. M.; Allara, D. L.; Wang, Q. *Advanced Materials* **2004**, *16*, 823.
6. Hoeben, F. J. M.; Jonkheijm, P.; Meijer, E. W.; Schenning, A. P. H. J. *Chemical Reviews* **2005**, *105*, 1491.

7. Jonkheijm, P.; van Duren, J. K. J.; Kemerink, M.; Janssen, R. A. J.; Schenning, A. P. H. J.; Meijer, E. W. *Macromolecules* **2006**, *39*, 784.
8. Van Herrikhuyzen, J.; Jonkheijm, P.; Schenning, A. P. H. J.; Meijer, E. W. *Organic & Biomolecular Chemistry* **2006**, *4*, 1539.
9. Matthews, J. R.; Goldoni, F.; Schenning, A. P. H. J.; Meijer, E. W. *Chemical Communications* **2005**, 5503.
10. Disney, M. D.; Zheng, J.; Swager, T. M.; Seeberger, P. H. *Journal of the American Chemical Society* **2004**, *126*, 13343.
11. Wu, C. F.; Szymanski, C.; McNeill, J. *Langmuir* **2006**, *22*, 2956.
12. Kurokawa, N.; Yoshikawa, H.; Hirota, N.; Hyodo, K.; Masuhara, H. *Chemphyschem* **2004**, *5*, 1609.
13. Kietzke, T.; Neher, D.; Landfester, K.; Montenegro, R.; Guntner, R.; Scherf, U. *Nature Materials* **2003**, *2*, 408.
14. Qiang, L. L.; Fan, Q. L.; Ma, Z.; Zheng, Z.; Wang, Y. Y.; Zhang, G. W.; Huang, W. *Chemistry Letters* **2005**, *34*, 1164.
15. Liu, S. Y.; Zhang, G. Z.; Jiang, M. *Polymer* **1999**, *40*, 5449.
16. Wang, M.; Jiang, M.; Ning, F. L.; Chen, D. Y.; Liu, S. Y.; Duan, H. W. *Macromolecules* **2002**, *35*, 5980.
17. Zhang, Y. W.; Jiang, M.; Zhao, J. X.; Zhou, J.; Chen, D. Y. *Macromolecules* **2004**, *37*, 1537.
18. Jiang, M.; Duan, H. W.; Chen, D. Y. *Macromolecular Symposia* **2003**, *195*, 165.
19. Liu, S. Y.; Jiang, M.; Liang, H. J.; Wu, C. *Polymer* **2000**, *41*, 8697.

20. Yuan, X. F.; Zhao, H. Y.; Jiang, M.; An, Y. L. *Acta Chimica Sinica* **2000**, *58*, 118.
21. Yuan, X. F.; Jiang, M.; Zhao, H. Y.; Wang, M.; Zhao, Y.; Wu, C. *Langmuir* **2001**, *17*, 6122.
22. (a) Pang, Y.; Chu, Q. H. *Macromolecules*, **2003**, *36*, 4614-4618. (b) Chu, Q.; Pang, Y. *Macromolecules* **2005**, *38*, 517-520.
23. Schwartz, B. J. *Annu. Rev. Phys. Chem.* **2003**, *54*, 141-172.
24. (a) Bouchard, J.; Belletête, M.; Durocher, G.; Leclerc, M. *Macromolecules* **2003**, *36*, 4624-4630. (b) Lee, Y. Z.; Chen, X.; Chen, S.; Wei, P. K.; Fann, W. S. *J. Am. Chem. Soc.* **2001**, *123*, 2296-2307. (c) Halkyard, C. E.; Rampey, M. E.; Kloppenburg, L.; Studer-Martinez, S. L.; Bunz, U. H. F. *Macromolecules*, **1998**, *31*, 8655-8659.
25. (a) Ickenroth, D.; Weissmann, S.; Rumpf, N.; Meier, H. *Eur. J. Org. Chem.* **2002**, 2808-2814. (b) Li, H.; Powell, D. R.; Firman, T. K.; West, R. *Macromolecules* **1998**, *31*, 1093-1098.
26. (a) Beeby, A.; Findlay, K.; Low, P. J.; Marder, T. B. *J. Am. Chem. Soc.* **2002**, *124*, 8280-8284. (b) James, P. V.; Sudeep, P. K.; Suresh, C. H.; Thomas, K. G. *J. Phys. Chem. A* **2006**, *110*, 4329-4337. (c) Liu, L. T.; Yaron, D.; Sluch, M. I.; Berg, M. A. *J. Phys. Chem. B* **2006**, *110*, 18844-18852.
27. (a) Kim, J.; Swager, T. M. *Nature (London)* **2001**, *411*, 1030-1034. (b) Kim, J.; Levitsky, I. A.; McQuade, D. T.; Swager, T. M. *J. Am. Chem. Soc.* **2002**, *124*, 7710-7718. (c) Zahn, S.; Swager, T. M. *Angew. Chem. Int. Ed.* **2002**, *41*,

4225-4230.

28. (a) Jenekhe, S. A.; Osaheni, J. A. *Science* **1994**, *265*, 765-768. (b) Kim, Y.; Bouffard, J.; Kooi, S. E.; Swager, T. M. *J. Am. Chem. Soc.* **2005**, *127*, 13726-13731. (c) Como, E. D.; Loi, M. A.; Murgia, M.; Zamboni, R.; Muccini, M. *J. Am. Chem. Soc.* **2006**, *128*, 4277-4281.
29. (a) Peng, K. Y.; Chen, S. A.; Fann, W. S. *J. Am. Chem. Soc.* **2001**, *123*, 11388-11397. (b) Wang, S.; Wu, P.; Han, Z. *Macromolecules* **2003**, *36*, 4567-4576. (c) Chen, Y.; Wang, S.; Zhuang, Q.; Li, X.; Wu, P.; Han, Z. *Macromolecules* **2005**, *38*, 9873-9877.

## CHAPTER FOUR

### Study on Optical Properties and Fluorescence Quenching of Water-Soluble Light-Emitting Nanoparticles

#### 4.1 Introduction

Fluorescent water-soluble conjugated polymers (FWSCPs) containing charged groups are promising candidates as novel chemo- or biosensors due to their amplified fluorescence quenching upon electrostatic attraction by ionic quenchers.<sup>1</sup> Anionic water-soluble sulfonated poly(phenylene vinylene) (MPS-PPV) was among the first FWSCPs to be studied and it was shown that its fluorescence can be effectively quenched by cationic electron acceptors, such as methyl viologen ( $MV^{2+}$ ).<sup>2</sup> FWSCPs can be used as a simple way to detect different types of biomolecules through observing the fluorescence quenching/recovering process. Recently FWSCPs containing charged groups have been successfully developed to detect proteins and DNA.<sup>3</sup>

It is known that the fluorescence sensitivity of FWSCPs is influenced by the local chemical environment since their optical properties are strongly controlled by the conformation of conjugated main chains which varies according to the variation in the chemical environment, such as ionic strength,<sup>4</sup> pH,<sup>5,6</sup> charge on quencher,<sup>7</sup> concentration of surfactant<sup>8</sup> or polyelectrolyte.<sup>9,10</sup>

Ionic FWSCPs have been the subject of intensive studies.<sup>2-11</sup> Recently, novel water-soluble light-emitting nanoparticles with conjugated polymers or oligomers as



cores have been developed via simple non-covalent self-assembly. However, studies on fluorescence quenching of such conjugated polymer- or oligomer-containing water-soluble nanoparticles are little reported, which may have limited the use of these water-soluble nanoparticles as chemo- or biosensors.

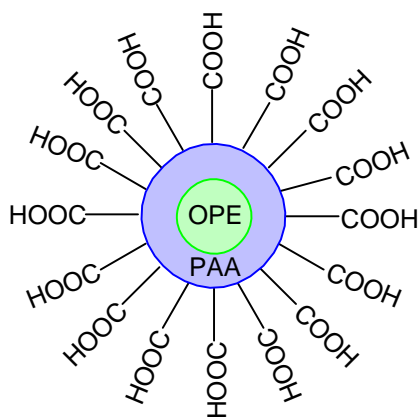
Poly(*p*-phenyleneethynylene) (PPE) or oligo(*p*-phenyleneethynylene) (OPE) have been widely used to study optical property-structure relationship because of their good optical response to change in environmental conditions through the facial changeable torsion angle and interchain aggregation. Their applications as chemosensors have been widely reported<sup>12-16</sup> and recently water-soluble PPEs were developed to detect DNA<sup>17</sup>. Furthermore, they were used to study the contribution of polymer aggregation on fluorescence quenching.<sup>18</sup> We reported in the last chapter the successful preparation of water-soluble light-emitting nanoparticles through non-covalent self-assembly of hydroxyl group functionalized OHOPEs with water-soluble polymers (PAA, PEG and PG). To develop these nanoparticles for chemo- or biosensor applications, we report here the study of optical properties of anionic light-emitting nanoparticles prepared from OHOPE<sub>L</sub> and PAA via non-covalent self-assembly and the effects of typical quenchers such as MV<sup>2+</sup> and Fe(CN)<sub>6</sub><sup>4-</sup> on these nanoparticles in different chemical environments.

## 4.2 Molecular Design

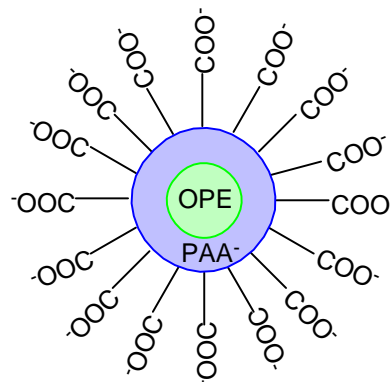
In order to prepare anionic light-emitting nanoparticles, the OHOPE<sub>L</sub>/PAA nanoparticles were neutralized with sodium hydroxide in solution to form anionic

light-emitting nanoparticles. The chemical structures of the nanoparticles and the quenchers are illustrated in Scheme 4. 1.

**Nanoparticles:**

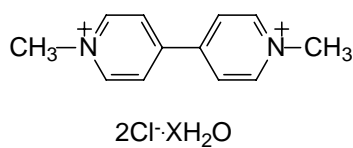


**OHPE/PAA nanoparticles**

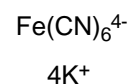


**OHPE/PAA<sup>-</sup> nanoparticles**

**Quencher:**



**MV<sup>2+</sup>**



**Scheme 4.1 Neutral/anionic water-soluble nanoparticles and quenchers**

### 4.3 Experimental

#### 4.3.1 Materials

Water-soluble conjugated oligomer-based light-emitting nanoparticles, OHPE<sub>L</sub>/PAA, were prepared according to the procedure described in Chapter 3. The quenchers, methyl viologen dichloride hydrate (MV<sup>2+</sup>) and K<sub>4</sub>Fe(CN)<sub>6</sub>, were obtained from

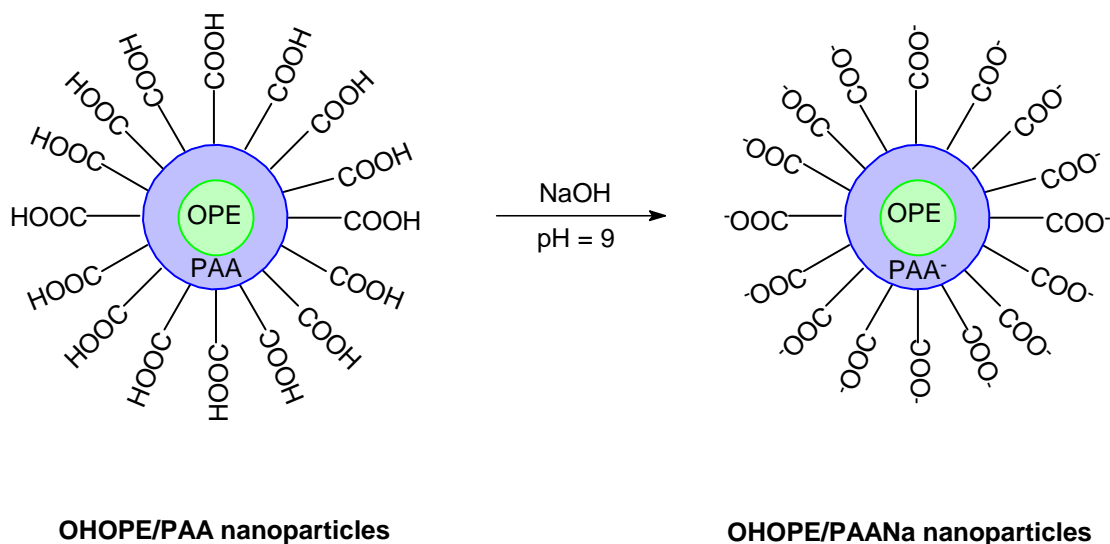
Aldrich Chemical Co. The chemical structures of the compounds are shown in Scheme 4.1. The Milli-Q water used in preparing the aqueous solutions of the polymers and quenchers was purged with nitrogen for 4 h before use.

#### **4.3.2 Characterization Methods**

UV-vis spectra were recorded on a Shimadzu 3101 PC spectrometer. Fluorescence measurement was carried out on a Perkin-Elmer LS 50B photoluminescence spectrometer with a xenon lamp as a light source. The quenching studies were realized *in situ* through comparing the photoluminescence intensities of the solutions with different water-soluble nanoparticle and quencher concentrations. All the quenched solutions were prepared by adding the calculated amount of quencher solution into the water-soluble light-emitting solution and purging with nitrogen for 1 min before taking their corresponding absorption and emission spectra with excitation at 386 nm. The optical properties of the anionic nanoparticle solution with no quencher were also determined for comparison purposes.

#### **4.3.3 Preparation of anionic nanoparticles**

The anionic OHOPE<sub>L</sub>/PAA<sup>-</sup> nanoparticles were obtained after adjusting the pH of 2 mL of OHOPE<sub>L</sub>/PAA nanoparticle aqueous solution (obtained in Chapter 3) to 9 by adding 0.01 N NaOH aqueous solution.



**Scheme 4.2 Preparation of anionic water-soluble nanoparticles**

## 4.4 Results and Discussion

### 4.4.1 General properties of OHOPE<sub>L</sub>/PAA<sup>-</sup> nanoparticles

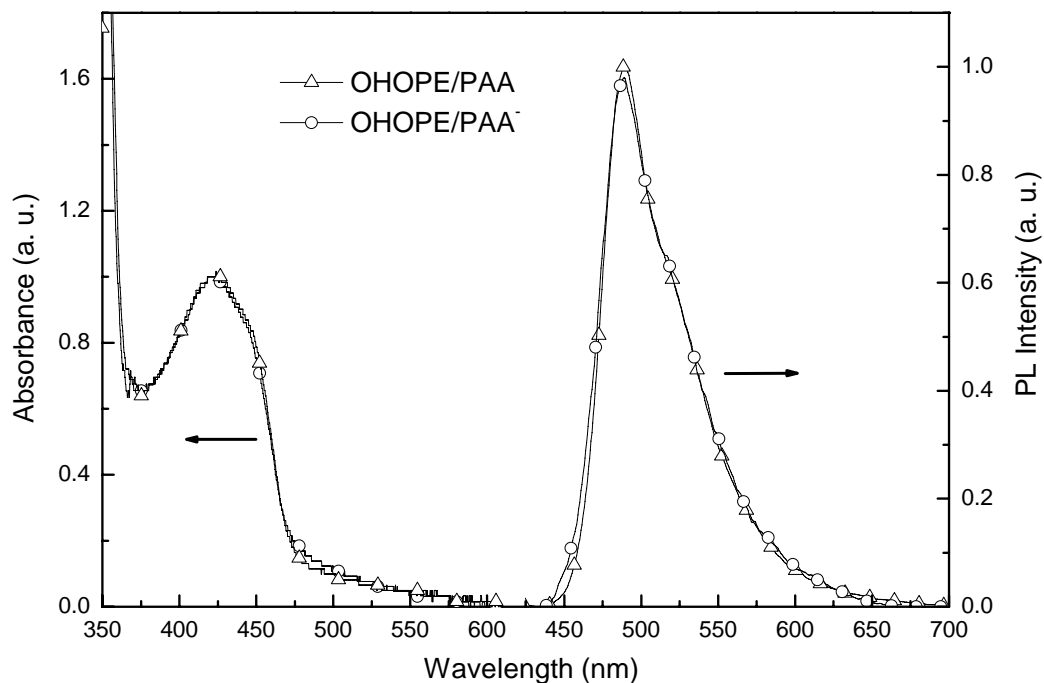


**Figure 4.1 UV-vis and PL spectra of the neutral OHOPE<sub>L</sub>/PAA and anionic OHOPE<sub>L</sub>/PAA<sup>-</sup> nanoparticles in aqueous solution**

The absorption and emission spectra of the neutral OHOPE<sub>L</sub>/PAA and anionic OHOPE<sub>L</sub>/PAA<sup>-</sup> nanoparticles in aqueous solution are shown in Figure 4.1 and other photophysical data are listed in Table 4.1. The results show that the ionized OHOPE<sub>L</sub>/PAA<sup>-</sup> nanoparticles exhibit similar optical properties to the neutral OHOPE<sub>L</sub>/PAA nanoparticles, indicating that the anionic groups has little effect on the optical properties of the nanoparticles.

**Table 4.1 Photophysical properties of the neutral OHOPE<sub>L</sub>/PAA and anionic OHOPE<sub>L</sub>/PAA<sup>-</sup> nanoparticles in aqueous solution**

micelles	Solution		$\tau$ /ns at 500 nm (amplitude/%)	$\Phi_f$
	absorption $\lambda_{\max}$ /nm	emission $\lambda_{\max}$ /nm		
OHOPE <sub>L</sub> /PAA	422	489	0.53 (25), 2.60 (75)	0.12
OHOPE <sub>L</sub> /PAA <sup>-</sup>	422	489	0.49 (20), 2.40 (80)	0.12

#### 4.4.2 Fluorescence quenching of nanoparticles by MV<sup>2+</sup>

The high fluorescence sensitivity of FWSCPs as chemo- or biosensors is derived from their rapid and collective response to quenchers.<sup>1</sup> Because of the facile electron and energy migration along the conjugated backbone and the strong binding force between the quencher and FWSCP by electrostatic attraction, the fluorescence emission of FWSCPs can be easily quenched by trace amount of quencher through electron or energy transfer.

Generally the fluorescence quenching includes static quenching and dynamic quenching. Each quenching behavior can be described by the Stern-Volmer

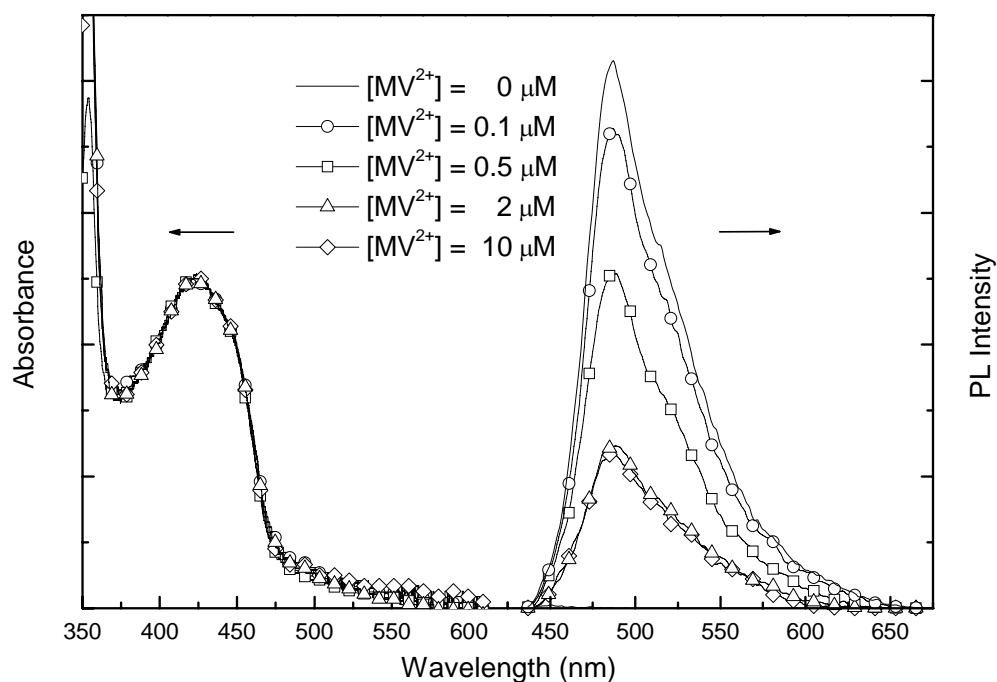
equation:<sup>19</sup>

$$F_0/F = 1 + K_{sv}[Q] \quad (1)$$

In this equation,  $F_0$  is the fluorescence intensity without adding quencher,  $F$  is the fluorescence intensity with quencher,  $[Q]$  is the quencher concentration and  $K_{sv}$  is the Stern-Volmer constant which represents the efficiency of fluorescence quenching. Both dynamic and static quenching follow linear Stern-Volmer plot ( $F_0/F \sim [Q]$ ). However, when the dynamic quenching and static quenching exist simultaneously, Equation (1) must be modified and the plot is curved upward.<sup>19</sup> Both the linear and upward Stern-Volmer curves have been observed in WSCPs.<sup>2,3,6,20</sup>

In this work the quenching behavior of OHOPE<sub>L</sub>/PAA<sup>-</sup> nanoparticles was studied by the reaction with cationic quencher MV<sup>2+</sup>. MV<sup>2+</sup> has previously been used as a quencher to investigate the quenching behavior of anionic PPV<sup>22</sup> and PPE.<sup>17</sup> Figure 4.2 shows the UV-vis and emission spectra of OHOPE<sub>L</sub>/PAA<sup>-</sup> nanoparticles at 1 μM (the concentration of OHOPE<sub>L</sub>) after addition of quencher MV<sup>2+</sup> of different concentrations. Both absorption and emission spectra exhibited very small spectral changes in terms of the shape and wavelength of the absorption and emission peaks as shown in Figure 4.2. This is different to the quenching of PPE-SO<sub>3</sub><sup>-</sup> by MV<sup>2+</sup>,<sup>17</sup> in which a new red-shifted absorption peak and broadened emission spectrum were observed which could be attributed to the formation of PPE-SO<sub>3</sub><sup>-</sup> aggregates induced by the addition of MV<sup>2+</sup>. These results show that the state of aggregation of OPE chains in the cores of the nanoparticles is not much influenced by the MV<sup>2+</sup> absorbed on the surface. Besides, the decrease in fluorescence intensity of the nanoparticles

with increase in concentration of the quencher indicates that it is not the interchain aggregation but the fluorophore-quencher interaction (electron transfer) that is responsible for the fluorescence quenching of nanoparticles in our system.



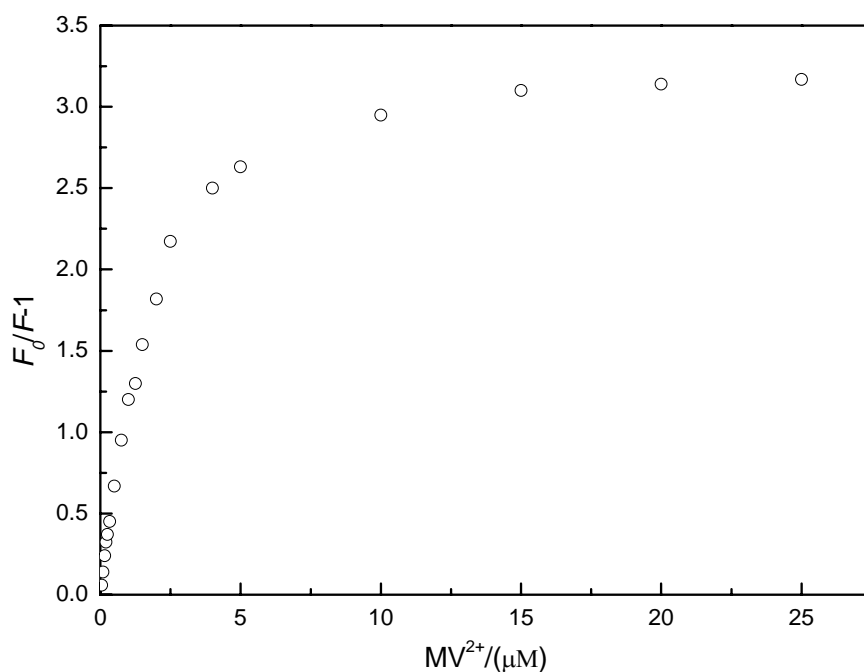
**Figure 4.2 UV-vis absorbance and PL emission spectra of nanoparticles in aqueous solution quenched by  $MV^{2+}$  in different concentrations**

Figure 4.3 shows the Stern-Volmer plot for OHOPE<sub>L</sub>/PAA<sup>-</sup> nanoparticles with  $MV^{2+}$  as the quencher. It describes an interesting Stern-Volmer plot which is curved upward and a constant level of quenching beyond about 15  $\mu M$  of  $MV^{2+}$ . Such a Stern-Volmer plot can be explained by the existence of two fluorophores: accessible and inaccessible fluorophores.<sup>21</sup> When a quencher is introduced, only those accessible fluorophores are quenched but the inaccessible ones remain unreacted. Based on this assumption, a modified equation was derived to describe the relationship between the fluorescence intensity and quencher concentration<sup>22</sup>:

$$F_0/(F_0 - F) = 1/(f_a K_{sv}[Q]) + 1/f_a \quad (3a)$$

$$f_a = F_{0a}/(F_{0a} + F_{0b}) \quad (3b)$$

where  $F_{0a}$  is the fluorescence intensity from an accessible fluorophore,  $F_{0b}$  is the fluorescence intensity from an inaccessible fluorophore and  $f_a$  is the fraction of fluorescence from an accessible fluorophore.



**Figure 4.3 Unmodified Stern-Volmer plot of anionic OHOPE<sub>L</sub>/PAA<sup>-</sup> nanoparticles quenched by MV<sup>2+</sup>**

The modified Stern-Volmer plot for OHOPE<sub>L</sub>/PAA<sup>-</sup> nanoparticles according to Equation (3a) is shown in Figure 4.4 and a linear dependence of  $F_0/(F_0 - F)$  on  $[1/MV^{2+}]$  can be observed.  $f_a = 0.78$  and  $K_{sv} = 2.2 \times 10^6 \text{ M}^{-1}$  were determined from the intercept and the slope of the plot, respectively. This  $K_{sv}$  value indicates an efficient fluorescence quenching of OHOPE<sub>L</sub>/PAA<sup>-</sup> nanoparticles by the quenchers through static electronic interaction. 22% of the inaccessible fluorophore probably



stems from the OHOPE<sub>L</sub> chains buried in the nanoparticle core which are hard to reach by the quenchers.

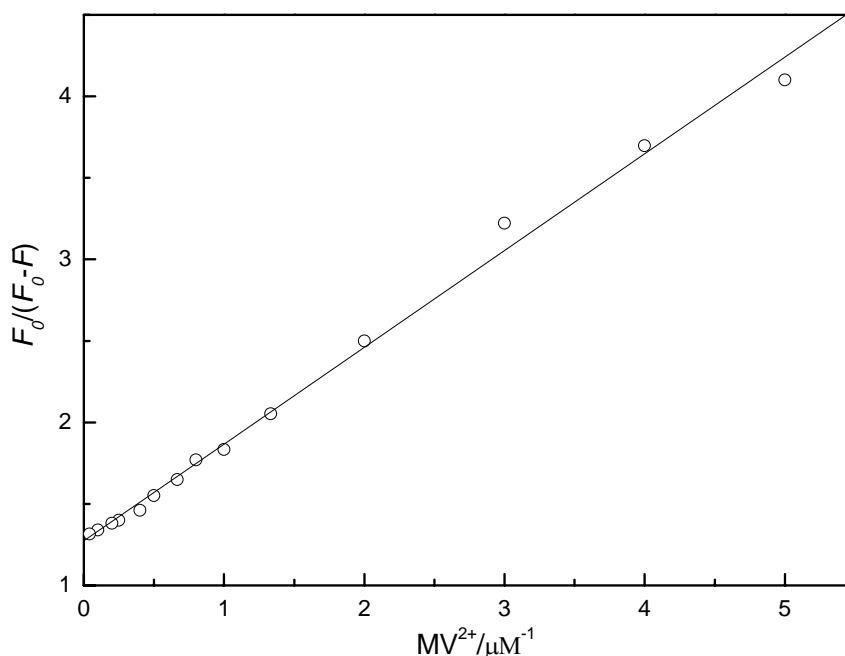


**Figure 4.4 Modified Stern-Volmer plot for anionic OHOPE<sub>L</sub>/PAA<sup>-</sup> nanoparticles in Figure 4.3**

#### 4.4.3 The influence of electrostatic interaction on fluorescence quenching

The influence of electrostatic interaction on the fluorescence quenching of nanoparticles was further investigated. Figure 4.5 shows the unmodified and modified Stern-Volmer plots of anionic OHOPE<sub>L</sub>/PAA<sup>-</sup> nanoparticles quenched by Fe(CN)<sub>6</sub><sup>4-</sup> and neutral OHOPE<sub>L</sub>/PAA nanoparticles quenched by MV<sup>2+</sup> as well as Fe(CN)<sub>6</sub><sup>4-</sup> in aqueous solution. In Figure 4.5 A, all the unmodified Stern-Volmer plots are curved upward but not linear which further confirmed the existence of inaccessible fluorophore. Anionic OHOPE<sub>L</sub>/PAA<sup>-</sup> nanoparticles are more sensitive to MV<sup>2+</sup> ( $K_{sv} = 2.2 \times 10^6 \text{ M}^{-1}$ , obtained from Figure 4.4) than Fe(CN)<sub>6</sub><sup>4-</sup> ( $K_{sv} = 190 \text{ M}^{-1}$ , obtained from

Figure 4.5 B), indicating that electrostatic attraction between ionic nanoparticles and quenchers is the main driving force to effect fluorescence quenching. Compared to anionic OHOPE<sub>L</sub>/PAA<sup>-</sup> nanoparticles, neutral OHOPE<sub>L</sub>/PAA nanoparticles showed lower fluorescence sensitive to MV<sup>2+</sup> ( $K_{sv} = 3.3 \times 10^3 \text{ M}^{-1}$ ) and Fe(CN)<sub>6</sub><sup>4-</sup> ( $K_{sv} = 810 \text{ M}^{-1}$ ), respectively. This further demonstrates the effects of electrostatic attraction on the quenching behavior of those nanoparticles.

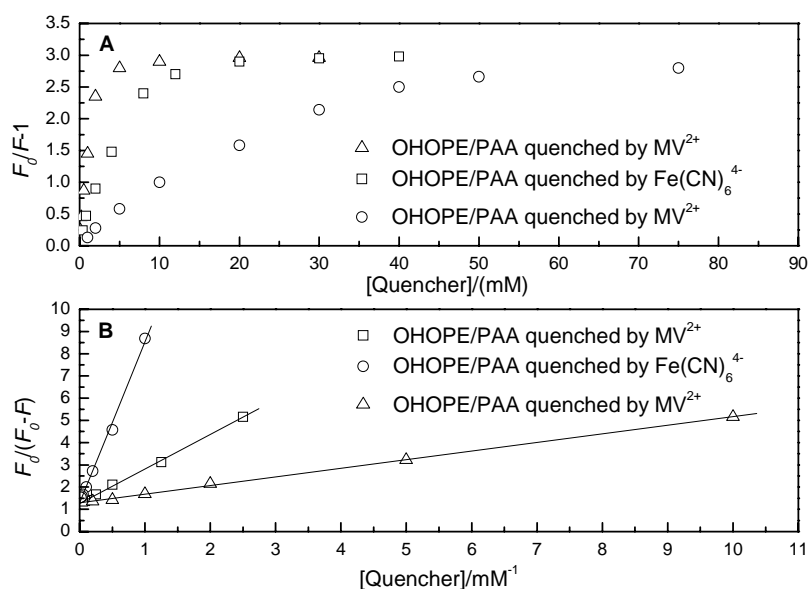


**Figure 4.5 A: Unmodified and B: Modified Stern-Volmer plots of OHOPE<sub>L</sub>/PAA<sup>-</sup> nanoparticles quenched by Fe(CN)<sub>6</sub><sup>4-</sup> and OHOPE<sub>L</sub>/PAA nanoparticles quenched by Fe(CN)<sub>6</sub><sup>4-</sup> and MV<sup>2+</sup>**

#### 4.4.4 The influence of the nanoparticles concentration on fluorescence quenching

Figure 4.6 shows the selected UV-vis absorption and emission spectra of OHOPE<sub>L</sub>/PAA<sup>-</sup> nanoparticles in different concentrations ( $c = 1, 10$  and  $50 \mu\text{M}$ ) in water. No spectra shift can be observed with the increase of OHOPE<sub>L</sub>/PAA<sup>-</sup>

nanoparticles concentration, which suggests that the conformation of  $\text{OHOPE}_L/\text{PAA}^-$  nanoparticles in water remains unchanged in different concentrations.

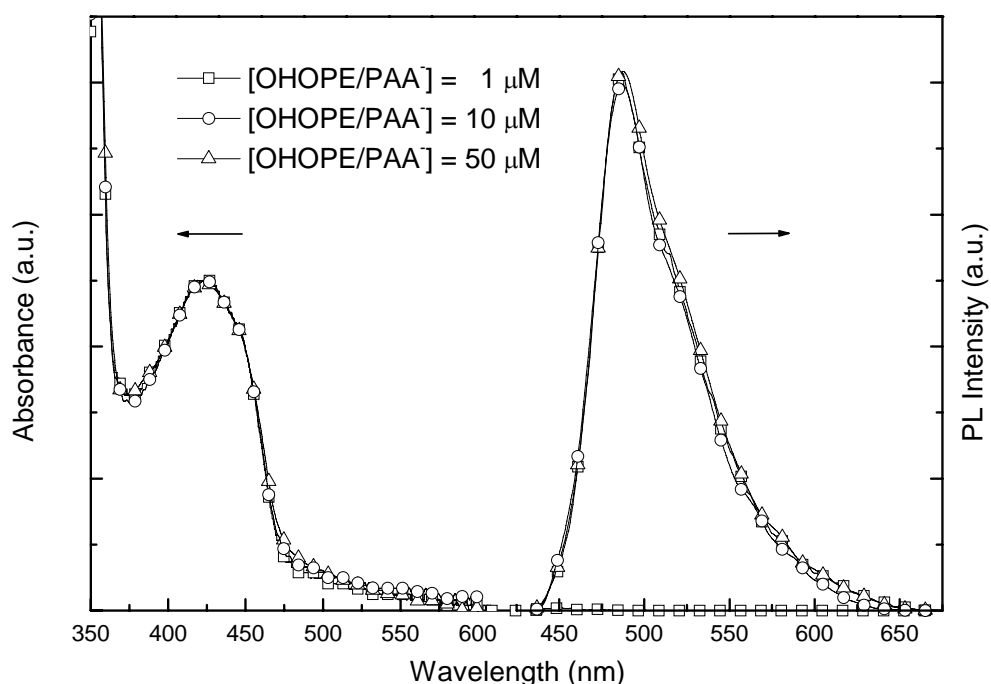


**Figure 4.6** UV-vis absorption and emission spectra of  $\text{OHOPE}_L/\text{PAA}^-$  nanoparticles in different concentrations ( $c = 1, 10$  and  $50 \mu\text{M}$ )

Figure 4.7 shows the  $K_{sv}$  values for  $\text{OHOPE}_L/\text{PAA}^-$  nanoparticles of different concentrations using  $\text{MV}^{2+}$  as the quencher. It is interesting to note that the quenching constant of  $\text{OHOPE}_L/\text{PAA}^-$  nanoparticles increases with decreasing concentrations of the nanoparticles. A similar result was also reported for  $\text{PPE-SO}_3^-$ ,  $\text{PPP-NEt}_3^+$  and  $\text{PPV-NEt}_3^+$  systems,<sup>17,20,23</sup> which suggests that the quenching constant  $K_{sv}$  is closely related to the concentration of the detectors. According to previous work,<sup>10</sup> the cationic ions ( $\text{Na}^+$ ) are better dissociated away from the negatively charged surface of nanoparticles at a low polymer concentration. This removal of ions decreases the electrostatic screening around nanoparticles surface and favors the interaction

between  $\text{OHOPE}_L$  and quencher.<sup>4,17</sup>

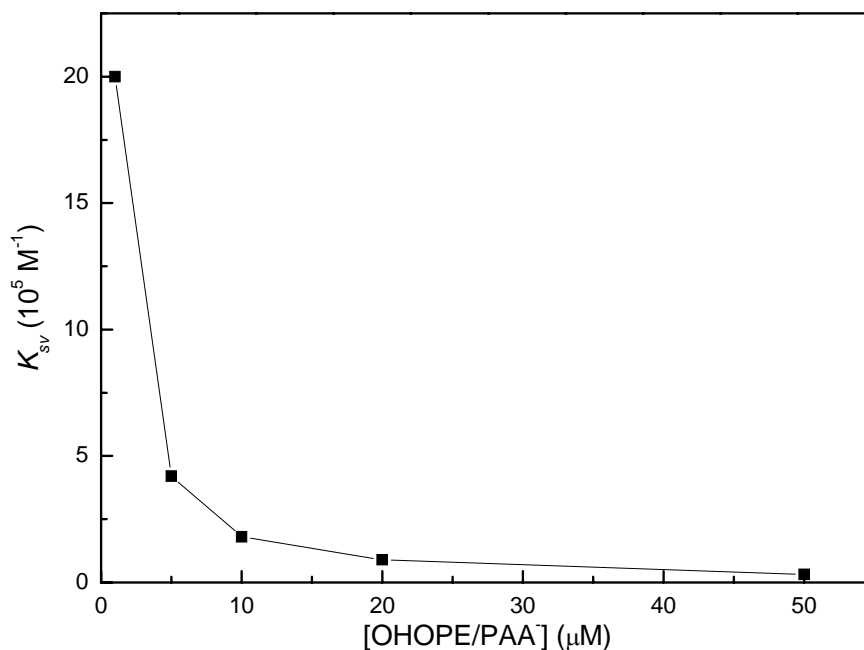


**Figure 4.7**  $K_{sv}$  versus the concentration of  $\text{OHOPE}_L/\text{PAA}^-$  nanoparticles ranging from 1 to 50  $\mu\text{M}$  in the presence of  $\text{MV}^{2+}$

#### 4.4.5 The influence of pH on fluorescence quenching

In practice, analysis carried out in environments of different pHs is common and a number of papers has discussed the related pH-influenced detective efficiency of conjugated polymers. Many reports showed that the pH greatly influenced the interchain aggregation and therefore the optical properties of conjugated polymers and their fluorescence sensitivity to quenchers.<sup>11</sup> Figure 4.8 shows the UV-vis absorption and emission spectra of  $\text{OHOPE}_L/\text{PAA}^-$  nanoparticle in aqueous solution of different pH values. We note that all the absorption and emission spectra are hardly affected by the pH. Previously it was reported that the interchain aggregation of  $\text{OHOPE}_L$ s appeared after their water-soluble nanoparticles have been formed. Thus

the pH change in the aqueous solution outside the nanoparticles cannot affect the chain aggregation inside and their optical properties, which is obviously different from the result for water-soluble conjugated polymers.

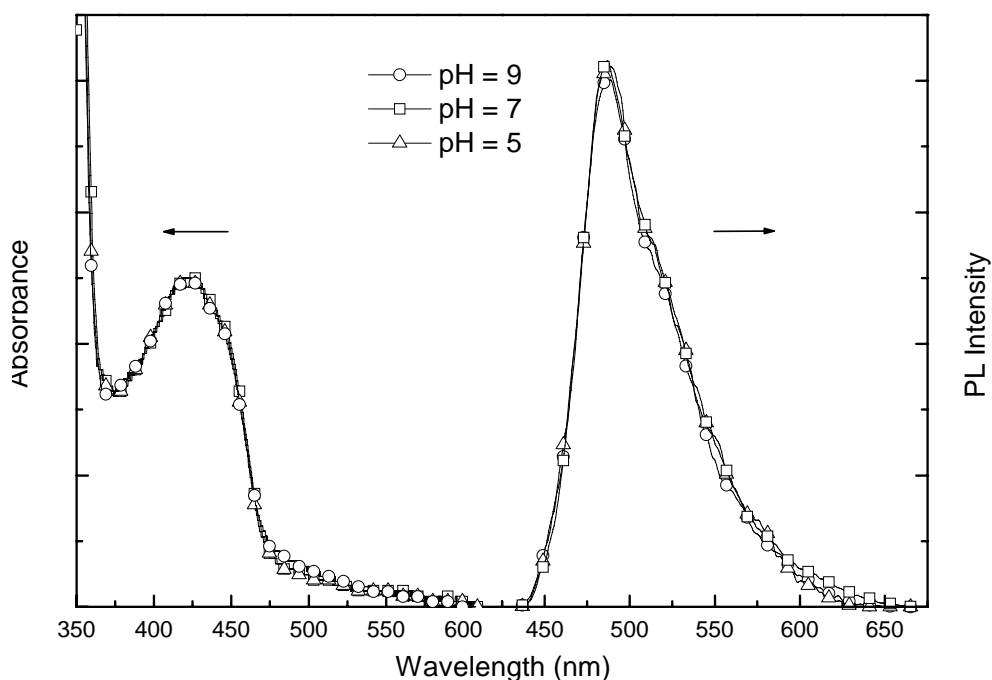


**Figure 4.8 UV-Vis absorbance and PL emission spectra of OHOPE<sub>L</sub>/PAA<sup>-</sup> nanoparticles in aqueous solution of different pHs**

The plot of  $K_{sv}$  values of OHOPE<sub>L</sub>/PAA<sup>-</sup> nanoparticles versus pH is shown in Figure 4.9. The  $K_{sv}$  value decreased by about eight times from pH of 9 to pH of 7. We believe that when  $\text{pH} > 9$ , the  $\text{COO}^-$  groups are the dominant species in the aqueous solution; but when the pH is lower than 9, the negative charges on the nanoparticles surface are partially neutralized by  $\text{H}^+$  ( $\text{COO}^- + \text{H}^+ \leftrightarrow \text{COOH}$ ). Consequently, the decreased charge density on polymer chains reduced the mutual electrostatic attraction by positive quencher  $\text{MV}^{2+}$ <sup>24-27</sup> and resulted in a lowering of  $K_{sv}$  value. As pH decreased further, all the  $\text{COO}^-$  groups on the surfaces of nanoparticles are

neutralized to COOH groups and behaved like neutral OHOPE<sub>L</sub>/PAA nanoparticles. Furthermore, the  $K_{sv}$  value can be recovered repeatedly through changing the pH, indicating that the fluorescence sensitivity of nanoparticles can be adjusted by controlling the pH.

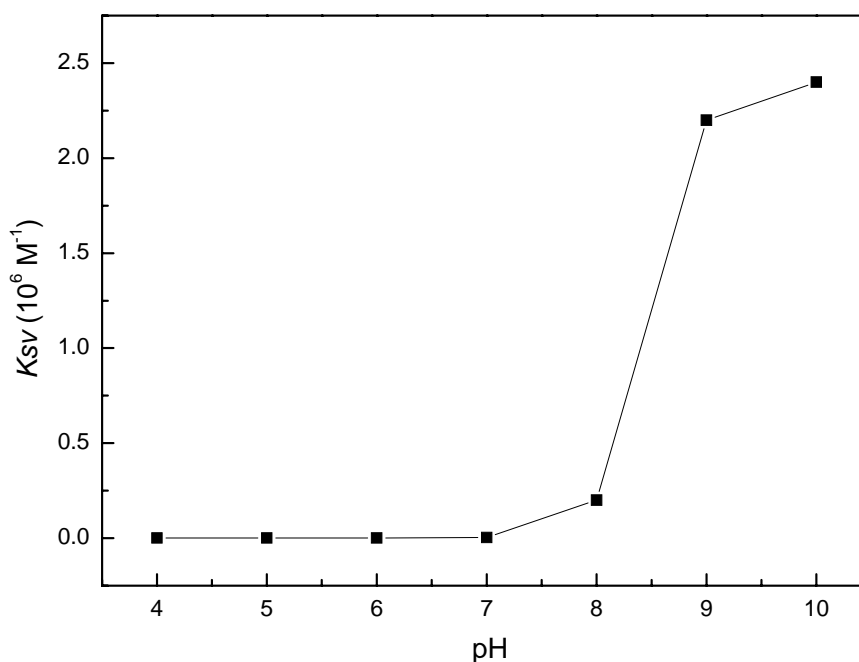


**Figure 4.9**  $K_{sv}$  values of OHOPE<sub>L</sub>/PAA<sup>-</sup> versus pHs

The plot of  $K_{sv}$  values versus pHs in different concentrations of OHOPE<sub>L</sub>/PAA<sup>-</sup> nanoparticles are shown in Figure 4.10. The data show that between pH values 7 to 9, a ten times increase of OHOPE<sub>L</sub>/PAA<sup>-</sup> nanoparticles concentration is accompanied by a nearly 10 folds decrease in the  $K_{sv}$  value. On the other hand, the  $K_{sv}$  value is not affected by the increase in concentration of the nanoparticles between pH values of 4 to 7 which is attributed to the fixed charge density obtained from the dissociation of carboxylic groups.

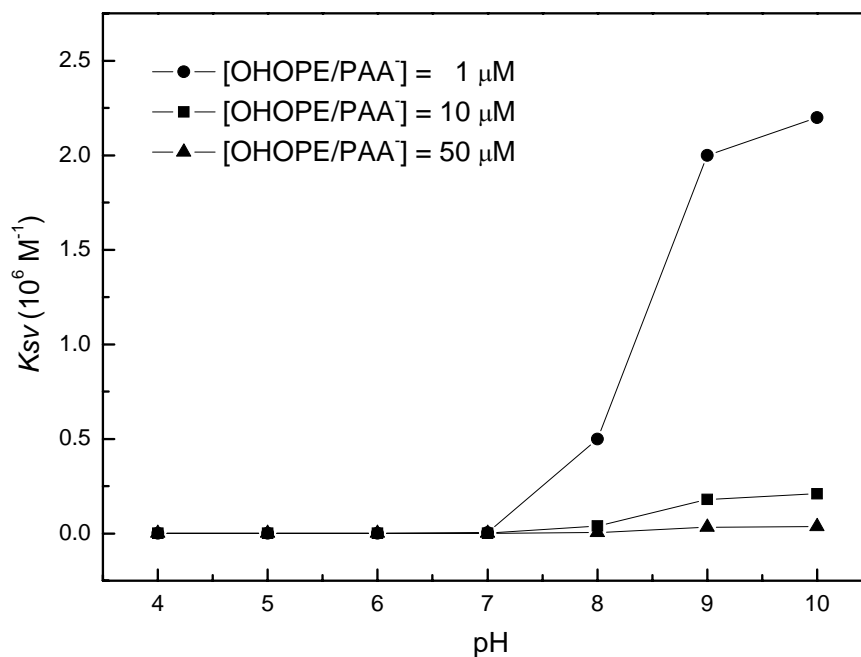


**Figure 4.10**  $K_{sv}$  values of OHOPE<sub>L</sub>/PAA<sup>-</sup> nanoparticles versus pHs in different nanoparticle concentrations

#### 4.4.6 The influence of ionic strength on fluorescence quenching

Influence of ionic strength on the optical properties of conjugated polymers has been studied by several researchers.<sup>3,28</sup> We have conducted a similar study in this work on the OHOPE<sub>L</sub>/PAA<sup>-</sup> nanoparticles in aqueous solution containing different amounts of NaCl to adjust the ionic strength. As shown in Figures 4.11a and 4.11b, the absorption and emission maxima are not affected by the increase of ionic strength. This result demonstrates that the optical properties of the nanoparticles are very stable with different pHs and ionic strengths, unlike the results obtained for ionic WSCPs. This may be attributed to the relatively stable interchain aggregation of OHOPEs in the cores of nanoparticles, which is difficult to be disturbed by chemical environments. This property made the nanoparticles attractive in practical applications where

stability over a broad range pHs and ionic strengths is required.

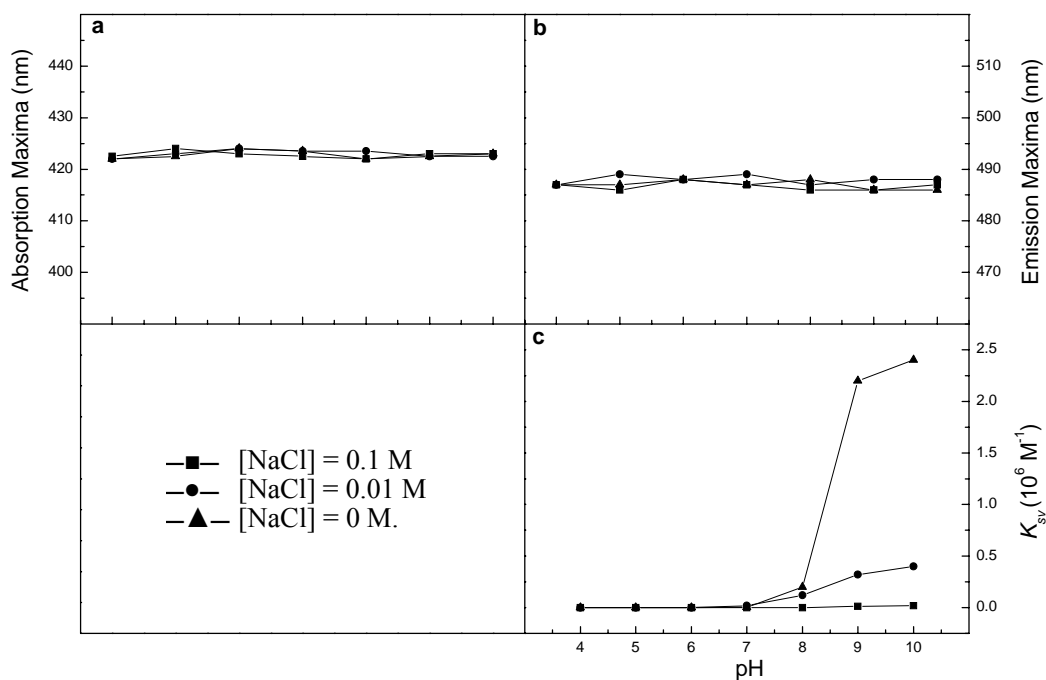


**Figure 4.11 (a) pH-dependence of UV-vis absorption maxima; (b) pH-dependence of emission maxima; (c) fluorescence quenching by  $MV^{2+}$  of  $OHOPE_L/PAA^- Na^+$  nanoparticles in aqueous solution with and without NaCl.**

The plots of  $K_{sv}$  values versus pHs with different ionic strengths are shown in Figure 4.11c. It can be observed that (i) the  $K_{sv}$  value decreased dramatically from no NaCl to 0.1 M of NaCl and (ii) the dependence of  $K_{sv}$  on pH is significantly reduced in the presence of NaCl. These results can be explained in terms of the effective screening of electrostatic interaction<sup>3</sup> by salts.

#### 4.5 Conclusion

We report in this chapter the successful preparation of anionic water-soluble light-emitting  $OHOPE_L/PAA^-$  nanoparticles through ionization of neutral



OHOPE<sub>L</sub>/PAA nanoparticles. The electronic spectra of the ionized nanoparticles present similar optical properties compared to that of the neutral nanoparticles. The optical properties and quenching effects of typical quenchers such as MV<sup>2+</sup> and Fe(CN)<sub>6</sub><sup>4-</sup> on these nanoparticles in different chemical environments are discussed. It is found that the optical properties of the OHOPE<sub>L</sub>/PAA<sup>-</sup> nanoparticles are stable in different nanoparticle concentrations, pHs and ionic strengths. Anionic OHOPE<sub>L</sub>/PAA<sup>-</sup> nanoparticles are more fluorescence sensitive to MV<sup>2+</sup> than Fe(CN)<sub>6</sub><sup>4-</sup>, indicating that electrostatic attraction between ionic nanoparticles and quenchers is the main driving force behind the quenching process. A Stern-Volmer plot curved upward is observed which could be explained by the existence of inaccessible fluorophores not reached by the quenchers. It reveals that the fluorescence quenching of the nanoparticles is limited by the effective contact between the OHOPE<sub>L</sub> and the quencher MV<sup>2+</sup>. Furthermore, the fluorescence quenching is closely related to the concentrations, pHs, and ionic strengths, all of them exert an effect on the electrostatic interaction between the quencher and the nanoparticles.

### References

1. McQuade, D. T.; Pullen, A. E.; Swager, T. M. *Chem. Rev.* **2000**, *100*, 2537.
2. Chen, L.; McBranch, D. W.; Wang, H.-L.; Helgeson, R.; Wudl, F.; Whitten, D. G. *Proc. Natl. Acad. Sci. U. S. A.* **1999**, *96*, 12287.
3. Liu, B.; Bazan, G. C. *Chem. Mater.* **2004**, *16*, 4467.
4. Wang, J.; Wang, D. L.; Miller, E. K.; Moses, D.; Bazan; G. C.; Heeger, A. J.

- Macromolecules* **2000**, *33*, 5153.
5. Pinto, M. R.; Kristal, B. M.; Schanze, K. S. *Langmuir* **2003**, *19*, 6523.
  6. Fan, Q.-L.; Zhou, Y.; Hou, X.-Y.; Huang, W. *Macromolecules* **2005**, *38*, 2927.
  7. Wang, D. L.; Wang, J.; Moses, D.; Bazan; G. C.; Heeger, A. J. *Langmuir* **2001**, *17*, 1262.
  8. Chen, L.; Xu, S.; McBranch, D.; Whitten, D. G. *J. Am. Chem. Soc.* **2000**, *122*, 9302.
  9. Jones, R. M.; Bergstedt, T. S.; McBranch, D. W.; Whitten, D. G. *J. Am. Chem. Soc.* **2001**, *123*, 6726.
  10. Stork, M.; Gaylord, B. S.; Heeger, A. J.; Bazan, G. C. *Adv. Mater.* **2002**, *14*, 361.
  11. Fan, C.; Plaxco, K. W.; Heeger, A. J. *J. Am. Chem. Soc.* **2002**, *124*, 5642.
  12. Zhou, Q.; Swager, T. M. *J. Am. Chem. Soc.* **1995**, *117*, 7017.
  13. Zhou, Q.; Swager, T. M. *J. Am. Chem. Soc.* **1995**, *117*, 12593.
  14. Yang, J.-S.; Swager, T. M. *J. Am. Chem. Soc.* **1998**, *120*, 5321.
  15. Yang, J.-S.; Swager, T. M. *J. Am. Chem. Soc.* **1998**, *120*, 11864.
  16. Kim, J.; McQuade, D. T.; McHugh, S. K.; Swager, T. M. *Angew. Chem. Int. Ed.* **2000**, *39*, 3869.
  17. DiCesare, N.; Pinto, M. R.; Schanze, K. S.; Lakowicz, J. R. *Langmuir* **2002**, *18*, 7785.
  18. Tan, C.; Mauricio, R. P.; Schanze, K. S. *Chem. Comm.* **2002**, 446.
  19. Lakowicz, J. R. in *Principles of Fluorescence Spectroscopy*, 2nd ed.; Plenum Press: New York, **1999**.

20. Harrison, B. S.; Ramey, M. B.; Reynolds, J. R.; Schanze, K. S. *J. Am. Chem. Soc.* **2000**, *122*, 8561.
21. Lehrer, S. S. *Biochemistry* **1971**, *10*, 3254.
22. Gong, Y.-K.; Miyamoto, T.; Nakashima, K.; Hashimoto, S. *J. Phys. Chem. B* **2000**, *104*, 5772.
23. Cheng, F; Zhang, G.-W.; Lu X.-M.; Huang Y.-Q.; Chen Y.; Zhou Y.; Fan Q.-L.; Huang W. *Macromolecular Rapid Communications*, **2006**, *27*, 799.
24. Balanda, P. B.; Ramey, M. B.; Reynolds, J. R. *Macromolecules* **1999**, *32*, 3970.
25. Liu, B.; Yu, W.; Lai, Y. H.; Huang, W. *Chem. Comm.* **2000**, 551.
26. Liu, B.; Yu, W.; Lai, Y. H.; Huang, W. *Macromolecules* **2002**, *35*, 4975.
27. Fan, Q.-L.; Lu, S.; Lai, Y.-H.; Huang, W. *Macromolecules* **2003**, *36*, 6976.
28. Kim, B.-S.; Chen, L.; Gong, J.; Osada, Y. *Macromolecules* **1999**, *32*, 3964.

## CHAPTER FIVE

### Conclusion Remarks

Water-soluble conjugated polymers (WSCPs) have shown great potential to be used as fluorescent chemo- or biosensors due to their special solubility and optoelectronic properties. However, the general synthetic method to realize their water-solubility (i.e., introducing ionic hydrophilic groups onto their side chains via chemical bonds) is very complicated. We have developed an alternative approach involving convenient preparation of water-soluble light-emitting nanoparticles by combining light-emitting conjugated polymers/oligomers and water-soluble polymers via hydrogen bonds.

In this thesis, a series of functionalized PPEs and OPEs was firstly synthesized and characterized by FTIR, NMR, TGA, and GPC. The PPE and OPE-based water-soluble light-emitting nanoparticles were then successfully prepared through non-covalent bond self-assembly with water-soluble polymers and characterized by DLS, TEM and fluorescence microscopy. Conjugated oligomers OPEs with the same conjugated length but of different molecular architectures, i.e., linear (**OHOPE<sub>L</sub>**), cross-shaped (**OHOPE<sub>C</sub>**) and T-shaped structure (**OHOPE<sub>T</sub>**), were used to study the influence on the size and dispersity of the nanoparticles exerted by the conjugated length and the molecular architecture of the conjugated molecules. Furthermore, water-soluble polymers such as PEG, PG and PAA containing different active hydrogens were used to investigate the effect of strength of hydrogen bonds between

the conjugated molecules and the water-soluble polymers on the properties of the nanoparticles produced.

DLS data provide evidence that the nanoparticle size is highly related to the ratio of water-soluble polymers to functionalized conjugated molecules, i.e., the higher ratio of water-soluble polymers to conjugated molecules, the smaller the nanoparticle diameter. Compared with the PPE-based nanoparticles, OPE-based nanoparticles exhibit smaller size and lower dispersity, indicating that the structure of water-soluble nanoparticles is linked to the conjugated length. Surprisingly, the formation of the nanoparticles are little influenced by the molecular architecture of conjugated molecules. Furthermore, the **OHOPE<sub>L</sub>/PG** and **OHOPE<sub>L</sub>/PAA** systems produced smaller particles and lower dispersity than **OHOPE<sub>L</sub>/PEG** system. These results suggest a strong correlation between strength of hydrogen bonds and size and degree of dispersity of the nanoparticles so formed.

The optical properties of the nanoparticles were intensively investigated by UV-vis, PL, and time resolved photoluminescent analysis. The results indicate the existence of interchain  $\pi$ -aggregation of PPEs/OPEs in the nanoparticles. It was also found that the optical properties of anionic **OHOPE<sub>L</sub>/PAA<sup>-</sup>** nanoparticles remained stable in different chemical environments such as changes in concentrations, pHs and ionic strengths.

The fluorescence quenching behavior of the nanoparticles in different environments was investigated by using  $MV^{2+}$  and  $Fe(CN)_6^{4-}$  as the ionic quenchers. The results show that anionic **OHOPE<sub>L</sub>/PAA<sup>-</sup>** nanoparticles are more fluorescence sensitive to

MV<sup>2+</sup> than Fe(CN)<sub>6</sub><sup>4-</sup>, indicating that electrostatic attraction is the main force to drive the quenchers close to the fluorophores to effect fluorescence quenching. Furthermore, the fluorescence quenching behavior is closely related to the chemical environment, i.e., concentrations, pHs, and ionic strengths, which has a direct influence on the electrostatic attraction.

The results have demonstrated that the water-soluble light-emitting nanoparticles, especially OPE-based nanoparticles, are promising candidates for application in chemo- or bio-sensors. This aspect of the work will be carried out in the future.